

AD-A131 284

FUNDAMENTAL PROPERTIES OF SOILS FOR COMPLEX DYNAMIC
LOADINGS: DYNAMIC CON. (U) APPLIED RESEARCH ASSOCIATES
INC ALBUQUERQUE NM W C DASS ET AL. APR 83

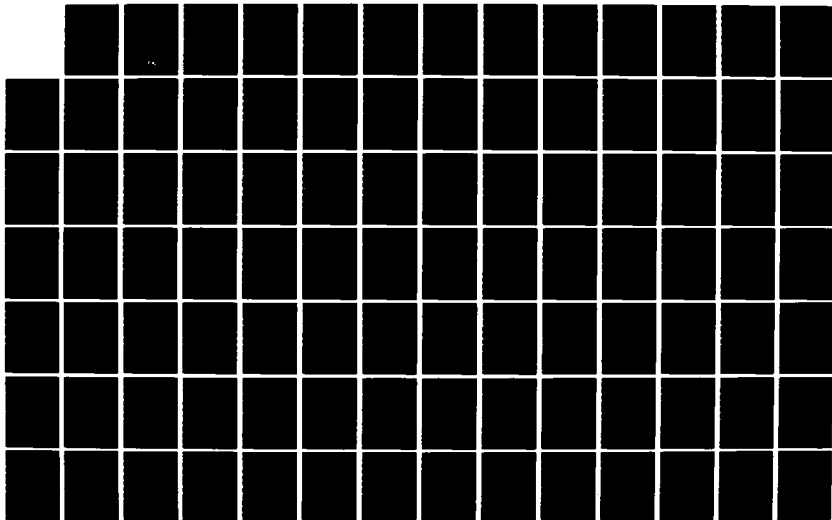
1/2

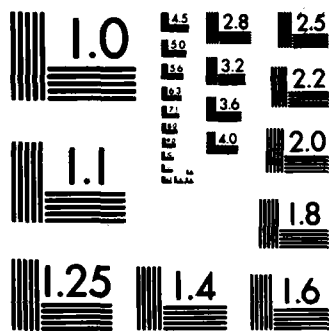
UNCLASSIFIED

AFOSR-TR-83-0653 F49620-80-C-0088

F/G 8/13

NL



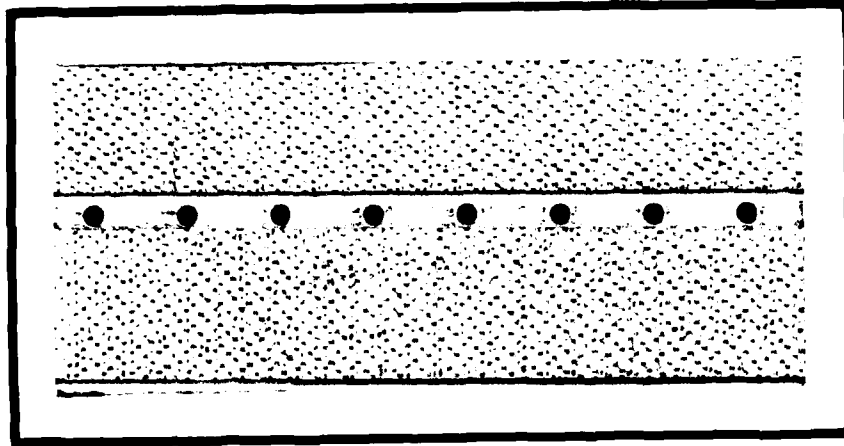


MICROCOPY RESOLUTION TEST CHART
NATIONAL BUREAU OF STANDARDS-1963-A

AFOSR-TR. 83-0653

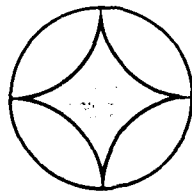
9

ADA131284



DTIC FILE COPY

APPLIED RESEARCH ASSOCIATES, INC.
AUG 11 1983
A



**APPLIED
RESEARCH
ASSOCIATES, INC.**

Engineering and Applied Science

Approved for public release; distribution unlimited. 83 08 08 006

**FUNDAMENTAL PROPERTIES OF SOILS FOR
COMPLEX DYNAMIC LOADINGS:**

ANNUAL TECHNICAL REPORT NO. 2

"Dynamic Constitutive Modeling of Sandy Soils"

by

**William C. Dass
Douglas H. Merkle
Jimmie L. Bratton**

April 1983

**Applied Research Associates, Inc.
2101 San Pedro NE, Suite A
Albuquerque, New Mexico 87110**

Prepared for

**Air Force Office of Scientific Research
Bolling Air Force Base
Washington, D.C. 20332**

Contract No. F49620-80-C-0088

Approved for Public Release; Distribution Unlimited

**AIR FORCE OFFICE OF SCIENTIFIC RESEARCH (AFSC)
NOTICE OF TRANSMITTAL TO DTIC**

**This technical report has been reviewed and is
approved for public release IAW AFR 190-12.
Distribution is unlimited.**

**MATTHEW J. KERPER
Chief, Technical Information Division**

Conditions of Reproduction

Reproduction, translation, publication, use and disposal in whole or in part by or for the United States Government is permitted.

Qualified requestors may obtain additional copies from the Defense Technical Information Service.

UNCLASSIFIED

SECURITY CLASSIFICATION OF THIS PAGE (When Data Entered)

REPORT DOCUMENTATION PAGE		READ INSTRUCTIONS BEFORE COMPLETING FORM
1. REPORT NUMBER AOSR-TR- 83-0658	2. GOVT ACCESSION NO. AD-A131284	3. RECIPIENT'S CATALOG NUMBER
4. TITLE (and Subtitle) FUNDAMENTAL PROPERTIES OF SOILS FOR COMPLEX DYNAMIC LOADINGS; Dynamic Constitutive Modeling of Sandy Soils		5. TYPE OF REPORT & PERIOD COVERED ANNUAL 1 Aug 81 - 31 Jul 82
7. AUTHOR(s) WILLIAM C DASS DOUGLAS H MERKLE JIMMIE L BRATTON		6. PERFORMING ORG. REPORT NUMBER
9. PERFORMING ORGANIZATION NAME AND ADDRESS APPLIED RESEARCH ASSOCIATES, INC 2101 SAN PEDRO, NE, SUITE A ALBUQUERQUE, NM 87110		8. CONTRACT OR GRANT NUMBER(s) F49620-80-C-0088
11. CONTROLLING OFFICE NAME AND ADDRESS AIR FORCE OFFICE OF SCIENTIFIC RESEARCH/NA BOLLING AFB, DC 20332		10. PROGRAM ELEMENT, PROJECT, TASK AREA & WORK UNIT NUMBERS 61102F 2307/C1
14. MONITORING AGENCY NAME & ADDRESS (if different from Controlling Office)		12. REPORT DATE 30 April 1983
		13. NUMBER OF PAGES 115
		15. SECURITY CLASS. (of this report) UNCLASSIFIED
		15a. DECLASSIFICATION/DOWNGRADING SCHEDULE
16. DISTRIBUTION STATEMENT (of this Report) Distributed unlimitedly		
17. DISTRIBUTION STATEMENT (of the abstract entered in Block 20, if different from Report)		
18. SUPPLEMENTARY NOTES		
19. KEY WORDS (Continue on reverse side if necessary and identify by block number) COHESIONLESS SOIL MATERIAL MODELING LABORATORY TESTING CIST DISC TEST		
20. ABSTRACT (Continue on reverse side if necessary and identify by block number) Constitutive modeling of cohesionless soil for both standard static test conditions and insitu impulsive dynamic load conditions is discussed in this annual report. Predicted laboratory response for several different types of models is evaluated using data from a coordinated testing program. The modeling of insitu soil response to explosive events (CIST and DISC Test) is considered, and the laboratory-derived models are tested for their convenience and accuracy in predicting ground motions. Several important laboratory and		

Abstract, continued

In situ phenomena which were not reflected by the model exercises are discussed. Based on the conclusions from this study, testing and modeling requirements for dynamic loading situations are proposed.

Accession For	
DTIC	1
By	
Date	
Dis	
A	



FUNDAMENTAL PROPERTIES OF SOILS FOR
COMPLEX DYNAMIC LOADINGS:

ANNUAL TECHNICAL REPORT NO. 2

"Dynamic Constitutive Modeling of Sandy Soils"

TABLE OF CONTENTS

<u>Section</u>		<u>Page</u>
1.0	INTRODUCTION AND SCOPE	1
2.0	PROGRESS SUMMARY	3
2.1	Soil Element Model Development	3
2.2	U.S. Army Engineer Waterways Experiment Station (WES) Testing Program	4
2.3	Application of Laboratory Data in Modeling	5
2.4	Strain Path Response	5
2.5	Wave Propagation Studies	6
2.6	Interactions	7
3.0	LABORATORY BEHAVIOR OF SAND	8
3.1	Introduction	8
3.2	Material Description	8
3.3	Laboratory Tests Performed	9
3.4	Laboratory Test Results	14
4.0	MODELING THE LABORATORY BEHAVIOR OF SAND	28
4.1	Constitutive Relationships	28
4.2	Model-Data Comparisons	28
4.3	Discussion of Comparisons	29
5.0	DYNAMIC INSITU BEHAVIOR OF SAND	42
5.1	Insitu Test Description	42
5.2	Insitu Test Results	42
6.0	MODELING THE INSITU BEHAVIOR OF SAND	50
6.1	Finite-Difference Calculations	50
6.2	Calculational Results	50

<u>Section</u>		<u>Page</u>
7.0	DISCUSSION OF SAND MODELING	62
7.1	Additional Laboratory Behavior of Sand	62
	7.1.1 Multiphase Effects	62
	7.1.2 Anisotropy and Work Hardening	62
	7.1.3 Strains	63
	7.1.4 Loading Rate Effects	65
	7.1.5 Cyclic Loading Effects	65
	7.1.6 High Pressure/Temperature Behavior	66
7.2	Additional Aspects of the Insitu Behavior of Sand	66
8.0	TESTING CONSIDERATIONS	73
	8.1 Ideal Testing Program	73
	8.2 Modeling Requirements	76
9.0	SUMMARY	78
REFERENCES		79
APPENDICES		
A	WES Laboratory Tests	81
B	Material Model Descriptions	84
C	Sample Results from SEM Finite Difference Calculations	90
D	Publications	100

ILLUSTRATIONS

<u>Figure</u>		<u>Page</u>
1	Average Grain Size Distribution Curves for MB, RB, and RV Sands	10
2	Example Determination of a Representative UX Compression Curve	12
3	Comparison of Representative MB and RB UX Compressibility Relations	15
4	Representative UX Compressibility for RV Alluvium 0-6 m Depth	17
5	Representative UX Stress Paths for MB and RB Sands	18
6	Variation of Poisson's Ratio During UX Tests on MB and RB Sands	20
7	Representative TX Stress-Strain and Effective Stress Path Relations for MB Sand	21
8	Representative TX Stress-Strain and Effective Stress Path Relations for RB Sand	23
9	Representative Pore Pressure Response for Undrained-Saturated TX Tests on MB and RB Sand	25
10	Typical TX Stress-Strain Response for Dry RV Alluvium	26
11	Dry MB Sand UX Model-Data Comparisons	30
12	Drained Saturated MB Sand UX Model-Data Comparisons	31
13	Dry RB Sand UX Model-Data Comparisons	32
14	Drained Saturated RB Sand UX Model-Data Comparisons	33
15	MB Sand TX Model-Data Comparisons (Confining Pressure = 3.45 MPa)	34
16	RB Sand TX Model-Data Comparisons (Confining Pressure = 3.45 MPa)	35
17	RV Alluvium UX and TX Model-Data Comparisons	36
18	MB and RB Sands Hyperbolic Model-Data Comparisons	37

<u>Figure</u>		<u>Page</u>
19	Effective Stress Cap Model, RB Undrained Saturated TX Model-Data Comparisons	38
20	AFWL Engineering Model with Multilinear Unload-Reload Behavior	40
21	CIST 22 Experimental Setup	43
22	DISC Test II Experimental Setup	44
23	CIST 22 Composite Radial Velocity Data	46
24	CIST 22 Observed Attenuation and Arrival Times	47
25	DISC Test II Composite Vertical Velocity Data	48
26	DISC Test II Observed Attenuation and Arrival Times	49
27	One-Dimensional Computational Setups for CIST 22 and DISC Test II	51
28	CIST 22 Elastic Calculation Compared with Data	54
29	CIST 22 Calculated Radial Velocity Waveforms Compared with Data	55
30	DISC Test II Calculated Vertical Velocity Waveforms Compared with Data	56
31	Comparison of Calculated and Measured Attenuation Rates for CIST 22 and DISC Test II	57
32	Comparison of Calculated and Measured Times of Arrival for CIST 22 and DISC Test II	58
33	DISC Test II Calculated (2D STEALTH) Velocity Waveforms	59
34	Hardening Behavior	64
35	Types of Explosive Loading	67

TABLES

<u>Table</u>		<u>Page</u>
1	Average Physical Properties for MB, RB, and RV Sands	11
2	Laboratory Tests on MB and RB Sands	13
3	Matrix of Finite Difference Calculations	52
4	Summary of Major Explosive Events in Sandy Soils	68
5	Important Response Phenomena for Dynamic Loadings	71
6	Controlling Soil Behavior for Various Dynamic Response Phenomena in Sands	72

ABBREVIATIONS AND ACRONYMS

AFWL	Air Force Weapons Laboratory
BP	Blast Pressure
CIST	Cylindrical Insitu Test
DISC	Dynamic Insitu Compressibility
DS	Drained Saturated
ELPLA	Elastic-Perfectly Plastic
HE	High Explosive
MB	Misers Bluff
RB	Reid Bedford
RV	Ralston Valley
SEM	Soil Element Model
TX	Triaxial
TXC	Triaxial Compression
TXE	Triaxial Extension
UD	Undrained Dry
US	Undrained Saturated
UX	Uniaxial Strain
WES	Waterways Experiment Station

1.0 INTRODUCTION AND SCOPE

The subject of this annual report is constitutive modeling of cohesionless soil, for both laboratory standard static test conditions and insitu impulsive dynamic load conditions. Laboratory test results are used to quantify the parameters for several different types of constitutive models. The ability of these models to predict laboratory behavior is then compared and evaluated. The modeling of insitu soil response to explosive events is considered, and the laboratory-derived models are tested for their convenience and accuracy in predicting ground motions. Several phenomena which occur in the laboratory and/or insitu, and which may be important in certain cases but were not reproduced by the models used, are discussed. An "ideal" testing device is proposed, which can exercise the important stress-strain mechanisms of explosively loaded cohesionless soils. The complexity of a constitutive model which includes all the above mechanisms is considered.

The following is the Statement of Work for this effort, as it appears in Contract Document No. F49620-80-C-0088, FY82 Modification:

- a. Use the Soil Element Model to study the response of soils to laboratory boundary conditions, utilizing a variety of dynamic soil models. Emphasis will be placed on understanding each model's capability to reproduce a large suite of laboratory test data and more complex stress/strain paths representing insitu dynamic loadings.
- b. Using the results from (a), characterize the "ideal" laboratory test(s) required to describe insitu response of soils to complex

dynamic loadings. Compare the resulting stress/strain paths with those of current laboratory tests.

- c. Continue the CISTFTON study of insitu soil response. Begin efforts to model the response of at least one soil for which insitu testing and large explosive event data are available. The purpose is to study the process of laboratory tests, insitu tests, model fitting and calculation of a dynamic event to confirm deficiencies in current models.
- d. Begin efforts, based on a, b, c, to outline a new approach for constitutive modeling for soils.

2.0 PROGRESS SUMMARY

2.1 Soil Element Model (SEM) Development

The SEM is a FORTRAN computer program which was written during the last reporting period (Ref. 1) to examine some of the questions regarding dynamic soil modeling. It consists of a driver, a set of boundary condition algorithms, and a set of constitutive relationships. The SEM allows comparison of material models when they are subjected to various kinds of static and dynamic stress and/or strain paths. It can also be used for parameter variation studies, and as a model parameter fitting tool.

During this reporting period, the SEM continued to be the primary tool for constitutive model evaluation and development. Two additional models were added to those already being studied: Duncan and Chang's hyperbolic curve-fitting model (Ref. 2), and a standard linear viscoelastic model. Also, Lade's model for cohesionless soil (Ref. 3) has been programmed and is currently being tested.

Several models already installed were refined to improve their behavior under various loading conditions. The AFWL Engineering model hydrostat was changed to a pressure versus volumetric strain formulation in place of a pressure versus excess compression relationship. This resolved some inconsistencies between assumed incrementally elastic properties. A multilinear unload-reload relation was added to the AFWL Engineering model, which increased the amount of strain recovery and allowed for hysteresis loops. The AFWL Engineering model failure surface was also modified to give different shear strengths in triaxial compression and extension, to produce a Mohr-Coulomb-like cross-section in

the octahedral plane. Tensile behavior in several models was studied and in most cases improved. It was found that in many loading situations the response to tensile stress significantly affected overall behavior. Various forms of tensile stress cutoff and volumetric strain tracking have been tested in the SEM.

The versatility of the SEM in subjecting a particular model to various stress/strain paths was greatly improved during the past year by addition of a one-dimensional wave propagation feature. The finite difference logic for this feature was adapted from SNEAKY (Ref. 4), and can use any of the SEM stress-strain models. The code can treat planar, cylindrical, and spherical geometries, and accommodates up to ten different material layers, each of which can have a different constitutive model. Although restricted to one dimension, inclusion of wave propagation in the SEM is an important step because it makes model evaluation under impulsive loading much easier, and the results directly applicable to finite difference techniques.

Improved plotting has made assessment of results from SEM studies easier and quicker. The curves resulting from several problems can be overlaid for qualitative comparison. Quantitative comparisons can be made by calculating the area between two curves as a continuous residual. In addition, any quantity resulting from a wave propagation calculation can be plotted versus time, another time varying quantity, or grid position.

2.2 U.S. Army Engineer Waterways Experiment Station (WES) Testing Program

Laboratory tests have been conducted on two recompacted sands, Misers Bluff sand and Reid Bedford Model sand. The data already available for

these materials, plus the above test results comprise a fairly complete and accurate definition of both sands' uniaxial strain and standard triaxial behavior under static and dynamic (rapid) loading. WES has published three reports (Refs. 5, 6, and 7) which document the testing program and provide initial analyses of the data.

2.3 Application of Laboratory Data in Modeling

The data from the WES program was utilized to study and model the behavior of cohesionless sands. The SEM was used to arrive at model fits to the data for most of the implemented constitutive relations. The ability of each model to predict laboratory responses was evaluated and compared. This work is described in detail in Section 4.0 of this report.

2.4 Strain Path Response

Model response comparisons were made under the "typical" strain path excursions postulated by Workman, et al. (Ref. 8). These strain paths are those expected from a truly spherical field of motion resulting from a buried explosion. The primary purpose of this exercise was to see if the models installed in the SEM predicted reasonable stress paths when exercised over the postulated strain paths. It was found that each model produced a reasonable stress path, and that the most important material parameters affecting the results were shear strength and tensile behavior.

A complete study of the strain path response technique for modeling material response has not been made. However, some initial observations can be made. The method requires a stress path resulting from each strain path. Aside from the testing difficulties involved in measuring such response in the laboratory, the representative strain paths may not always

be unique, especially under conditions of tensile or shear failure. Under these circumstances it would be difficult to utilize the resulting stress-strain relations as a complete material model.

2.5 Wave Propagation Studies

The models derived from the laboratory results were used to predict ground motions due to blast loading for uniaxial strain, plane-strain, and axisymmetric and spherically symmetric geometries. The wave propagation studies revealed much about the models which was not immediately obvious from laboratory behavior predictions, and forced them to become completely functional in a finite difference code. The dependency of model response on calculational details such as time step, grid size, and artificial viscosity was explored. For example, it was quickly confirmed that the cap model may require subcycling within a Courant-condition-defined time step to ensure correct model response. It was also found that the spherical and cylindrical one-dimensional wave propagation calculations exercised several important aspects of the models more completely than did the planar calculations. Expansive strains are produced in the cylindrical and spherical calculations which test the tensile relationships, and large stress differences are generated which test the adequacy of shearing behavior.

Calculated model responses were compared with available measured insitu responses. In some cases, the two did not compare well and model parameters were adjusted to give an insitu-based model. Observing the differences between laboratory-based and insitu-based models can help discern errors in material parameters based on a laboratory testing program.

2.6 Interactions

Appendix D contains a paper presented at the International Conference on Constitutive Laws for Engineering Materials, in Tuscon, Arizona on 13 January 1983, and published in the Proceedings. The paper discusses the goals of this research and briefly summarizes some of the work described above.

Also included in Appendix D is the abstract of a paper accepted for presentation at the Symposium on Interaction of Non-Nuclear Munitions with Structures, to be held at the USAF Academy from 9-13 May 1983. That paper describes the direct application of methods developed under this effort to an actual site and laboratory/insitu test program.

3.0 LABORATORY BEHAVIOR OF SAND

3.1 Introduction

Soil behavior observed in laboratory tests is generally limited in its nature by several factors. First, laboratory response is physically constrained by test item size and testing apparatus boundaries. Second, the variety of stress (or strain) paths to which a test item can be subjected is limited by test apparatus capability. Third, principal stress and strain directions are constant, and coincide with the test specimen axes in the uniaxial and triaxial apparatuses, which are the mainstay of standard soil testing. In addition, due to the cylindrical nature of the samples, two of the principal stresses and strains are always equal. Nevertheless, practical considerations dictate continued reliance on standard laboratory tests to develop constitutive relationships for most geologic materials. Many assumptions are then required to generalize the test results to predict response under more general states of stress and strain.

3.2 Material Description

The dynamic stress-strain behavior of three cohesionless sands was studied, using constitutive models based on laboratory test data. The three sands were: Misers Bluff (MB) sand, Reid Bedford Model (RB) sand, and Ralston Valley (RV) alluvium. The MB and RB sands were tested in conjunction with this project, and will receive the most attention. RV alluvium results are from a separate testing effort (Refs. 9 and 10), and are of interest because of the large amount of complementary insitu data also available for this material.

MB sand is a medium to coarse grained silty sand obtained at Planet Ranch, Arizona. Planet Ranch was the site of the Misers Bluff, Phase II HE experiments in 1978, and the CIST 19 material properties test in 1977. RB sand is a fine grained, uniform sand obtained along the Big Black River in Mississippi. It is often used by WES for test apparatus development and calibration work because of its easy availability, uniformity, and fairly well defined properties. RV alluvium is a medium to coarse grained silty sand obtained from the top six meters of the Ralston Valley geotechnical study site between Tonopah, Nevada and the northwest corner of the Nevada Test Site. Average grain size distribution curves for the three sands are shown in Figure 1. Average physical properties are given in Table 1.

3.3 Laboratory Tests Performed

Existing data was first collected for dry RB sand and saturated MB sand (Ref. 5). Uniaxial compression and triaxial shear tests were then performed on saturated RB sand and dry MB sand to complete the data base. A brief description of each laboratory test performed at WES is given in Appendix A (Refs. 5 and 6). Enough tests were done so that representative relations could be determined by weighting and averaging all test results (Fig. 2). However, there was not a sufficient number of tests done to warrant a statistical determination of mean curves or standard deviations. Table 2 shows the number of each type of test done on MB and RB sand during both previous WES efforts and the current ARA/WES effort.

The laboratory response of RV sand is less well defined than for MB or RB sand, but several static and dynamic uniaxial compression and triaxial shear tests were done on samples from the depth range of interest. Representative curves have been estimated from these results.

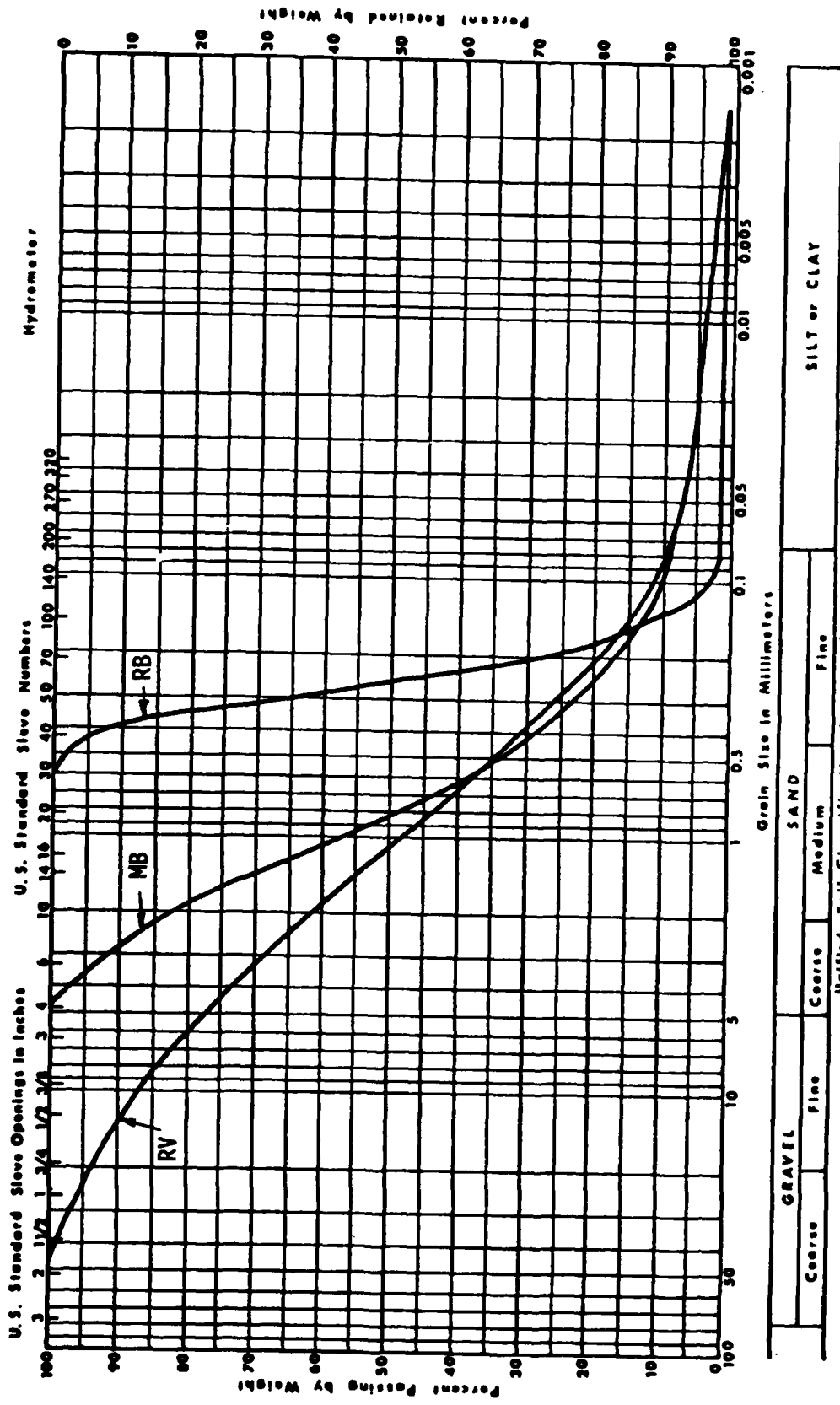
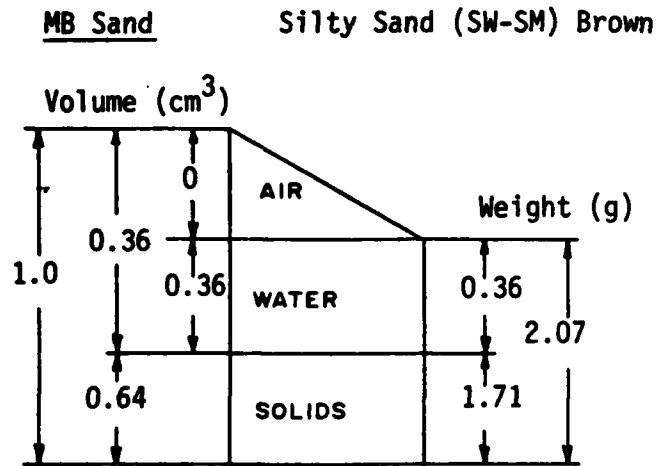
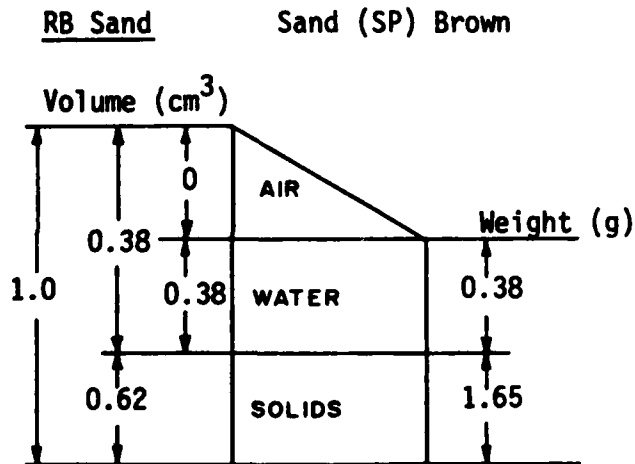


Figure 1. Average Grain Size Distribution Curves for MB, RB, and RV Sands

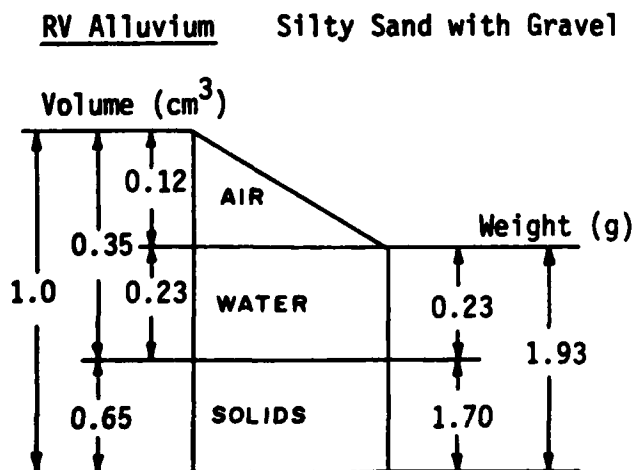
Table 1. Average Physical Properties of MB, RB, and RV Sands



$G_s = 2.67$
 $e = 0.57$
 $w = 21\%$
 $S = 100\%$
 $\gamma_t = 2.07$
 $w = 0.4\%$
 $S = 1.9\%$
 Air Dry: $\gamma_d = 1.72 \text{ g/cc}$



$G_s = 2.65$
 $e = 0.61$
 $w = 23\%$
 $S = 100\%$
 $\gamma_t = 2.03 \text{ g/cc}$
 $w = 0.1\%$
 $S = 0.3\%$
 Air Dry: $\gamma_d = 1.65 \text{ g/cc}$



$G_s = 2.63$
 $e = 0.54$
 $w = 14\%$
 $S = 56\%$
 $\gamma_t = 1.93 \text{ g/cc}$
 $\gamma_d = 1.70 \text{ g/cc}$

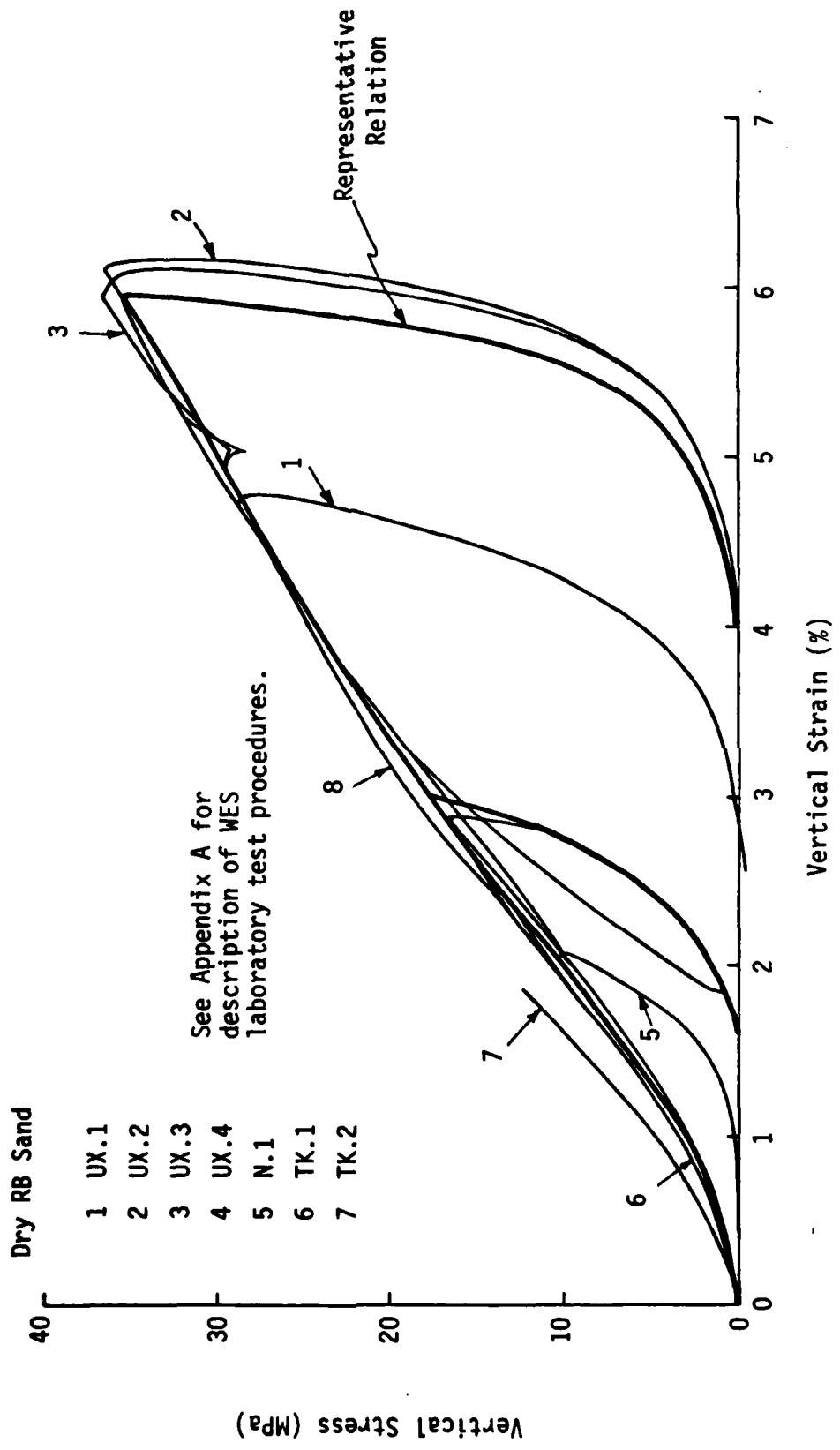


Figure 2. Example Determination of a Representative UX Compression Curve

Table 2. Laboratory Tests on MB and RB Sands

Test ⁺	Misers Bluff			Reid Bedford		
	Dry	Saturated		Dry	Saturated	
		Drained	Undrained		Drained	Undrained
Index Properties		X			X	
Grain Size Dist.		X			X	
Isotropic Compression (Static)	0	0	0	1*	1	2
Static	4	3*	8*	4*	1	3
Uniaxial Strain						
Dynamic	3	6*	0	0	0	2
Uniaxial Strain/K ₀	4	4*	6*	2*	2	3
Uniaxial Strain/Null	0	0	0	1*	0	0
Triaxial Compression	6	11*	23*	5*	3	7
Triaxial Extension	3	0	0	0	0	0

*Tests performed under an earlier WES Effort.

+See Appendix A for descriptions of test procedures.

Three types of tests were conducted on remolded MB and RB sand: undrained-dry (UD), drained-saturated (DS), and undrained-saturated (US). The initial void ratio was the same for each sand. Results discussed below are only a summary in the form of representative curves. References 6 and 7 should be consulted for the complete data set.

3.4 Laboratory Test Results

Uniaxial compressibility is shown in Figure 3 for MB and RB sand. These representative curves combine both static and dynamic test results. The curves marked UD are not undrained in the conventional sense (i.e., saturated with constant water content). If that were the case there would be little deformation in a uniaxial compression test. As Appendix A indicates, a UD test is a test on an air dry specimen with pore air flow prevented. The apparent compressibility difference between the representative UD and DS curves may be due to the same water lubricating effect which also influences compaction test results. However, it must be noted that the representative UD and DS curves were each constructed by a judgmental process, from sets of curves exhibiting far greater compressibility differences than that between the two resulting representative curves. Thus, the apparent compressibility difference between the representative UD and DS curves may not be significant. WES reported the difference because it was observed. The difference is acknowledged here because associated with it are two types of initial compressibility relations (concave and convex to the strain axis) which both need to be constitutively modeled.

MB and RB sands are nonlinear, fairly compressible in the UD or DS conditions, and recover only a relatively small amount of strain upon

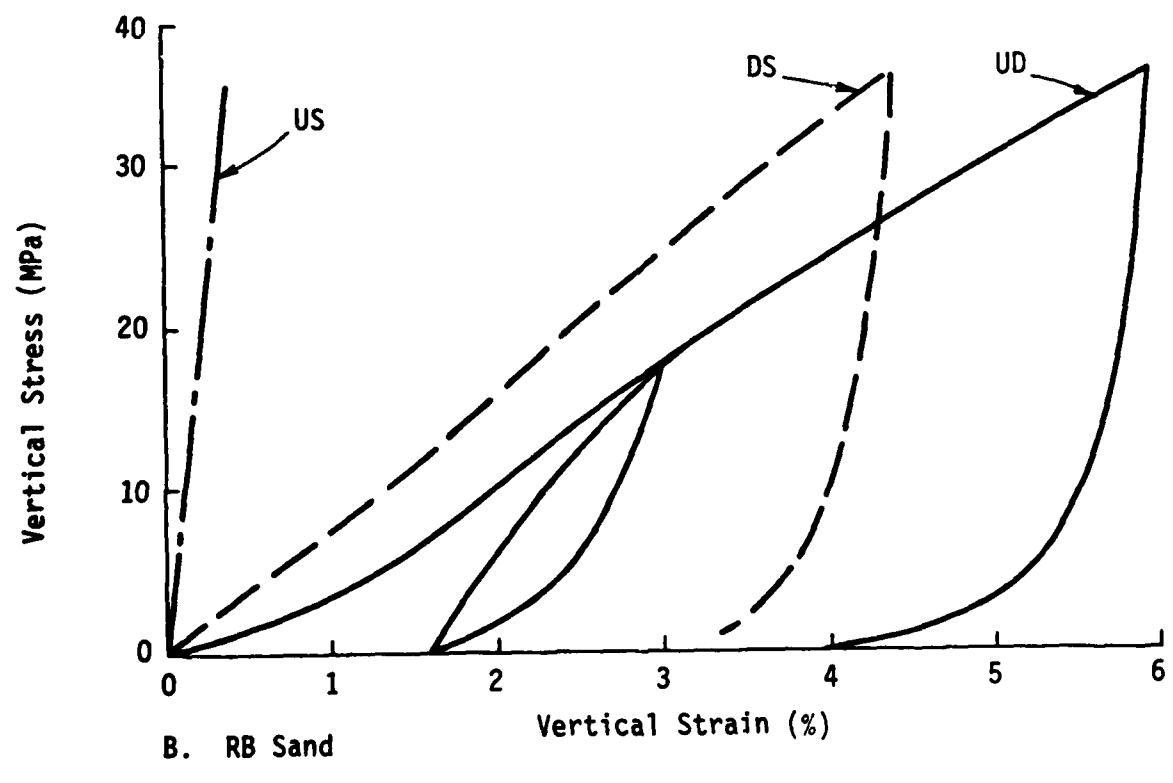
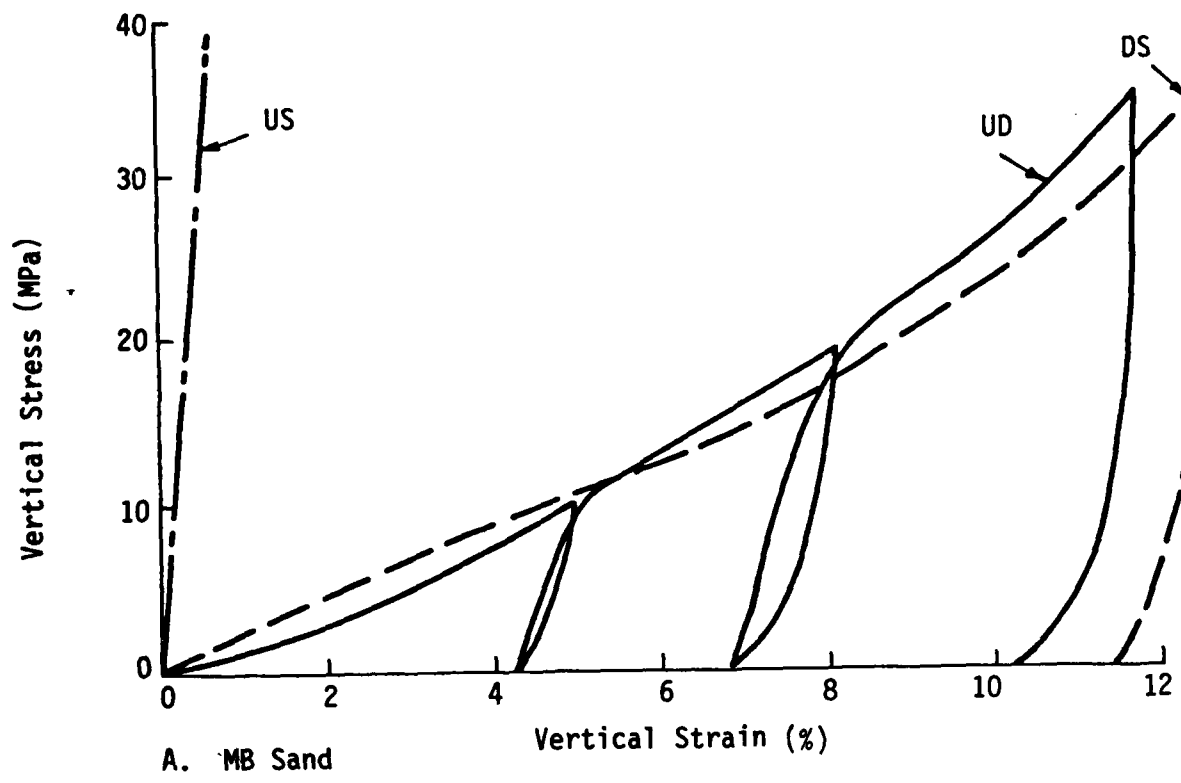


Figure 3. Comparison of Representative MB and RB UX Compressibility Relations

unloading. At lower stress levels (below 10 MPa) the DS response is apparently stiffer than the UD response. Above 10 MPa both the UD and DS samples show similar response. The US uniaxial strain response is linear and elastic, with a modulus predictable from mixture theory, using the bulk modulus of water, soil porosity, and an assumed Poisson's Ratio for the water-sand mixture. For MB sand, with $n = 0.36$ and with the bulk modulus of water, $K_w = 2070$ MPa, the constrained modulus of the water-sand mixture, M_s , may be computed as follows:

$$M_s = \frac{3(1 - \nu)}{(1 + \nu)} \frac{K_w}{n}$$

$$M_s = \frac{3(1 - .49)2070}{(1 + .49)} \frac{K_w}{0.36} = 5900 \text{ MPa}$$

This compares well with the observed representative value of 6000 MPa. Also worth noting is the UD and DS hysteretic unload-reload behavior. The observed trend is for these loops to become larger when unloading and reloading from higher stress levels. This effect is particularly important when considering cyclic loading, because of the energy dissipation it causes.

Figure 4 is a representative UX compressibility curve for RV alluvium (Ref. 11), based on drained tests on undisturbed samples at their natural water content. The compressibility of RV sand is very similar to that of MB sand.

UX stress paths from UX/ K_0 tests are shown for MB and RB sand in Figure 5. For both materials the US responses were very close, as were the DS responses. Based on elastic theory, the slope of the UX stress path, $s = \Delta(\sigma_1 - \sigma_3) / \Delta p$, is directly related to Poisson's Ratio, ν , by the relation:

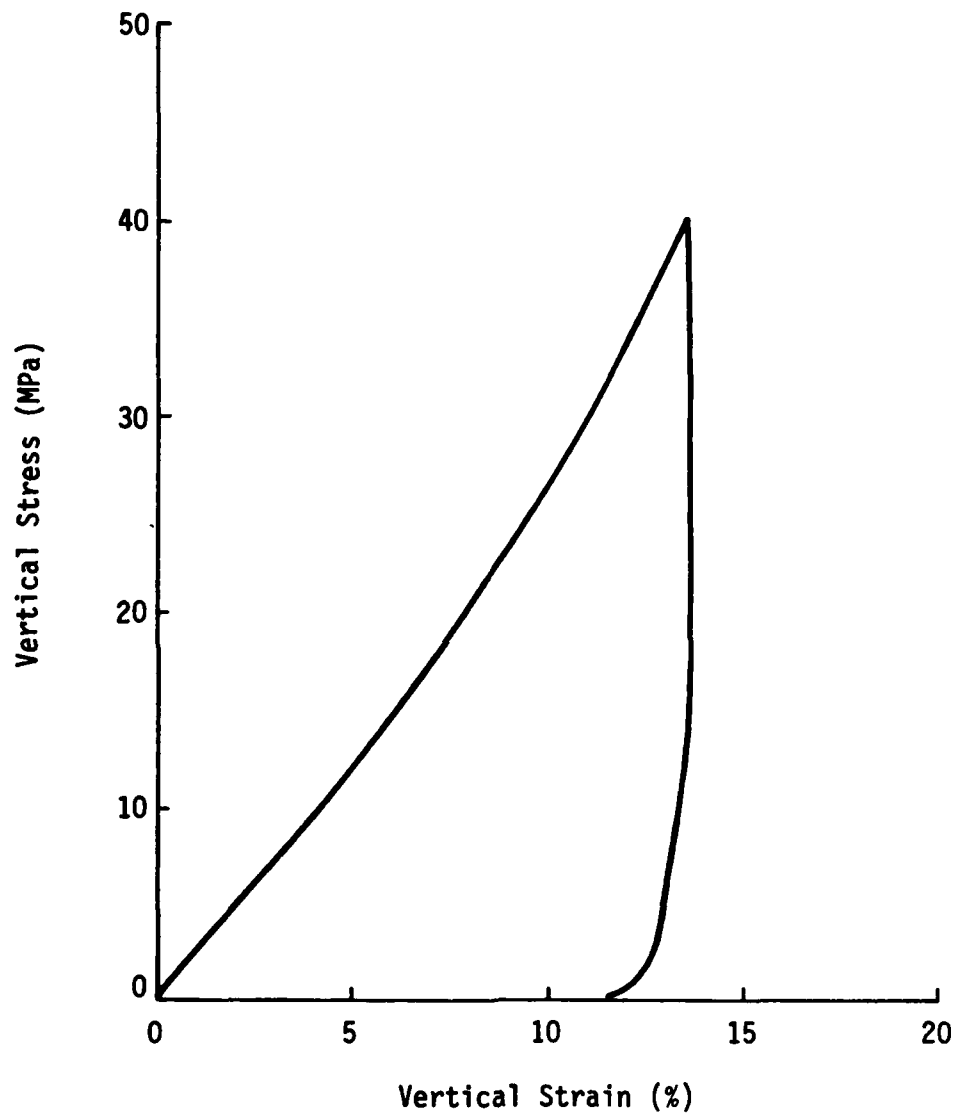


Figure 4. Representative UX Compressibility for RV Alluvium, 0-6 m Depth (Ref. 11)

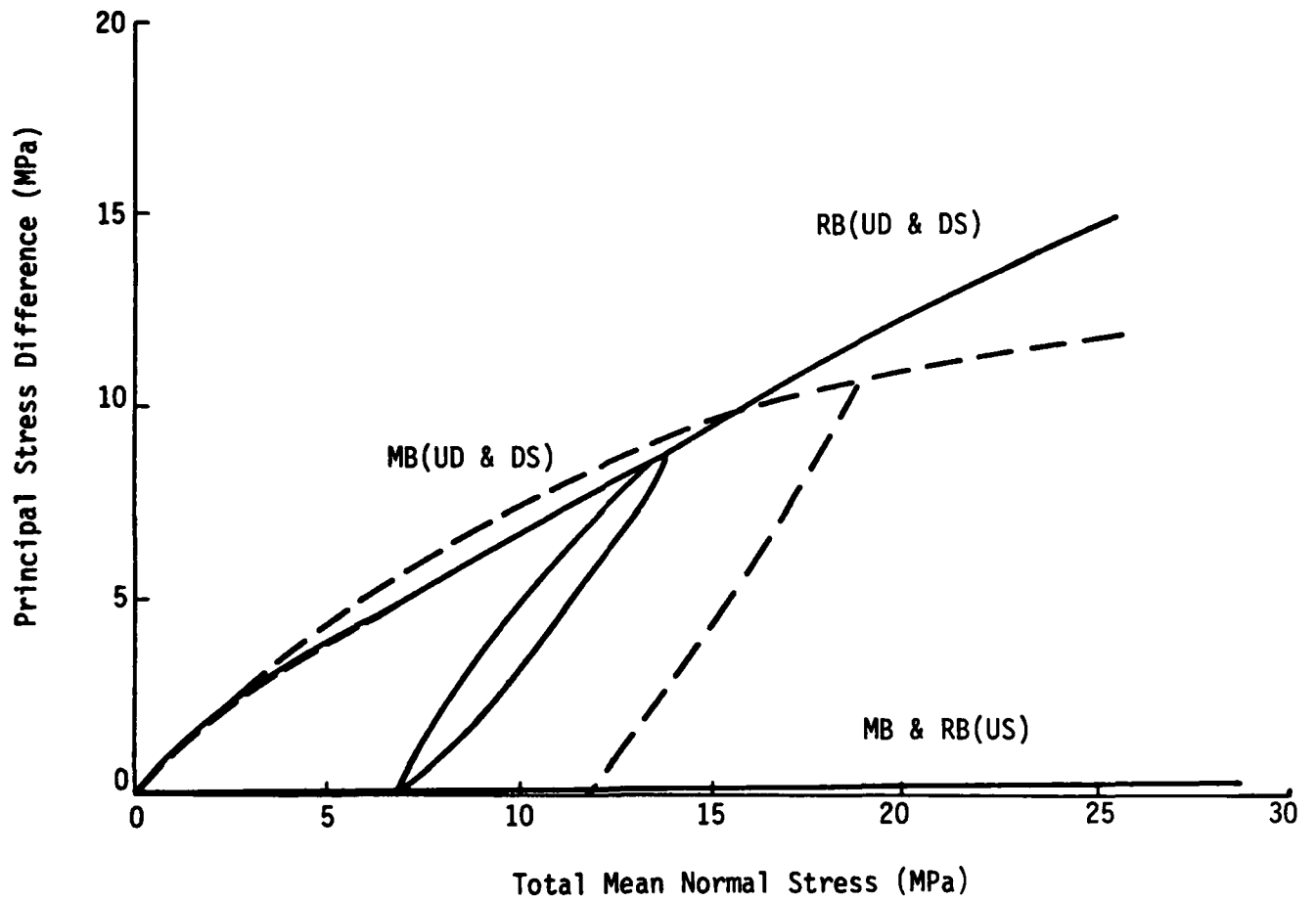
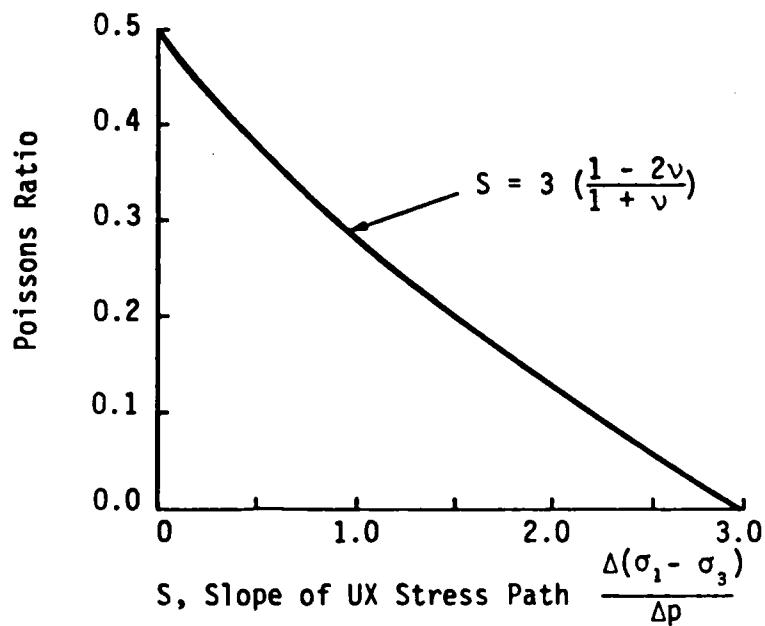


Figure 5. Representative UX Stress Paths for MB and RB Sands

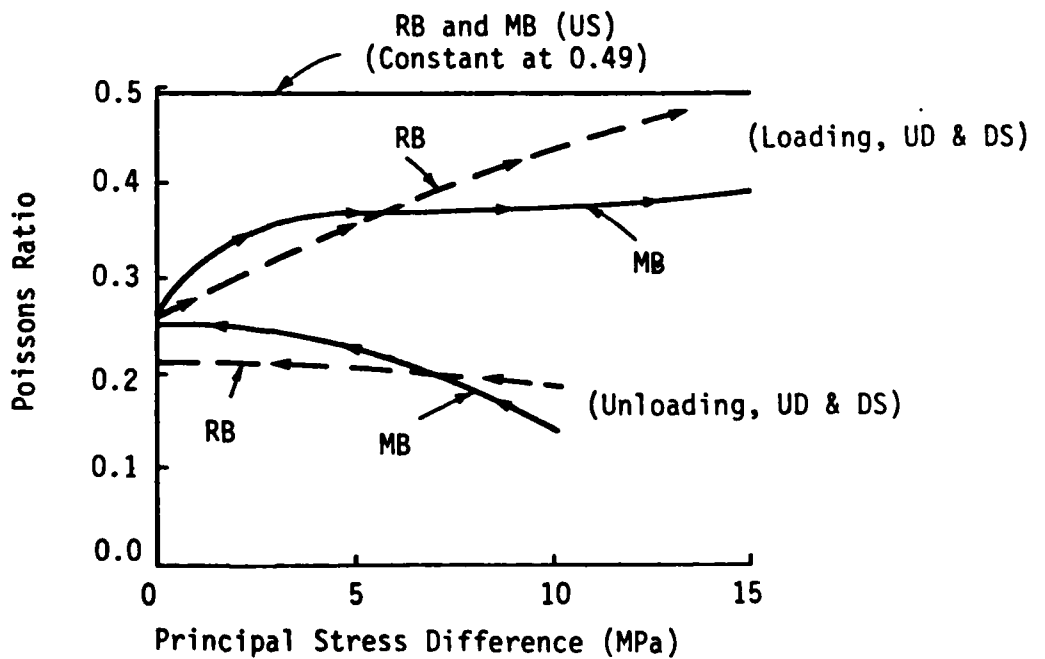
$$s = \frac{3(\Delta\sigma_1 - \Delta\sigma_3)}{\Delta\sigma_1 + 2\Delta\sigma_3} = \frac{3(1 - \frac{\nu}{1-\nu})}{1 + \frac{2\nu}{1-\nu}} = 3\left(\frac{1 - 2\nu}{1 + \nu}\right) \quad (3.1)$$

This equation is plotted in Figure 6A. Figure 6B shows the observed variation in Poisson's Ratio for MB and RB sands as calculated from the ratio of radial to axial strain increments. Poisson's Ratio increases from about 0.25 to 0.45 on loading, displays a sharp discontinuity at the start of unloading, and then increases again from 0.15 to 0.25. For the US case, the water-sand mixture is very nearly incompressible, and loads and unloads at $\nu = 0.49$.

The standard triaxial shear response of MB and RB sands was evaluated for three constant confining pressures: 0.14, 1.72, and 3.45 MPa. A few additional tests were done on RB sand at a constant confining pressure of 6.90 MPa. As in the uniaxial tests, the sand was tested under three conditions: undrained-dry (UD), drained-saturated (DS), and undrained-saturated (US). The representative UD and DS triaxial responses for MB sand were very similar, and in Figure 7 the two curves are overlaid. The US responses are also shown in Figure 7. When the DS and US results are compared, it is evident that effective stress controls behavior in the undrained state. The slope of the US effective stress path indicates whether the sample is attempting to dilate (and therefore generate negative excess pore pressure) or compress (and therefore generate positive excess pore pressure). A positive slope less than 3 on 1 indicates a tendency to dilate; a positive slope greater than 3 on 1 or a negative slope indicates a tendency to compress. This is because when σ_3 is constant, as it was in the above tests, then:

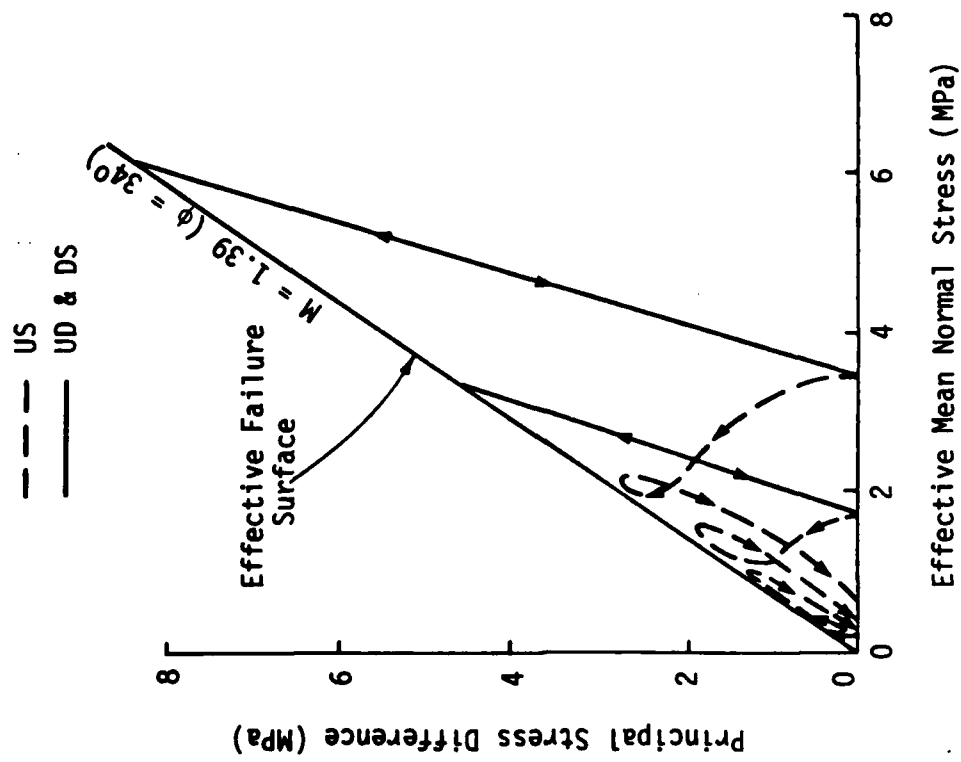


A. Elastic Relationship Between ν and Slope of UX Stress Path

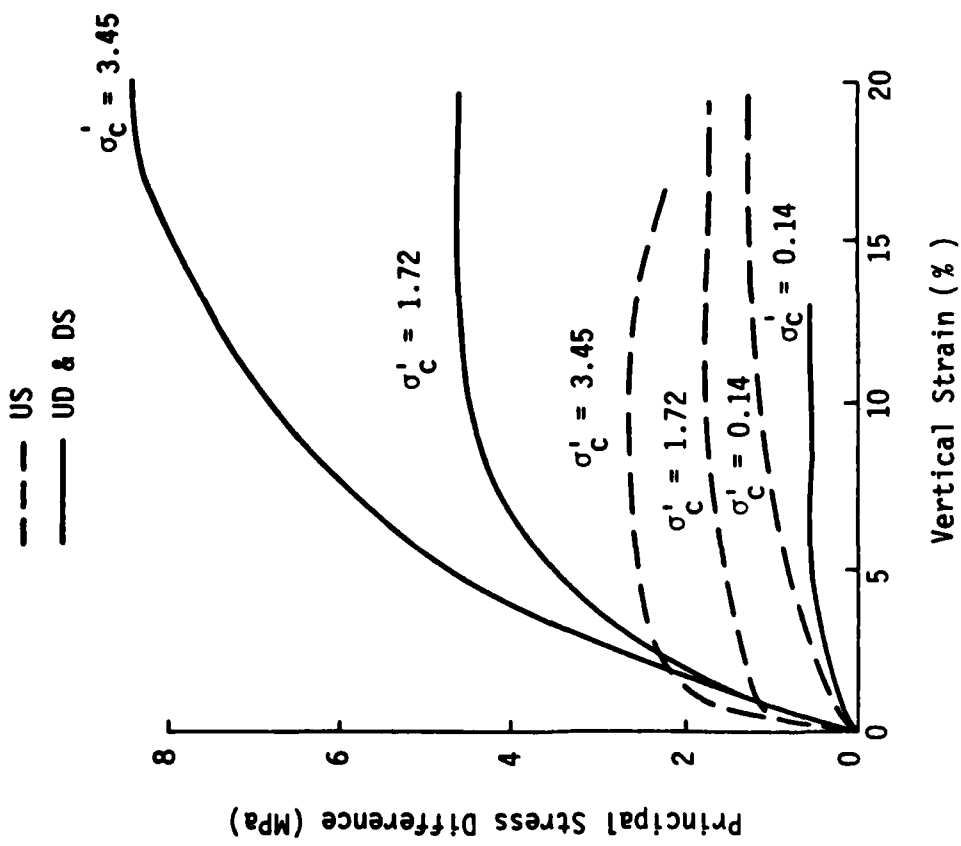


B. Observed Variation in Poisson's Ratio

Figure 6. Variation of Poisson's Ratio During UX Tests on MB and RB Sands



A. Stress-Strain Response



B. Stress Path Response

Figure 7. Representative TX Stress-Strain and Effective Stress Path Relations for MB Sand

$$\frac{\frac{\Delta\sigma_1 - \Delta\sigma_3}{3} - \Delta u}{\Delta\sigma_1 - 3\Delta u} = \frac{3\Delta\sigma_1}{\Delta\sigma_1 - 3\Delta u} = \frac{3}{1 - 3\frac{\Delta u}{\Delta\sigma_1}}$$

Clearly the coupling between shear strain and volumetric strain is a fundamental soil stress-strain mechanism which must be constitutively modeled.

In order to explore the symmetry of the failure surface about the p-axis in the triaxial plane, three triaxial extension (TXE) tests were done on MB sand. They showed a slope of -0.88 for the extension failure surface, compared with a slope of +1.39 in triaxial compression. This observed asymmetry is consistent with test results on other sands. The calculated friction angles for triaxial compression and extension are:

$$\phi_C = 2(\text{arc tan } \sqrt{\frac{3 + 2M_C}{3 - M_C}} - 45^\circ) = 34.4^\circ$$

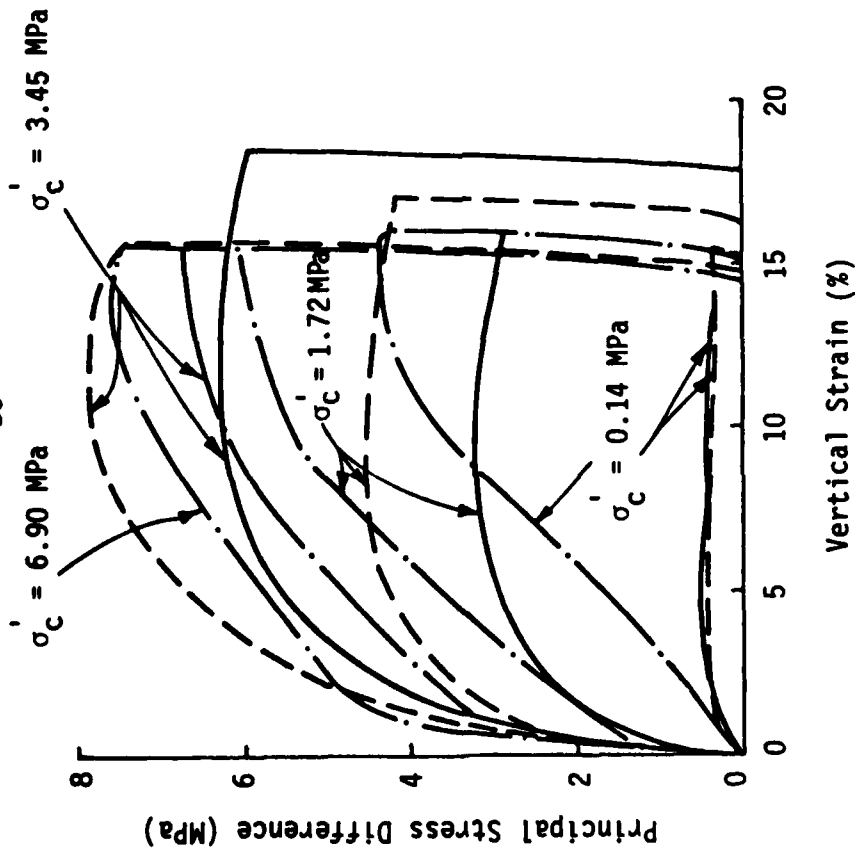
$$\phi_E = 2(\text{arc tan } \sqrt{\frac{3 - M_E}{3 + 2M_E}} - 45^\circ) = 31.0^\circ$$

Triaxial behavior for RB sand is shown in Figure 8. For this material the US and DS responses indicate slightly different apparent effective stress failure surfaces, as seen in Figure 8B. The dry specimens fail along a linear failure surface which displays a small amount of cohesion (0.6 MPa intercept in Figure 8B, b'), and a slope of $M = 1.09$. The calculated friction angle and cohesion for the UD tests on RB sand are:

$$\phi_C = 2(\text{arc tan } \sqrt{\frac{3 + 2M_C}{3 - M_C}} - 45^\circ) = 27.5^\circ$$

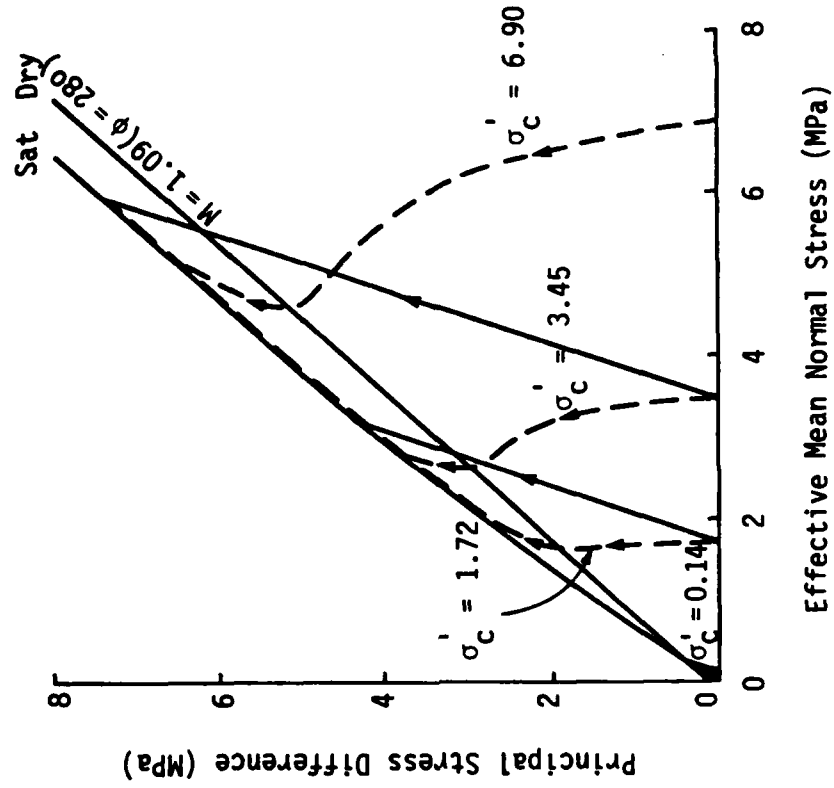
σ'_c - Confining Pressure

UD
US
DS



A. Stress-Strain Response

UD & DS
US



B. Stress Path Response

Figure 8. Representative TX Stress-Strain and Effective Stress Path Relations for RB Sand

$$c' = \frac{3b'}{2\sqrt{(3 + 2M_c)(3 - M_c)}} = 0.29 \text{ MPa}$$

However, the saturated effective stress failure envelope is slightly curved and lies above the UD envelope. The undrained TXC behavior of RB sand is similar to that of MB sand, but the undrained stress paths travel much further up the effective stress failure envelope, indicating a greater dilatant tendency (Figure 8B). This can also be seen in Figure 9. The relatively large drop in excess pore pressure associated with yielding in RB sand causes an increased shear stress capacity. The pore pressure increases upon unloading, which means the effective stress is dropping faster than total stress because the sample is trying to compress.

Figure 10 shows the triaxial shear stress-strain response for dry RV alluvium at several confining pressures, all considerably higher than those used in the RB and MB laboratory tests. For practical purposes these curves can be considered to be drained, in the sense that there was no excess pore pressure. The qualitative TX response of RV alluvium is typical of many dry sands, including MB and RB sands.

The observed behavior of MB, RB and RV sands under laboratory conditions can be summarized as follows:

- a) loading compressibility is nonlinear;
- b) a relatively small amount of strain is recovered upon unloading, resulting in substantial net compaction;
- c) assumed elastic relationships are not linear, and display large discontinuities at the transition from loading to unloading;
- d) shear stress-strain response is gradually softening in nature,

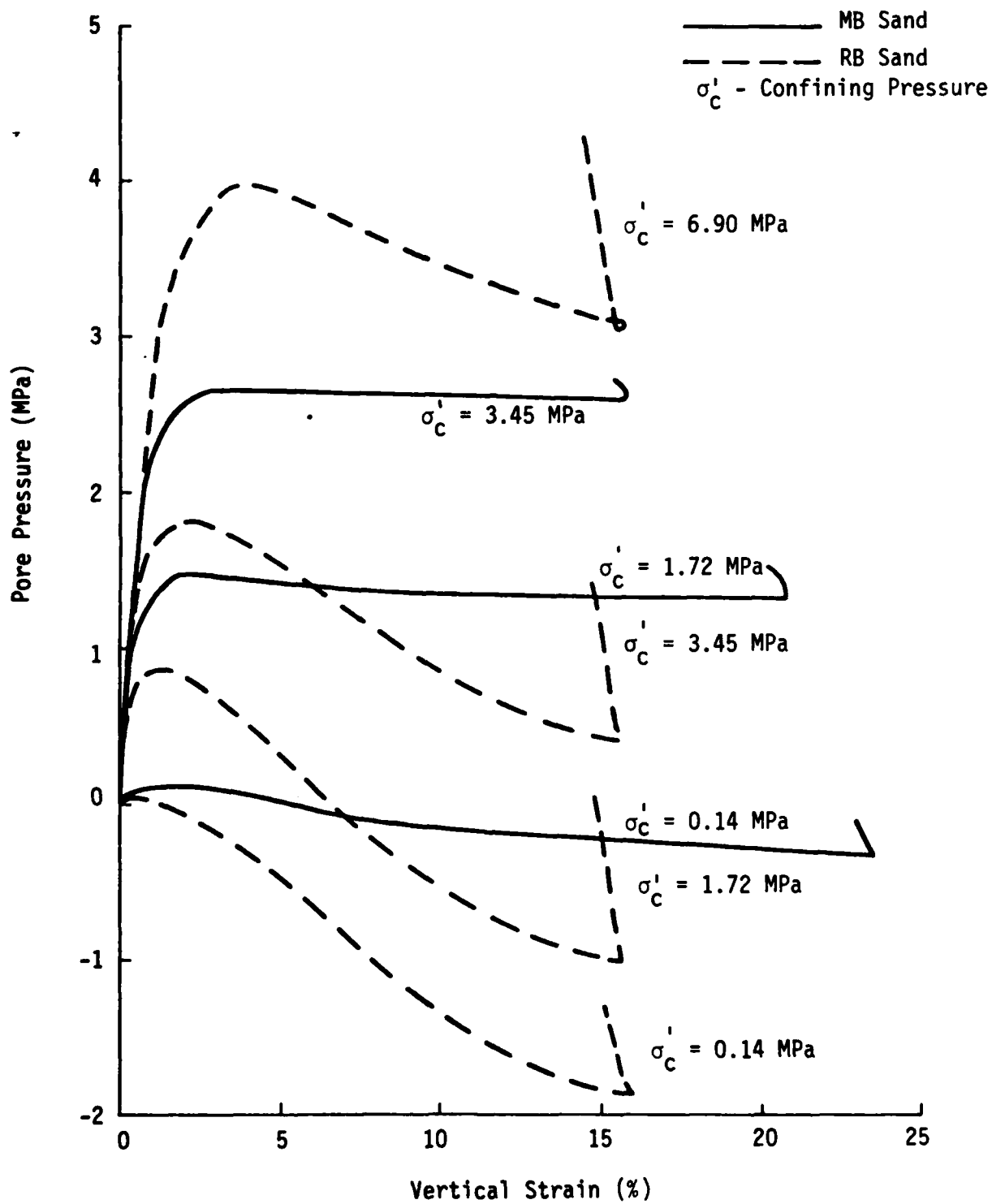


Figure 9. Representative Pore Pressure Response for Undrained-Saturated TX Tests on MB and RB Sand

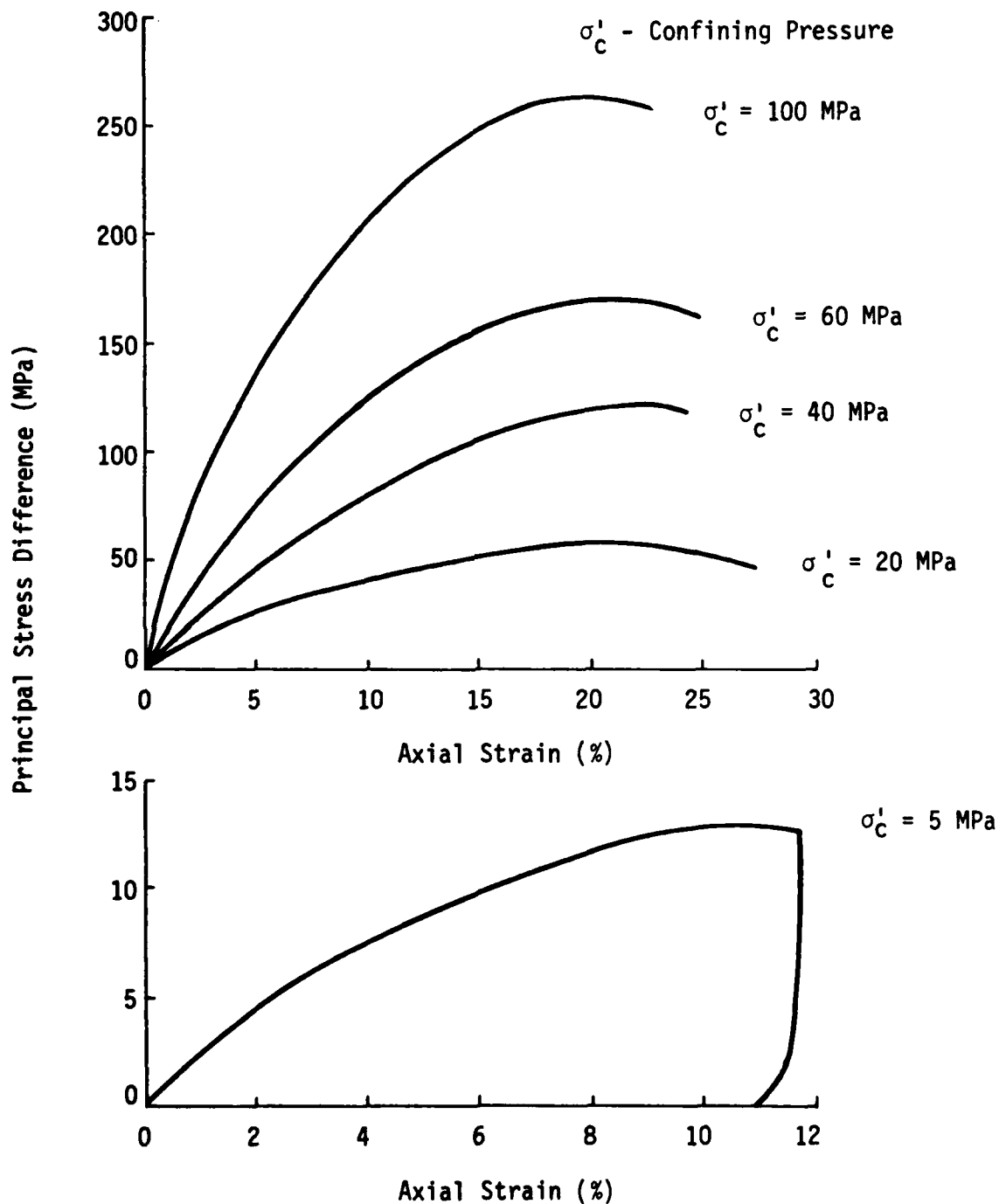


Figure 10. Typical Stress-Strain Response for Dry RV Alluvium (Ref. 11)

and large strains (>15 percent) may be reached before actual shear failure occurs;

- e) effective stress controls shearing behavior;
- f) the failure surface is not symmetric about the p-axis in the triaxial plane ($\sigma'_2 = \sigma'_3$), but the calculated friction angles in compression and extension are approximately equal.

4.0 MODELING THE LABORATORY BEHAVIOR OF SAND

4.1 Constitutive Relationships

Modeling the laboratory stress-strain response of any material is essentially curve-fitting. Curves generated in the laboratory are used to define the parameters for a model of interest. The model is then used to predict stress-strain response for conditions not created in the laboratory. One key to developing a model which can accurately predict stress-strain behavior over a wide range of load situations is using all pertinent information from the available test results. More important than the number of model parameters (although it is desirable to minimize that number) is the degree to which all significant stress-strain behavior mechanisms have been accounted for.

The primary behaviors studied in the WES testing program were: uniaxial compressibility (loading shape and compaction), shear response during uniaxial loading and unloading (UX stress path), and triaxial shear stress-strain behavior including shear failure. Four constitutive models were chosen to describe these behaviors and to illustrate varying degrees of thoroughness in utilizing laboratory data: an elastic-perfectly plastic model (ELPLA), the AFWL Engineering model (AFWL), the Weidlinger effective stress cap model (CAP), and a hyperbolic curve-fit (HYPER). These models are described in Appendix B.

4.2 Model Data Comparisons

Parameters were selected for each model based on the above representative data for MB, RB, and RV sands. The model parameters were adjusted until they yielded results which came within measured data

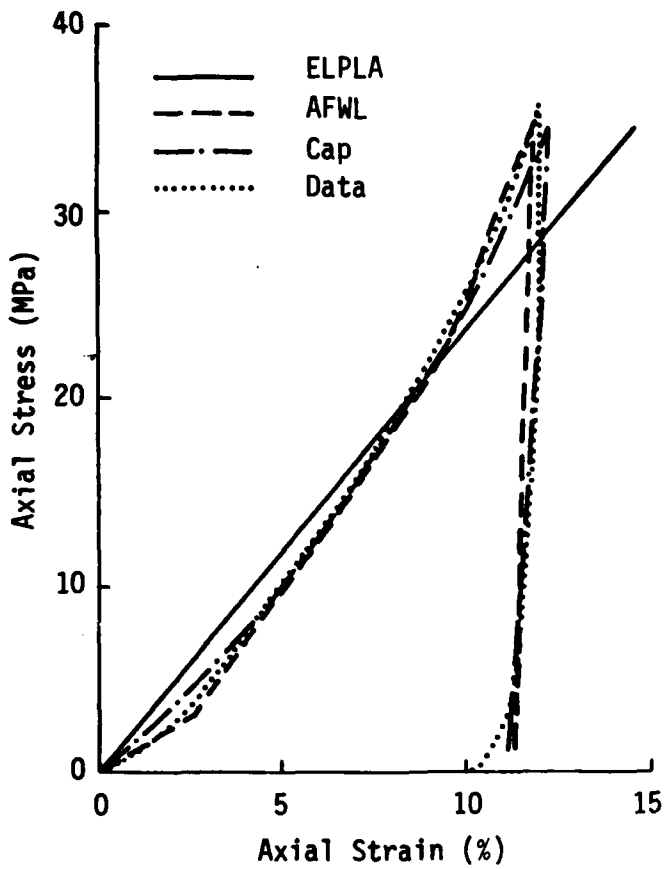
scatter, at least for those responses which the models can predict. In some cases, a model was developed for each material test condition: undrained dry (UD), drained saturated (DS), and undrained saturated (US). The undrained saturated response of all three sands is essentially linearly elastic in uniaxial (confined) compression, with a von Mises failure surface in shear, and only the effective stress cap model was formulated for US response. Pore pressure generation during triaxial shear was then predicted with this model. Specific values for the model parameters are given in Appendix B.

Figures 11 through 16 show comparisons between calculated and measured responses for MB sand and RB sand. RV alluvium results are shown in Figure 17. The curves labeled "Calculation vs. Data" represent the integrated differences between the calculated model response and the measured soil behavior, normalized to the total area under the representative data curve. This area difference is then divided by one hundred to yield a percent. The residual has been calculated for loading only. A calculation which had a constant area difference of zero would lie exactly along the data curve. The rate at which the residual deviates from zero indicates the quality of the model response.

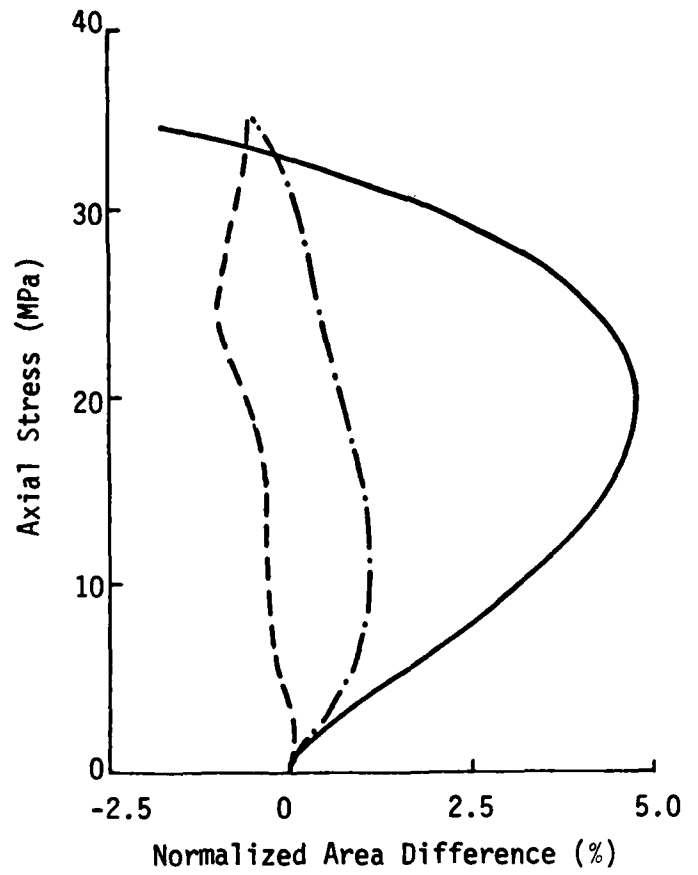
Figure 18 shows how the hyperbolic curve-fitting technique may be used to model triaxial stress-strain response at varying confining pressures. An example of results using the effective stress cap model to simulated undrained behavior is shown in Figure 19.

4.3 Discussion of Comparisons

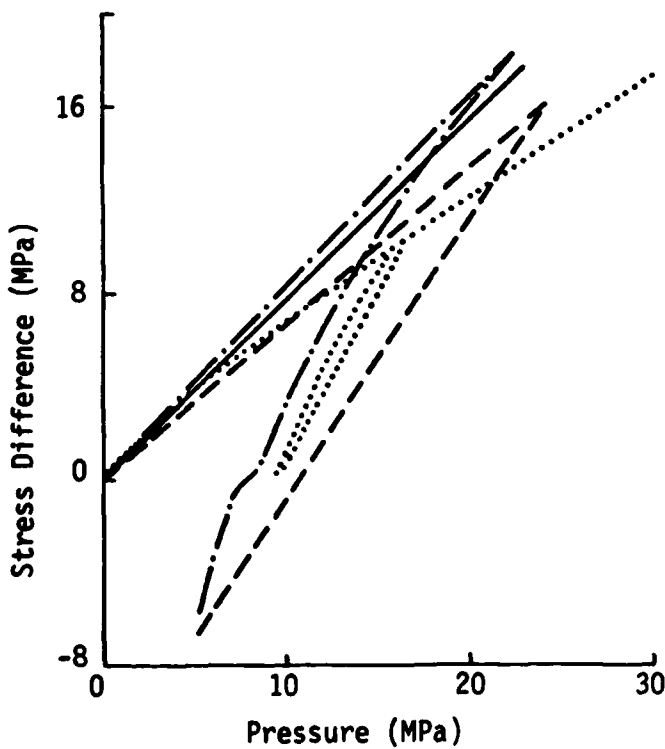
The elastic-plastic model does fairly well in defining two primary material behaviors: loading compressibility and limited shearing



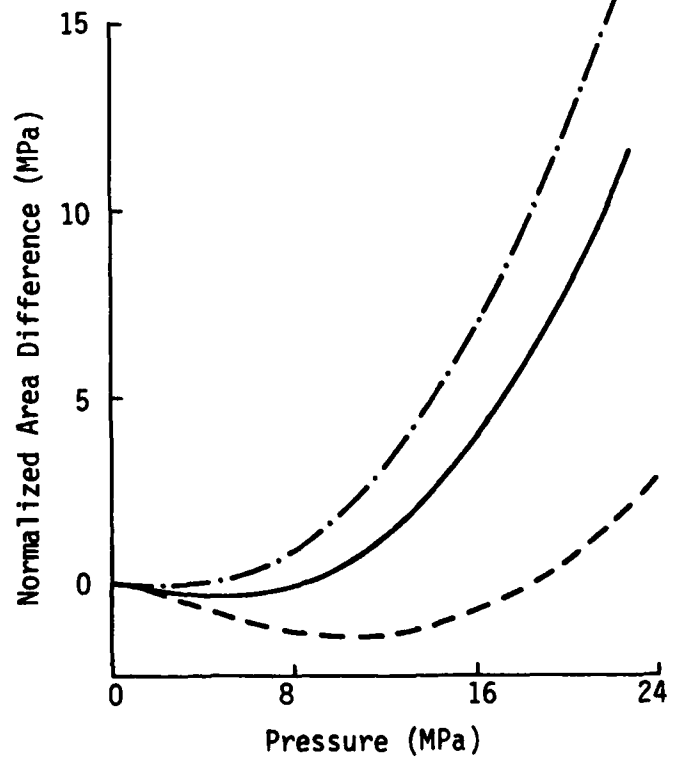
A. Uniax



B. Calculations vs. Data

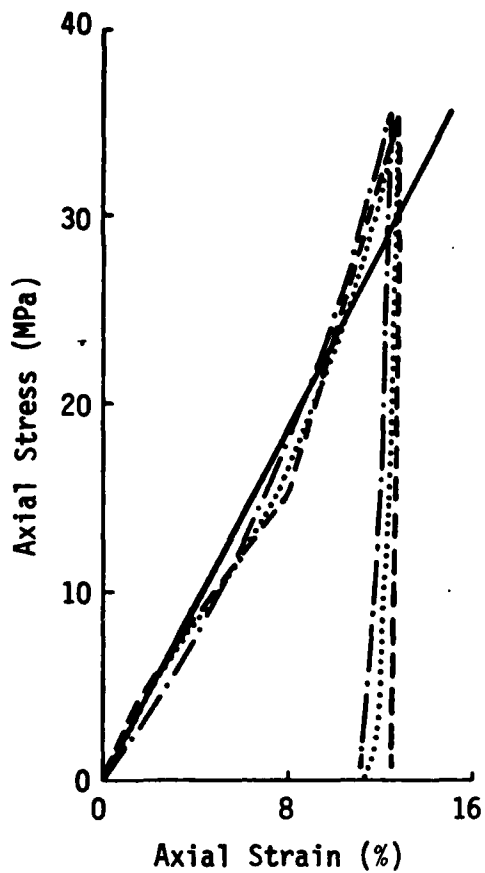


C. Stress Path

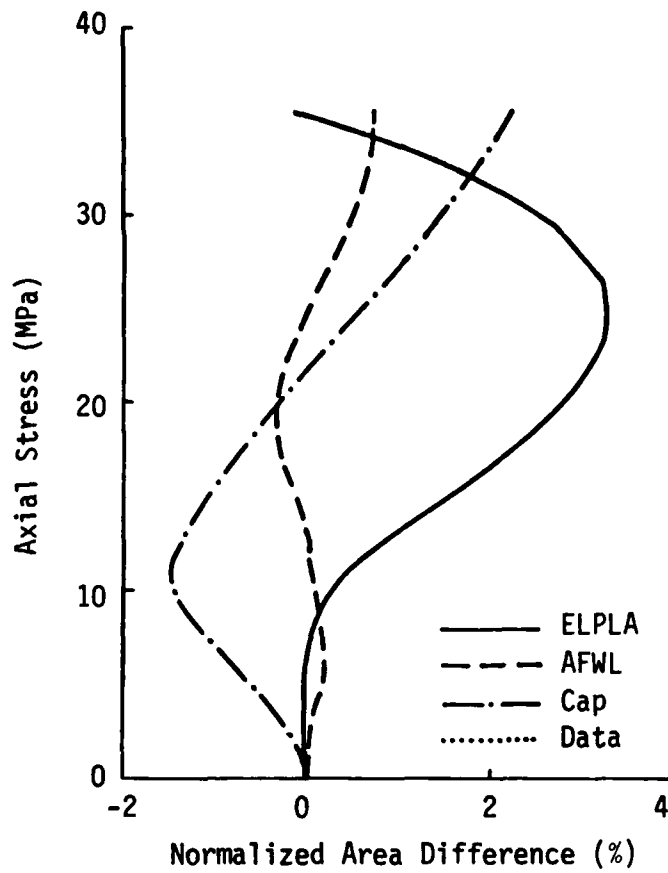


D. Calculation vs. Data

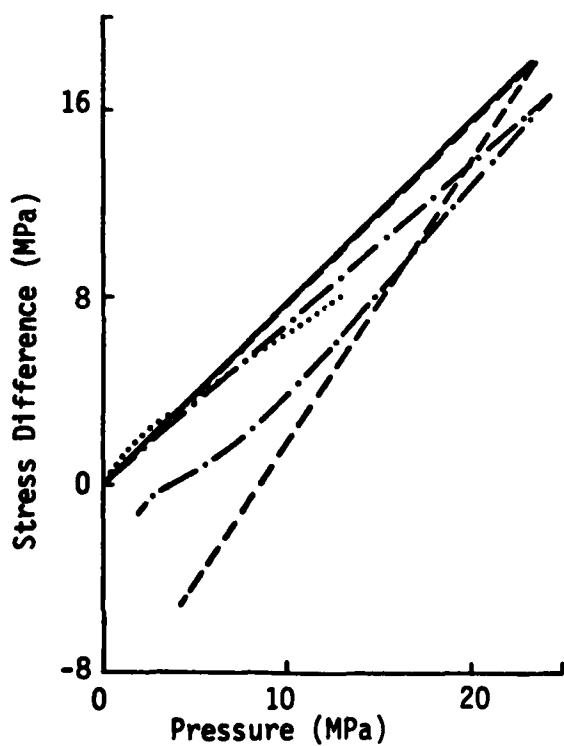
Figure 11. Dry MB Sand UX Model-Data Comparisons



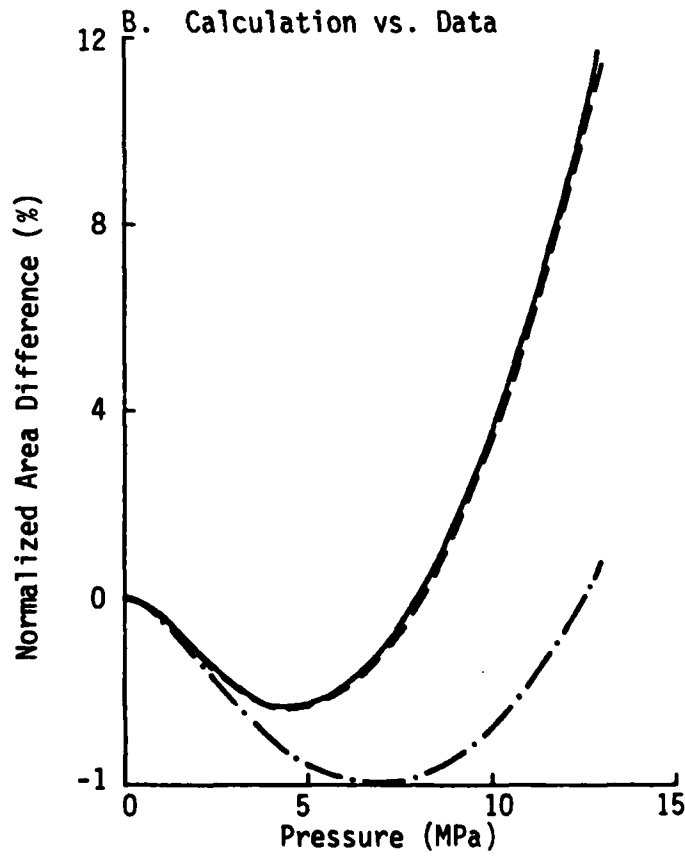
A. Uniax



B. Calculation vs. Data

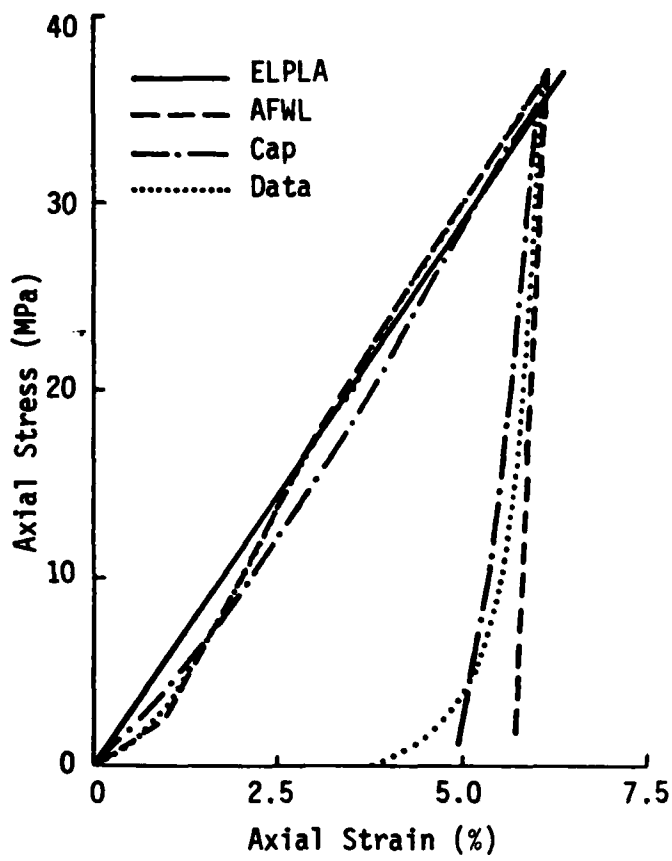


C. Stress Path

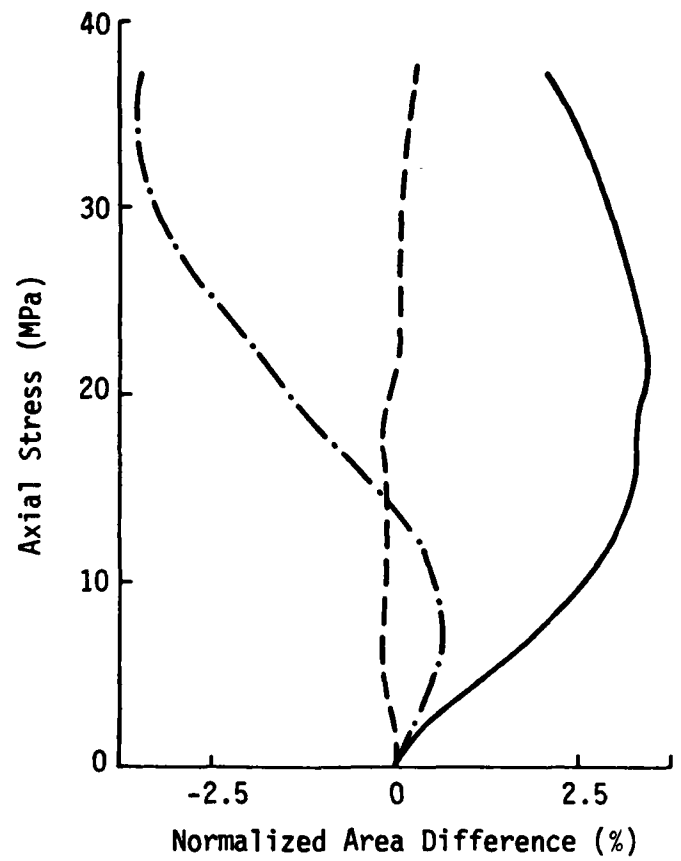


D. Calculation vs. Data

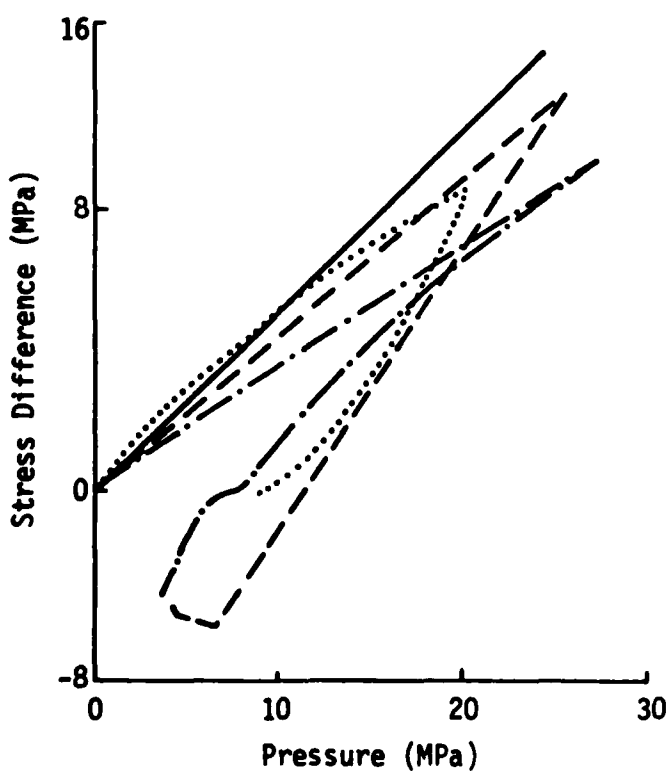
Figure 12. Drained Saturated MB Sand UX Model-Data Comparisons



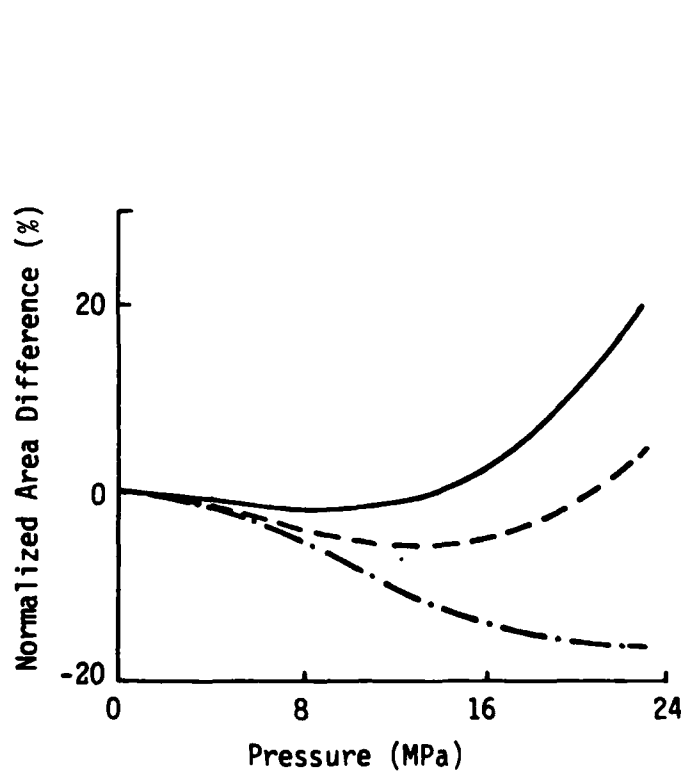
A. Uniax



B. Calculation vs. Data

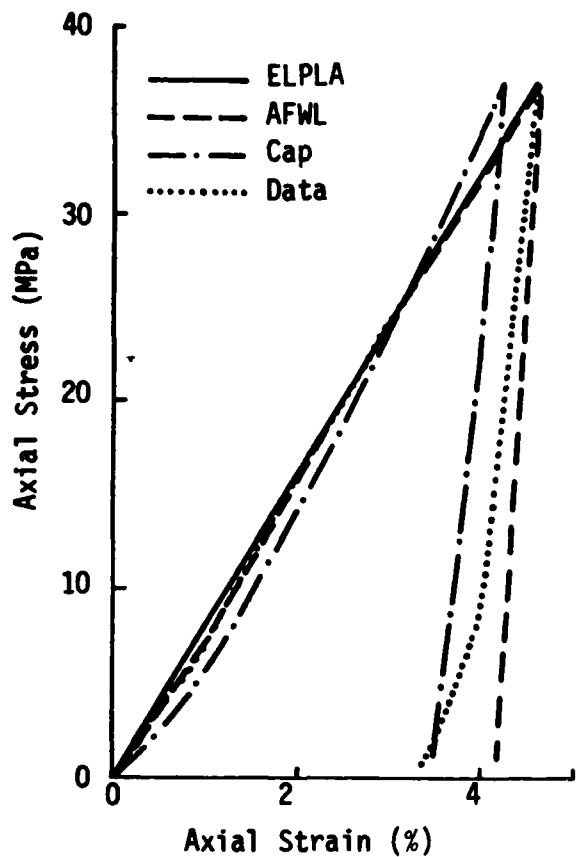


C. Stress Path

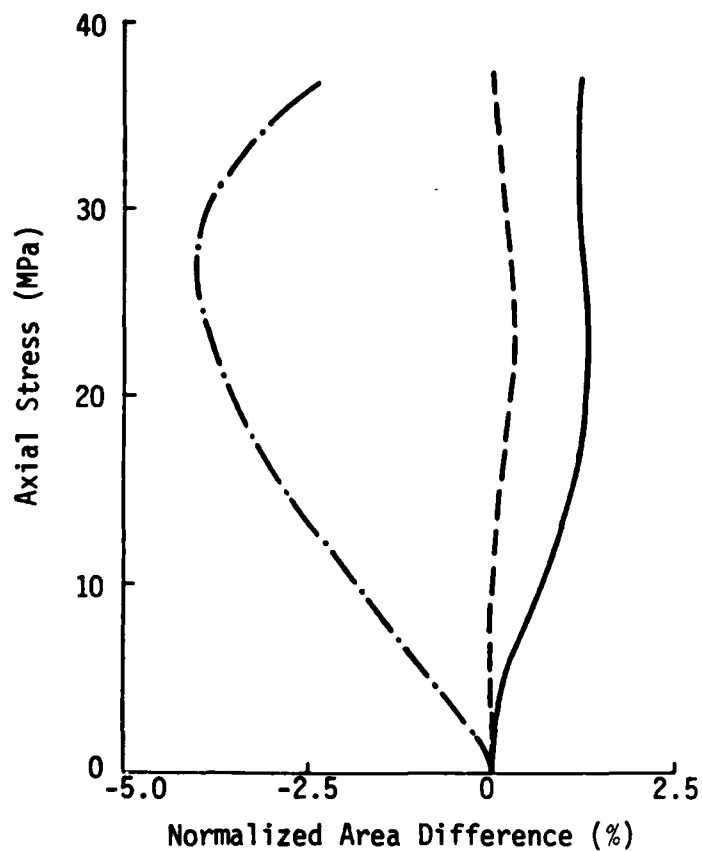


D. Calculation vs. Data

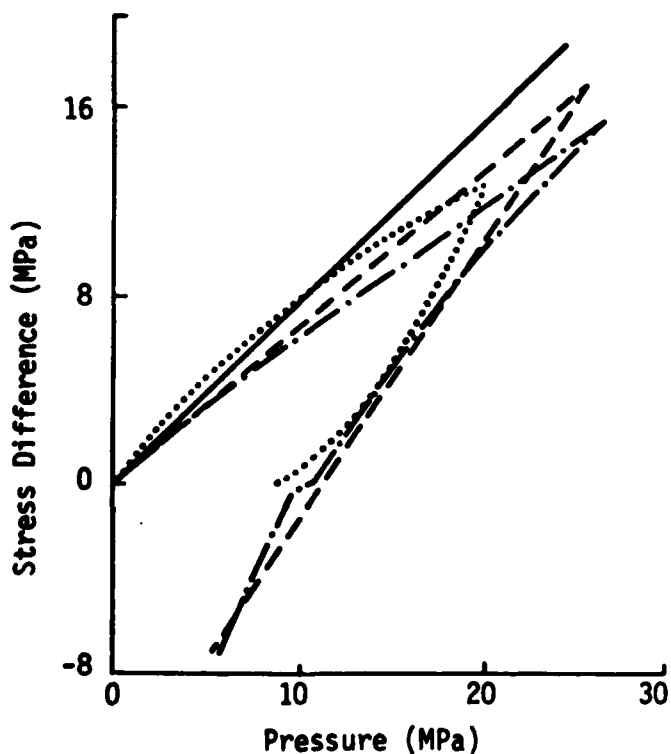
Figure 13. Dry RB Sand UX Model-Data Comparisons



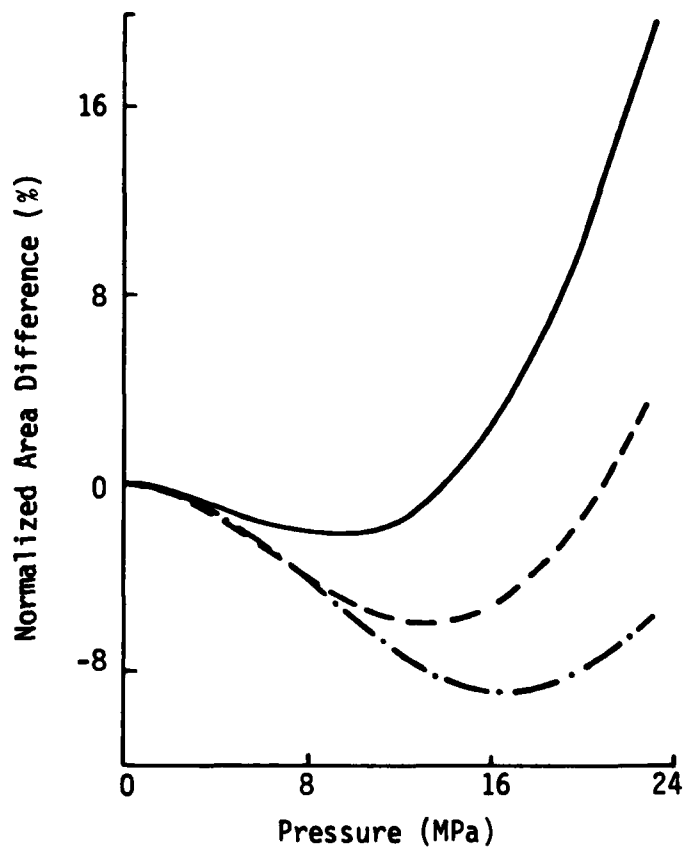
A. Uniax



B. Calculation vs. Data

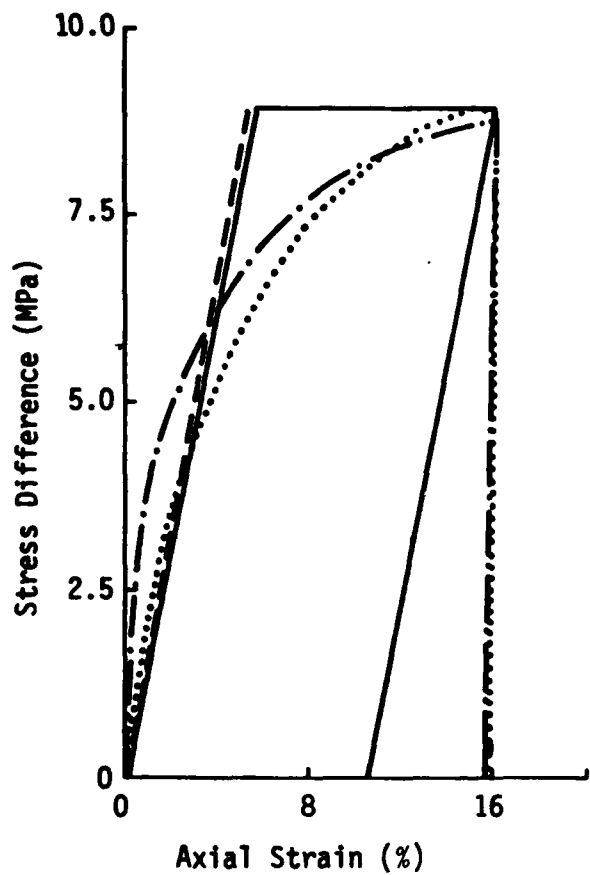


C. Stress Path

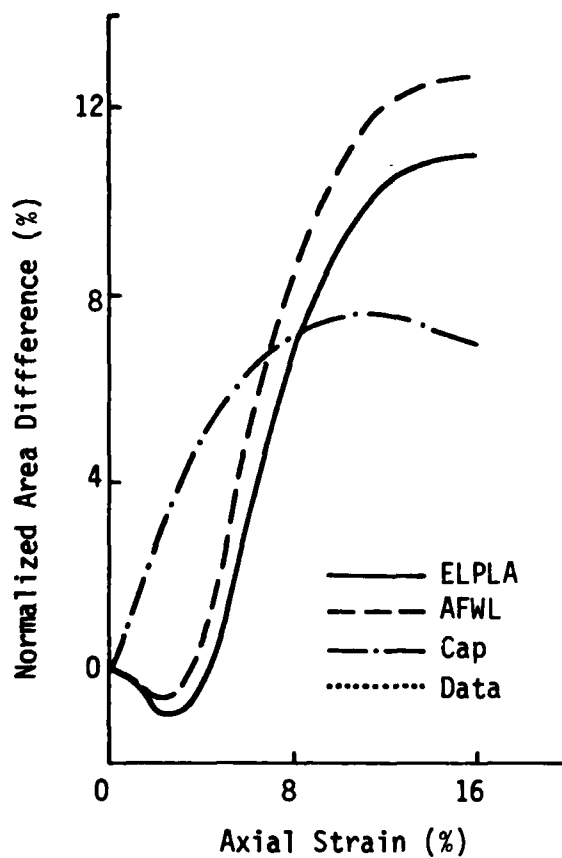


D. Calculation vs. Data

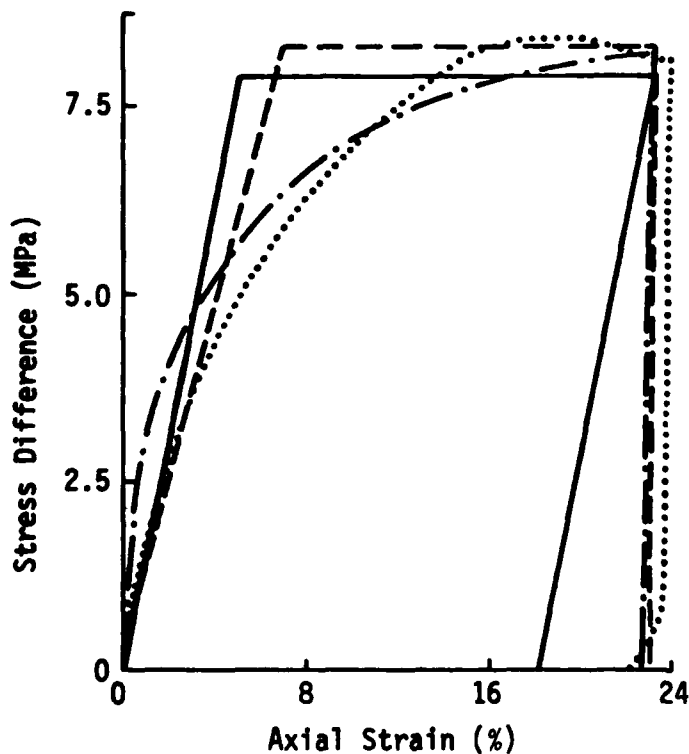
Figure 14. Drained Saturated RB Sand UX Model-Data Comparisons



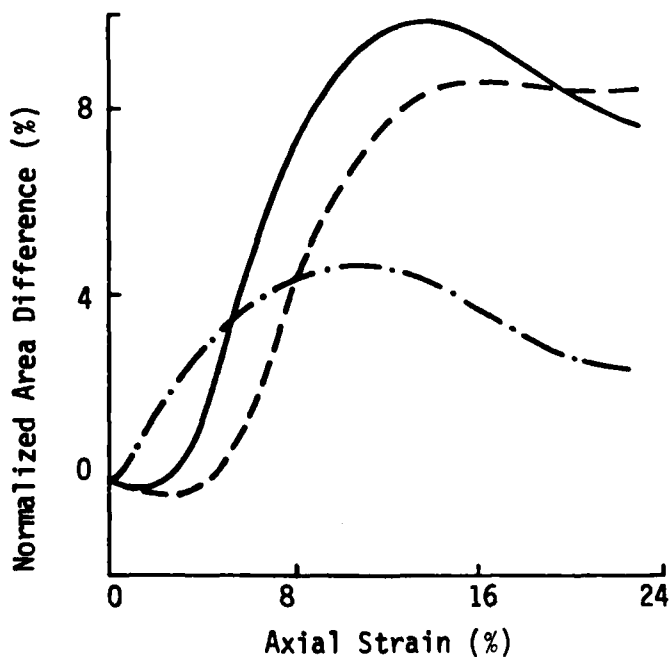
A. Dry MB Sand TX Stress-Strain



B. Calculation vs. Data

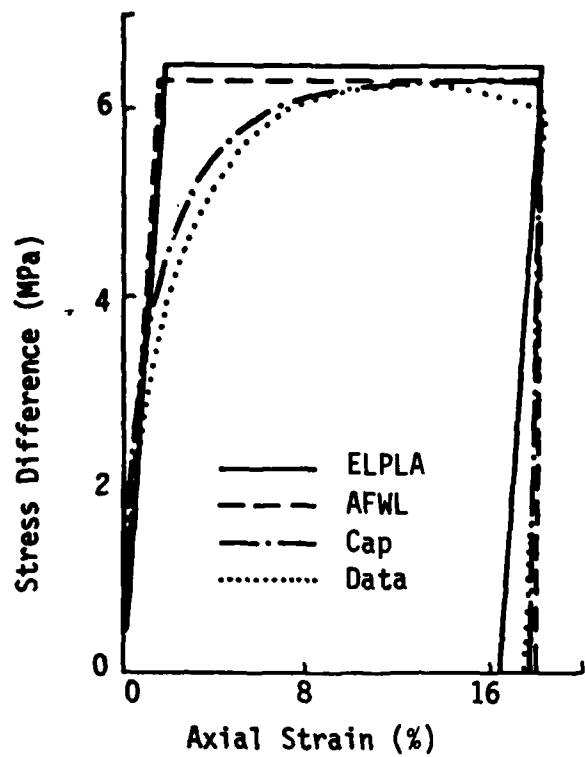


C. DS MB Sand TX Stress-Strain

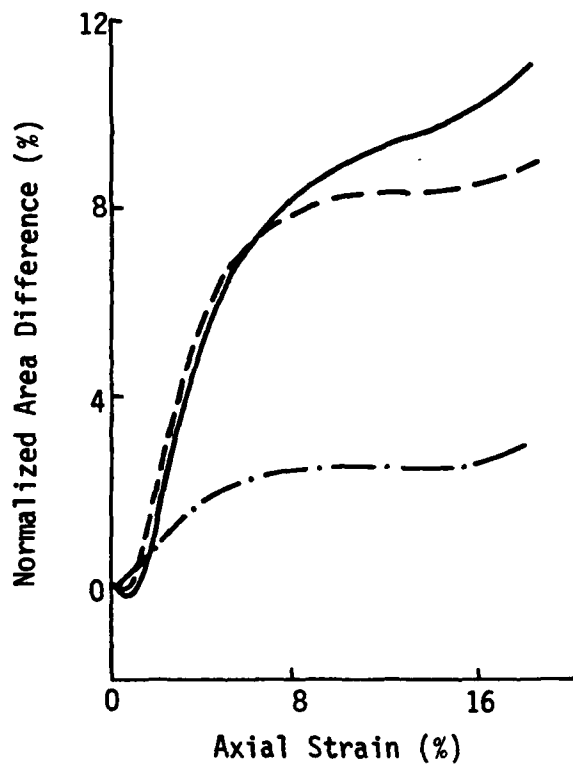


D. Calculation vs. Data

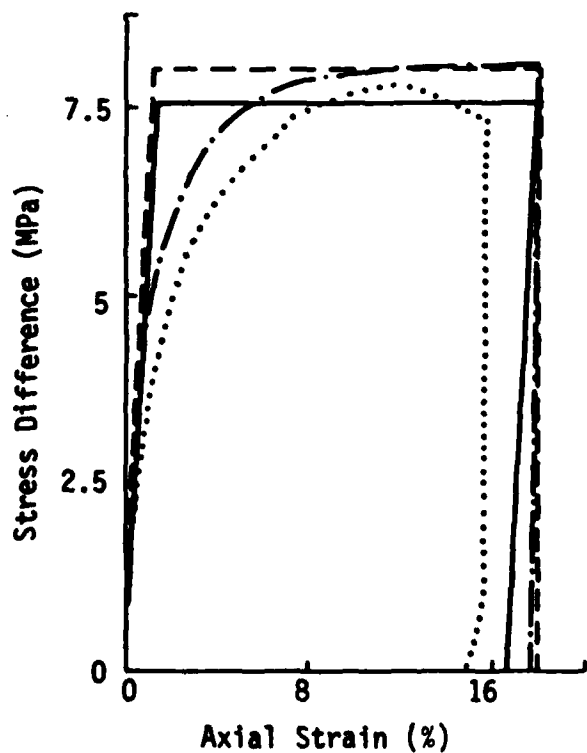
Figure 15. MB Sand TX Model-Data Comparisons (confining pressure = 3.45 MPa)



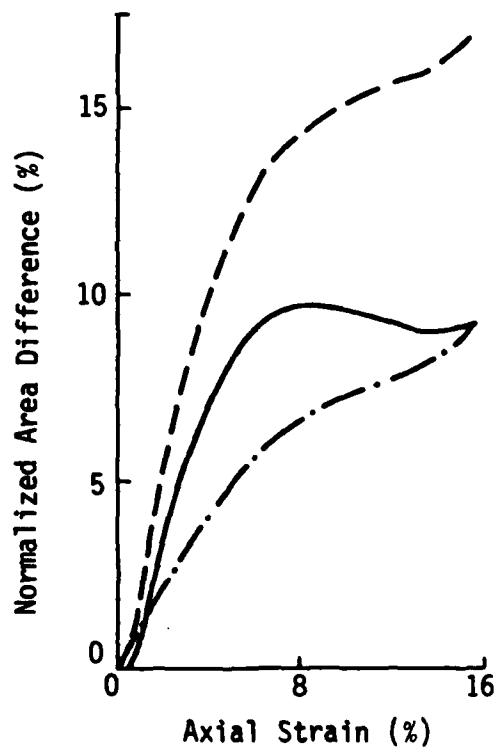
A. Dry RB Sand TX Stress-Strain



B. Calculation vs. Data

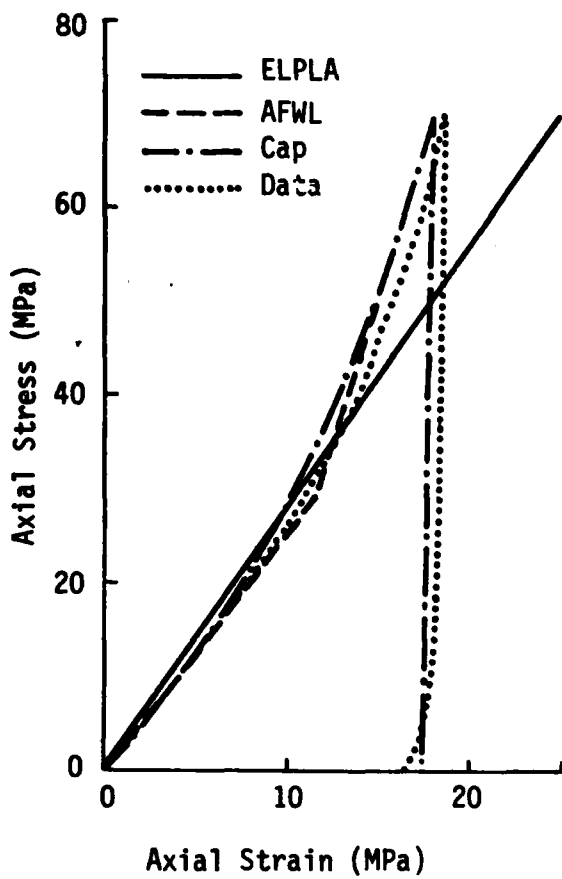


C. DS RB Sand TX Stress-Strain

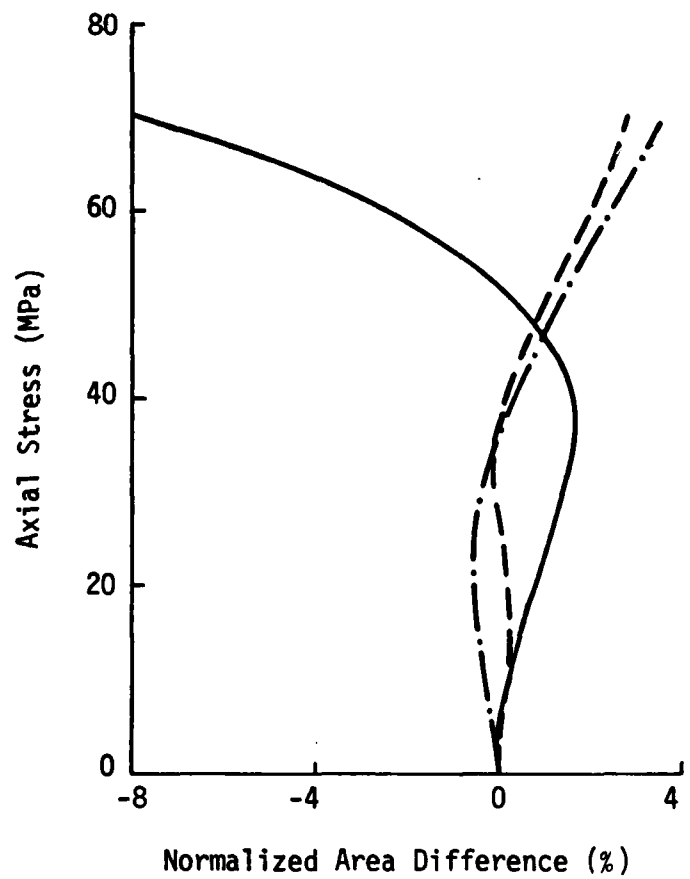


D. Calculation vs. Data

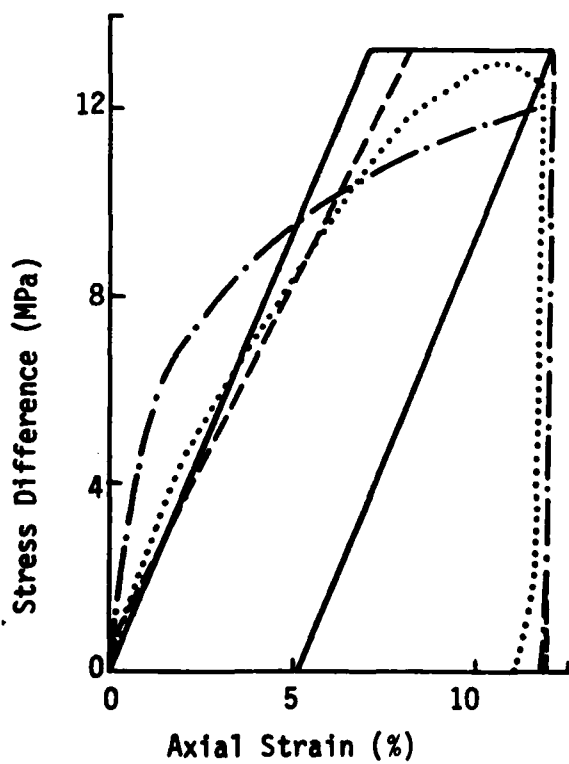
Figure 16 RB Sand TX Model-Data Comparisons (confining pressure = 3.45 MPa)



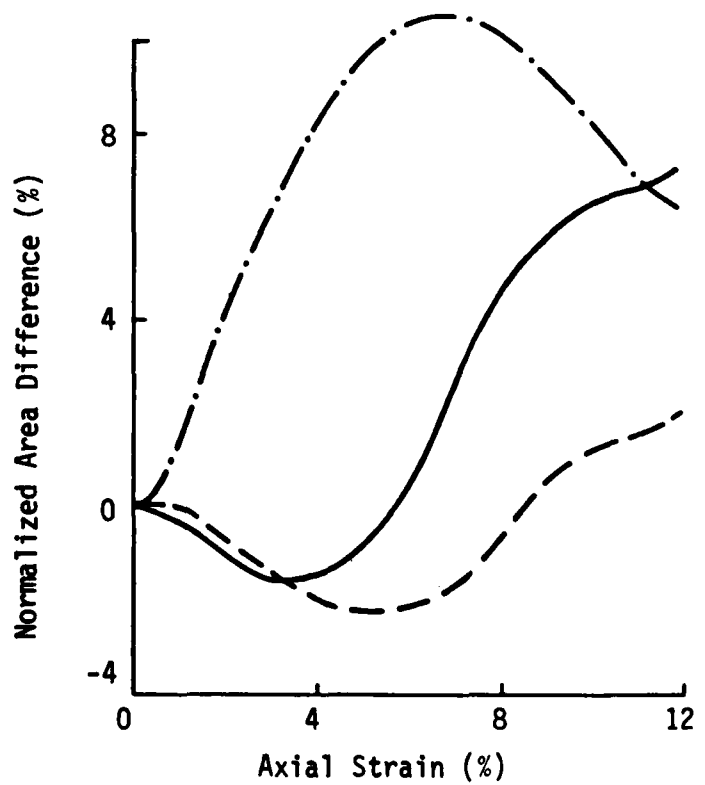
A. Uniax



B. Calculation vs. Data

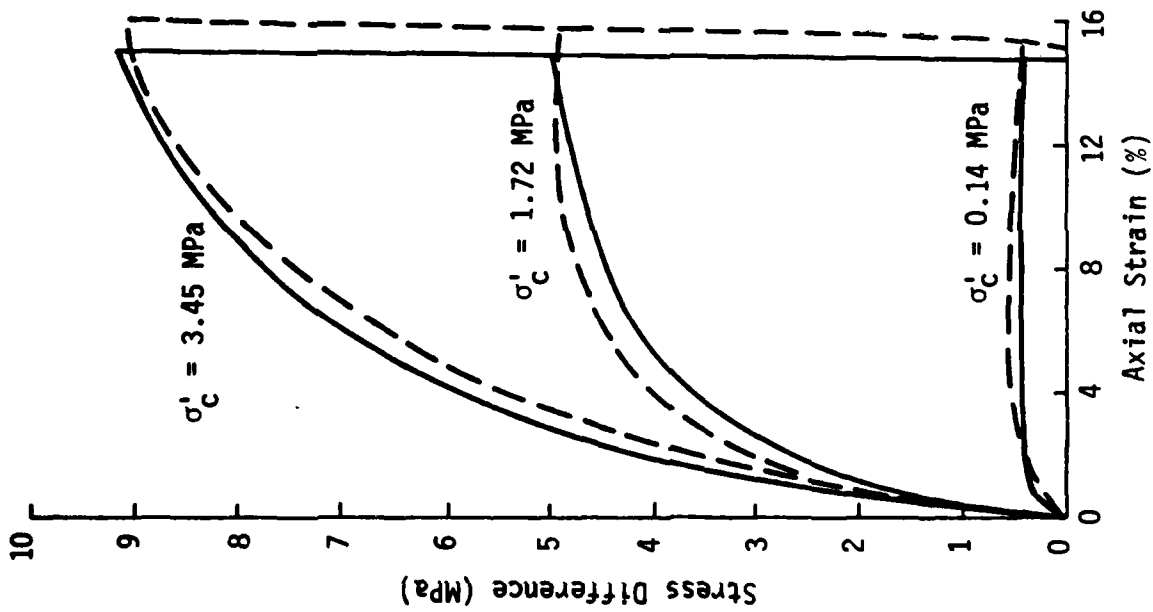


C. TX Stress-Strain

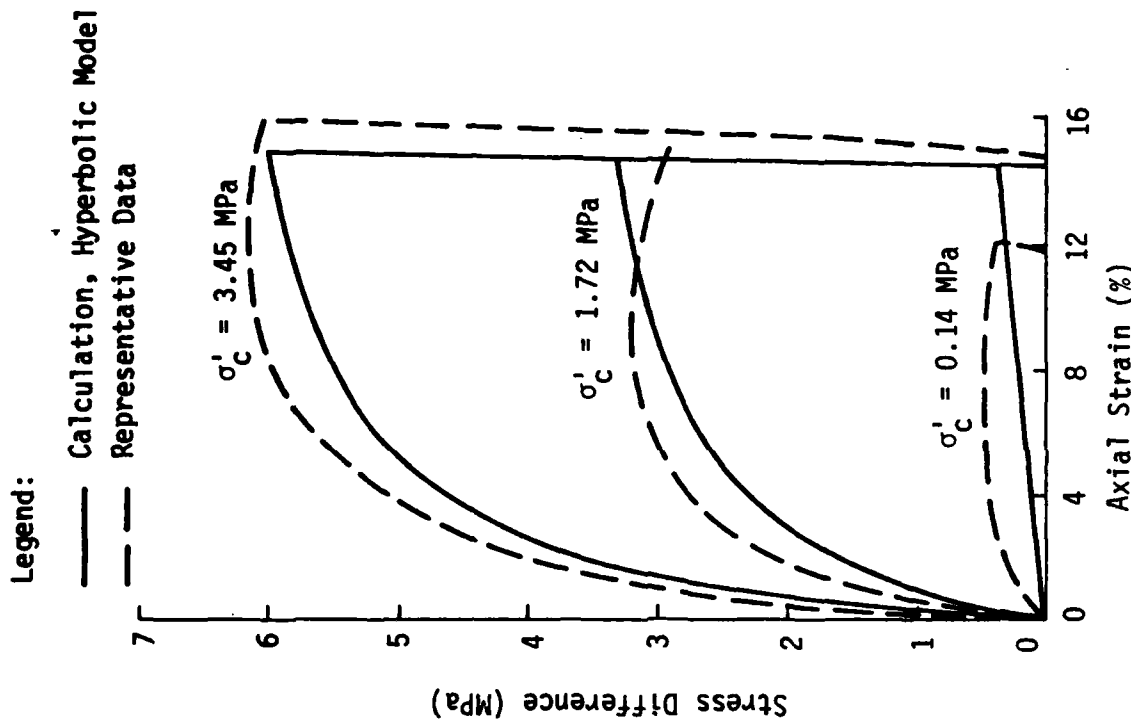


D. Calculation vs. Data

Figure 17. RV Alluvium UX and TX Model-Data Comparisons



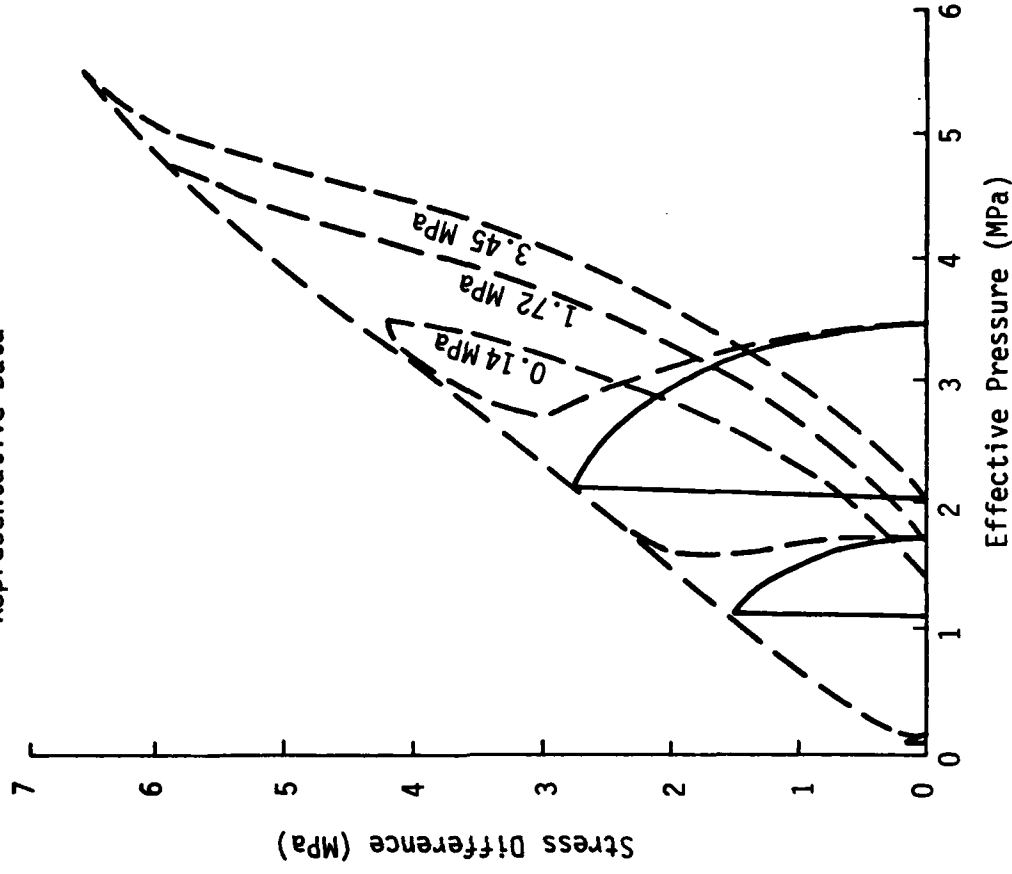
B. Misers Bluff Sand



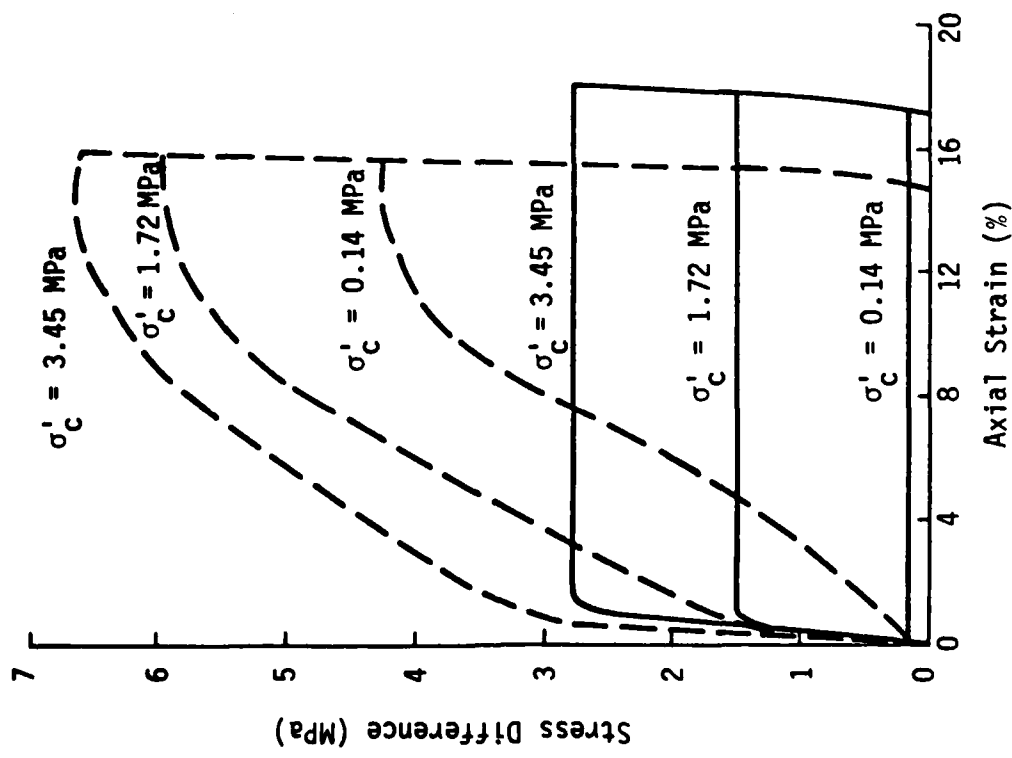
A. Reid Bedford Sand

Figure 18. MB and RB Sands Hyperbolic Model-Data Comparisons

Legend:
 — Calculation; Effective Stress Cap Model
 - - - Representative Data



A. Stress-Strain



B. Stress Path

Figure 19. Effective Stress Cap Model, RB Undrained Saturated TX Model-Data Comparisons

resistance. In the range of axial stress used to test the sands, a linear approximation to the UX loading curve is satisfactory, although the different sands showed different degrees of nonlinearity. The materials tested were much stiffer on unloading than on loading, and recovered only about twenty percent of accumulated axial strain. The elastic-plastic model predicts no compaction and a constant for both loading and unloading modulus, which is a substantial modeling deficiency for sands.

The AFWL Engineering model predicts nonlinear loading compressibility quite well, and is limited only by the chosen number of linear segments. The model uses a constant modulus for unloading, and predicts net compaction fairly accurately. On unloading from low stress levels the sands tend to recover strain at a greater rate than from higher stress levels, but this is not well modeled by the AFWL model. This can be remedied by including a multilinear unload-reload relationship, as shown in Figure 20. Since Poisson's Ratio in the AFWL model may be different for loading and unloading, the observed UX stress path may be approximately (i.e., linearly) matched. The AFWL model triaxial shear behavior is essentially the same as for the elastic-plastic model. The ultimate shear strength is well predicted by the linear failure surface, but the shape of the TX stress-strain curve is not. The shear modulus is directly proportional to the bulk modulus, and so the model may even predict a stiffening shear modulus if a hydrostat breakpoint is encountered during triaxial shear. The poor prediction of shear stress-strain behavior is a weakness of the AFWL model.

The cap model (as installed in the SEM) predicts only a concave (to the stress axis) UX loading compressibility curve. Thus, changes in

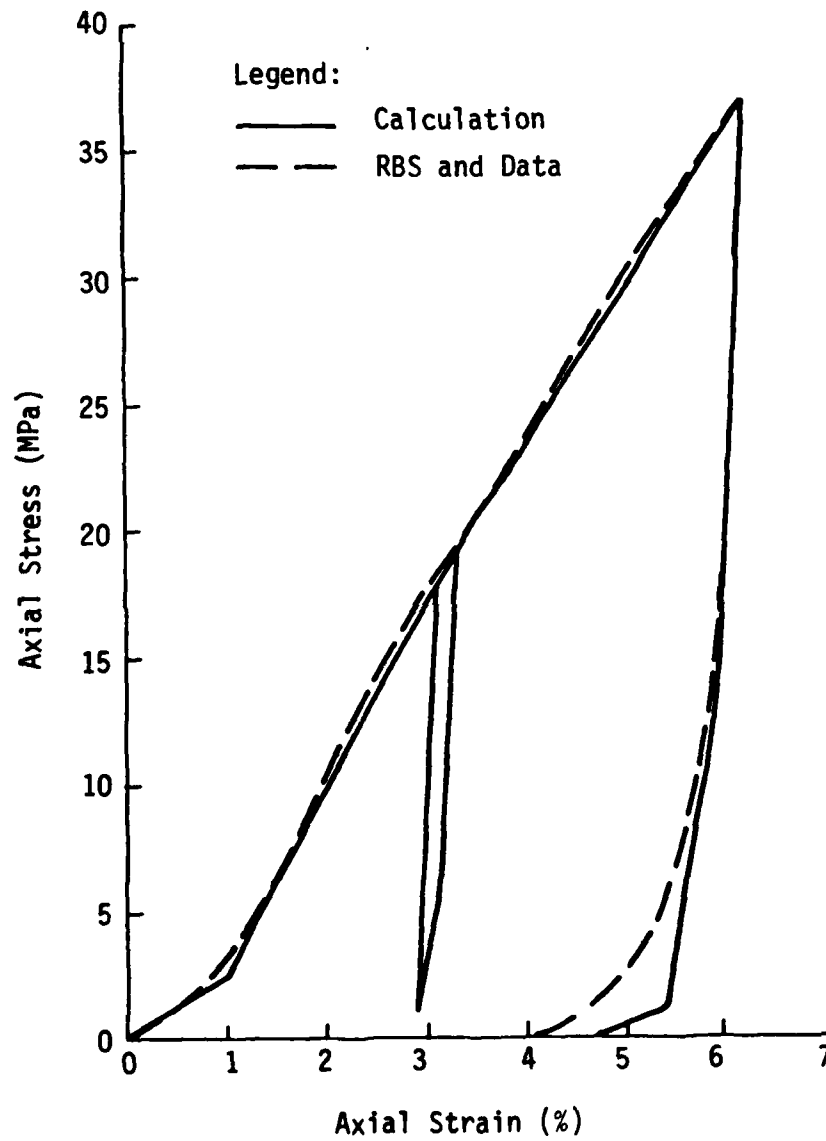


Figure 20. AFWL Engineering Model with Multilinear Unload-Reload Behavior

curvature in the UX curve are not modeled. Most of the sand data is consistently convex, so the cap model does as good a job as does the AFWL model. The nonlinear nature of the UX unloading behavior is handled much better by the cap model, as seen in the model-data comparisons (e.g. Fig. 13). The UX stress path is somewhat hard to control, but can be made to follow the trend of the data. Since the cap model parameters are fit to follow TX stress-strain curvature, the model is considerably more accurate in predicting these results than are either the elastic-plastic or AFWL models. The cap model cannot predict a post peak softening behavior, as was observed in drained saturated RB sand (Fig. 16).

The cap model was used to predict undrained behavior, since it can calculate both total and effective stress. The primary cap modeling deficiency in this exercise (as seen in Figure 19 for RB sand) was its inability to follow the effective stress failure envelope upwards after initially reaching it. In the actual material response, a significant post "failure" increase in shear strength was observed, due to the sample's tendency to dilate. The model does not consider this behavior, and therefore did not do well in predicting stress-strain relations, shear strength, or pore pressure response. A total stress approach with a von Mises type failure surface fit to ultimate strength would be more accurate, but fundamentally lacking, since effective stress actually controls shear behavior. The problem lies in predicting excess pore pressure, i.e., in predicting the coupling between shear strain and the tendency of the soil skeleton to change volume.

5.0 DYNAMIC INSITU BEHAVIOR OF SAND

5.1 Insitu Test Description

The insitu behavior of sand will be discussed here with reference to two types of insitu dynamic material property tests: the Cylindrical Insitu Test (CIST) and the Dynamic Insitu Compressibility Test (DISC Test). These tests have each been performed at the Ralston Valley Geotechnical Study Site in Nevada. The laboratory properties of RV alluvium are available (Ref. 11) and have been discussed previously.

CIST 22 (Ref. 12) fielded gages on several redundant radials at a single depth of 4.72 m. Accelerometers measured radial and vertical motions, and flat pack stress gages measured stress time histories. DISC Tests I and II (Refs. 13 and 14) were performed at approximately the same site as CIST 22. Their purpose was to define insitu vertical uniaxial strain compressibility to a depth of about fifteen meters. Approximately thirty ground motion gages were placed for each test (vertical and horizontal) along with 10 airblast gages. (Before edge effects appear, the tests maintain a condition of essentially uniaxial strain.) Figure 21 shows the experimental configuration for CIST 22, and Figure 22 shows the experimental configuration for DISC Test II.

5.2 Insitu Test Results

Several important features of CIST and DISC Test data help define insitu material properties:

- 1) Attenuation of peak motions (acceleration, velocity, and displacement;
- ii) Arrival times of first motion and peaks;

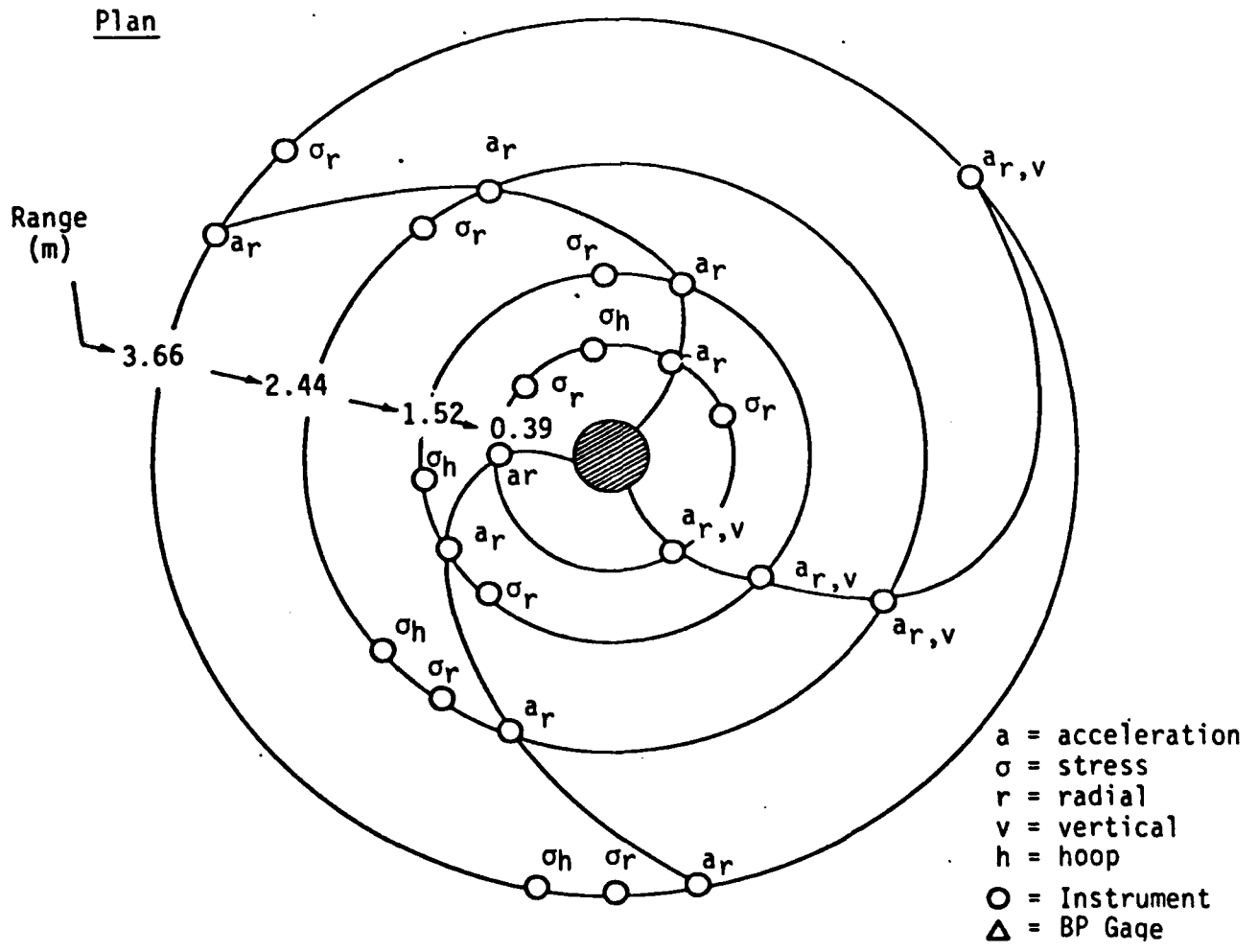
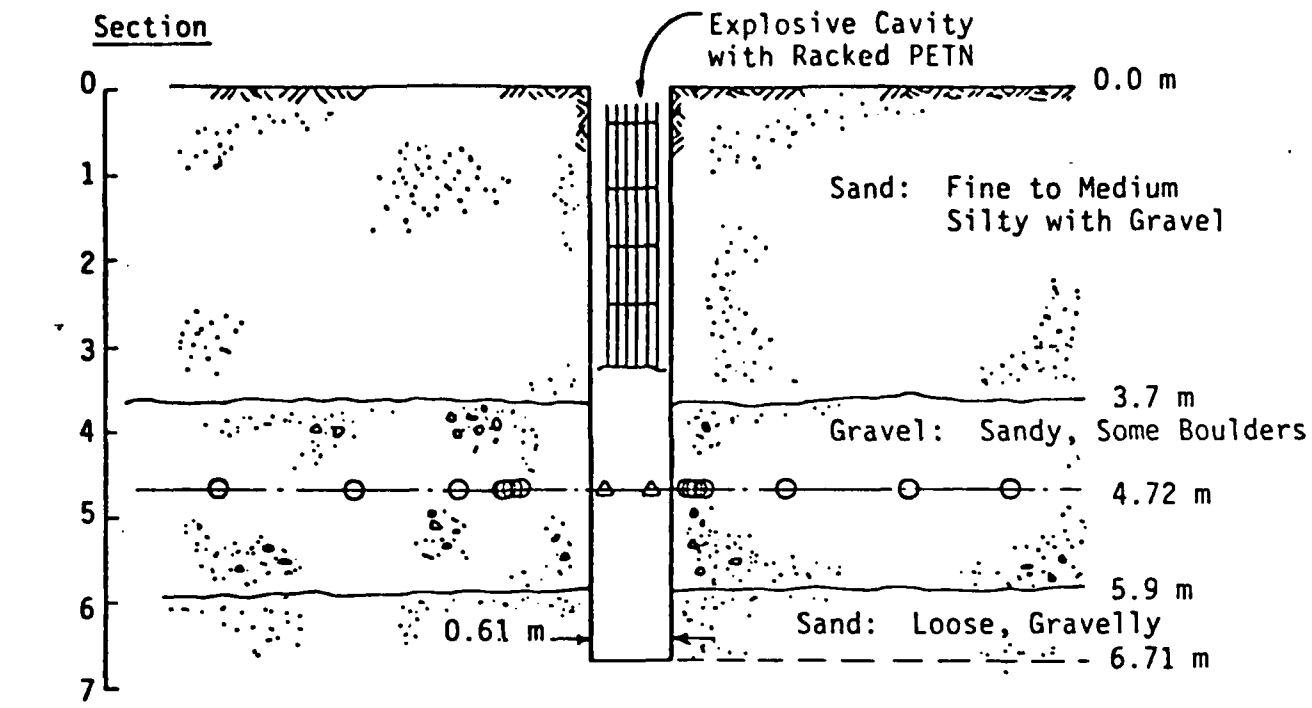
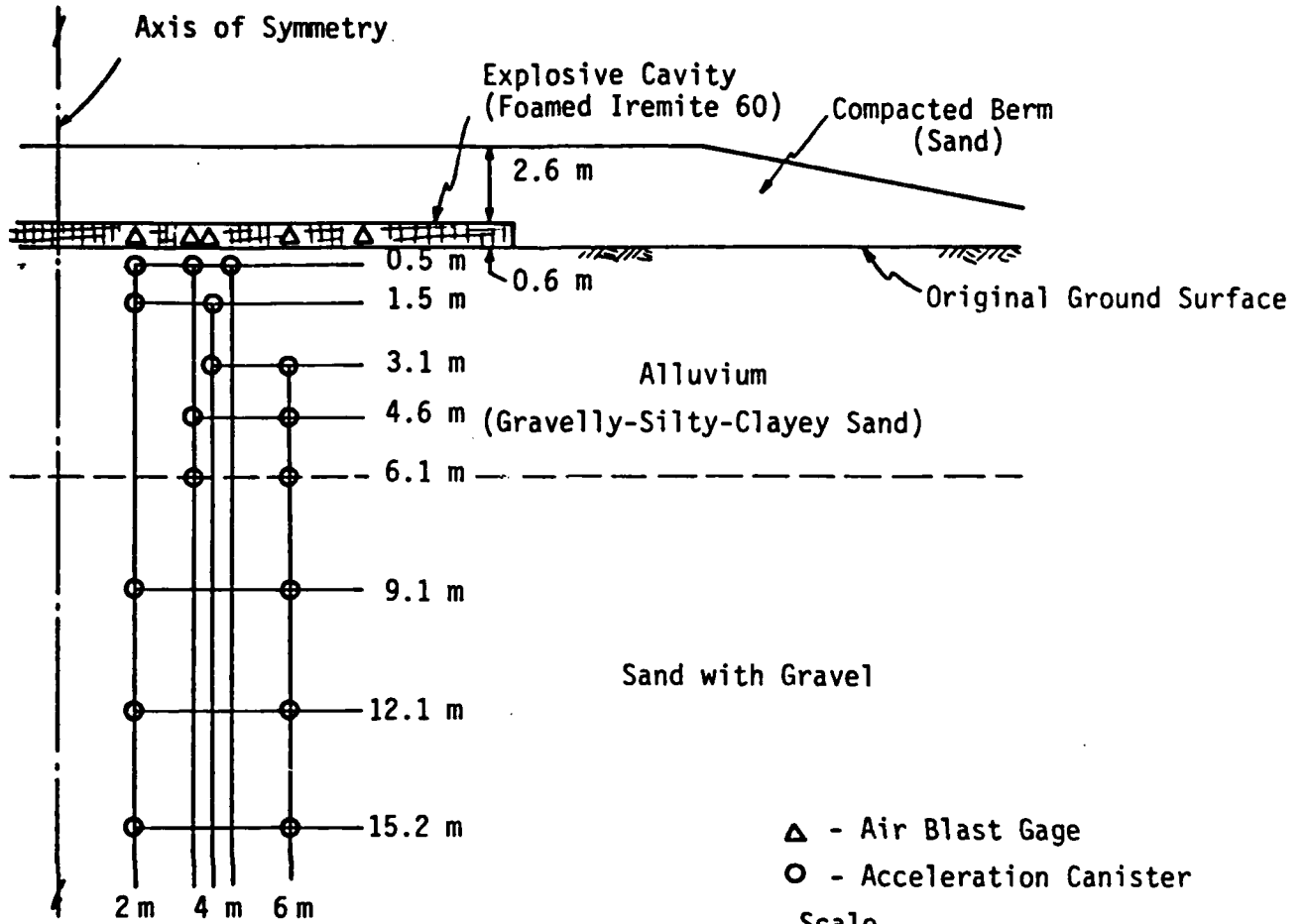


Figure 21. CIST 22 Experimental Setup
43

Section



Plan

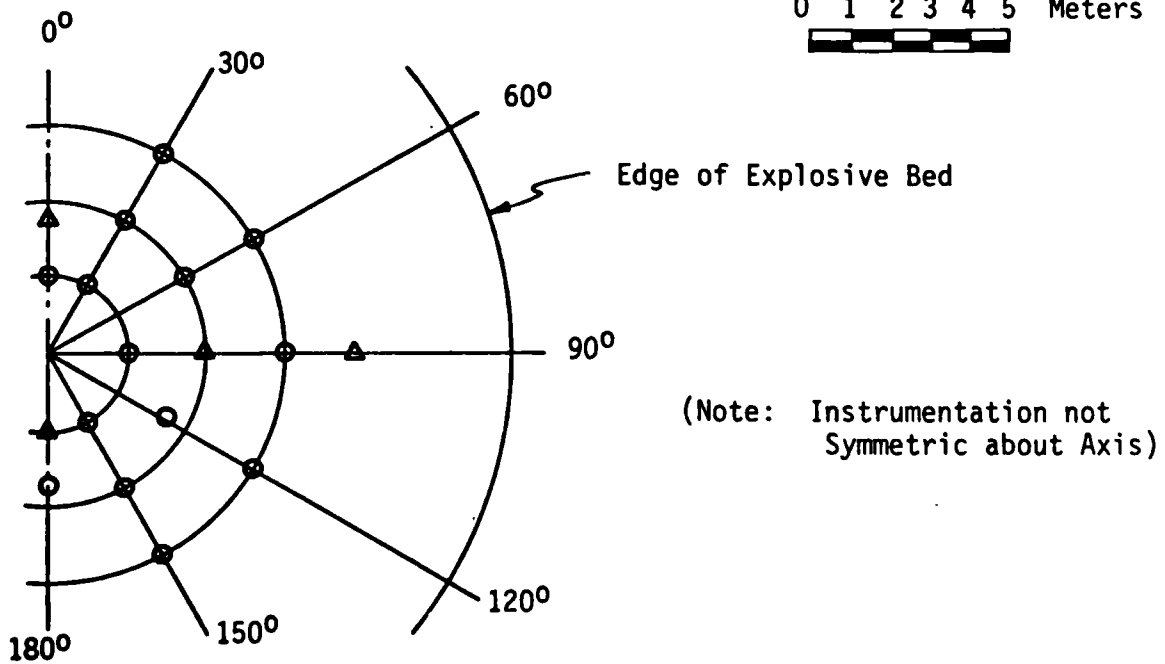


Figure 22. DISC Test II Experimental Setup

iii) Waveform shape (rise time, post peak rate of decay, and number of cycles of motion);

iv) Two-dimensional effects as reflected in the waveforms.

Figure 23 shows composite velocity waveforms and Figure 24 shows how peak velocity and arrival times varied with range in CIST 22. The data is consistent with other tests in dry sand, although the quality (based on redundancy) is not good. Definition of the actual cavity pressure was not totally successful, but some gages did survive and a reasonable estimate can be made based on the gages which did survive.

The primary (but not the only) difference between a DISC Test and a CIST is the direction of motion. A CIST is designed to test each individual soil layer by inducing radial displacement. A DISC Test includes the effects of reflection and refraction due to layering by inducing vertical displacement. Waveforms are shown for DISC Test II in Figure 25. Note the effect of layering (i.e. reflections) and explosive cavity venting through the berm, which give the waveforms more character than shown by CIST waveforms. Attenuation and arrival times for DISC Test II are shown in Figure 26.

Both the CIST and DISC Test results are influenced by two-dimensional effects. Relief waves propagate into the fields of recorded motions from the edge of the explosive cavity, and the free surface affects propagating waves in both test geometries.

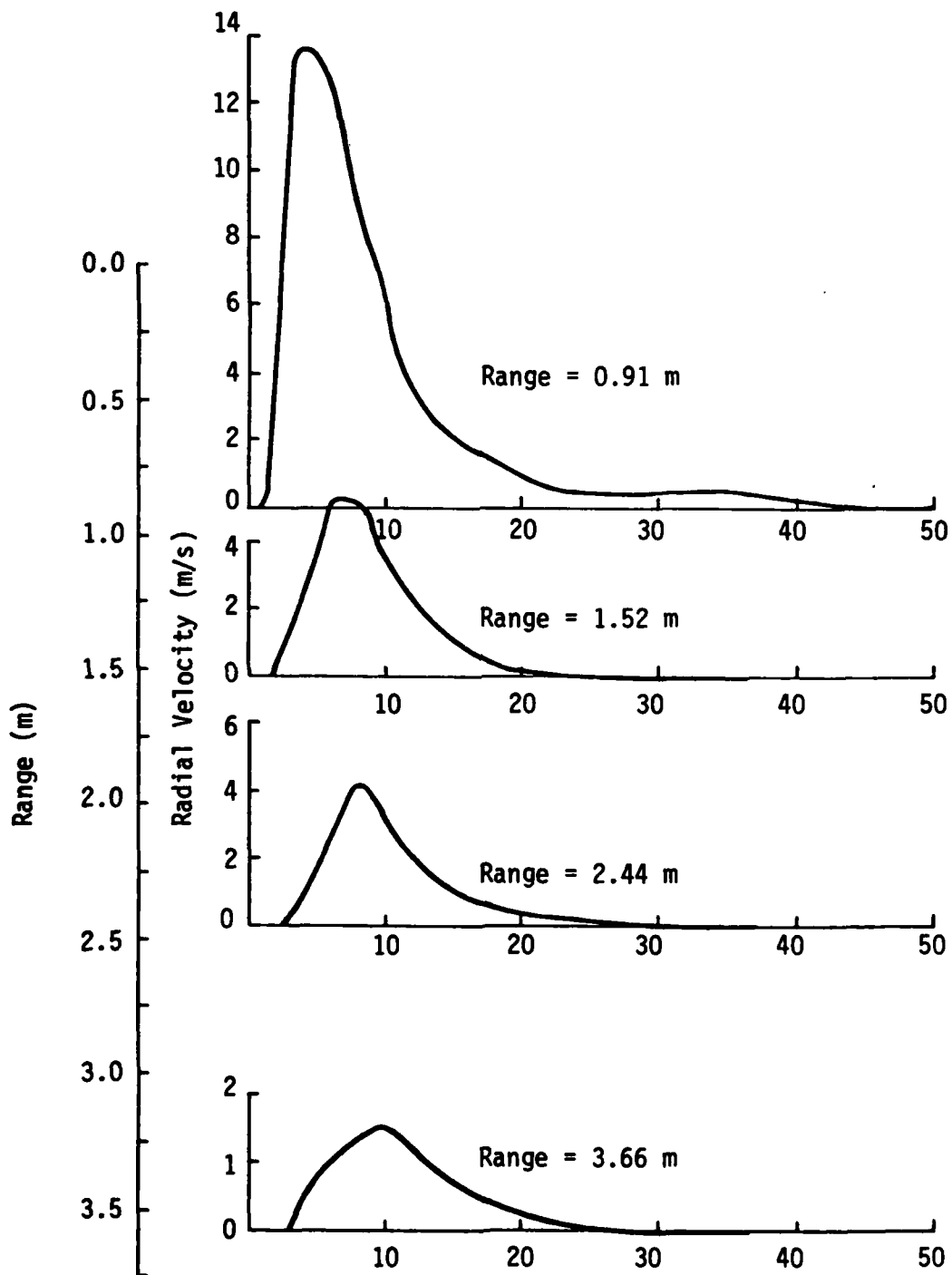
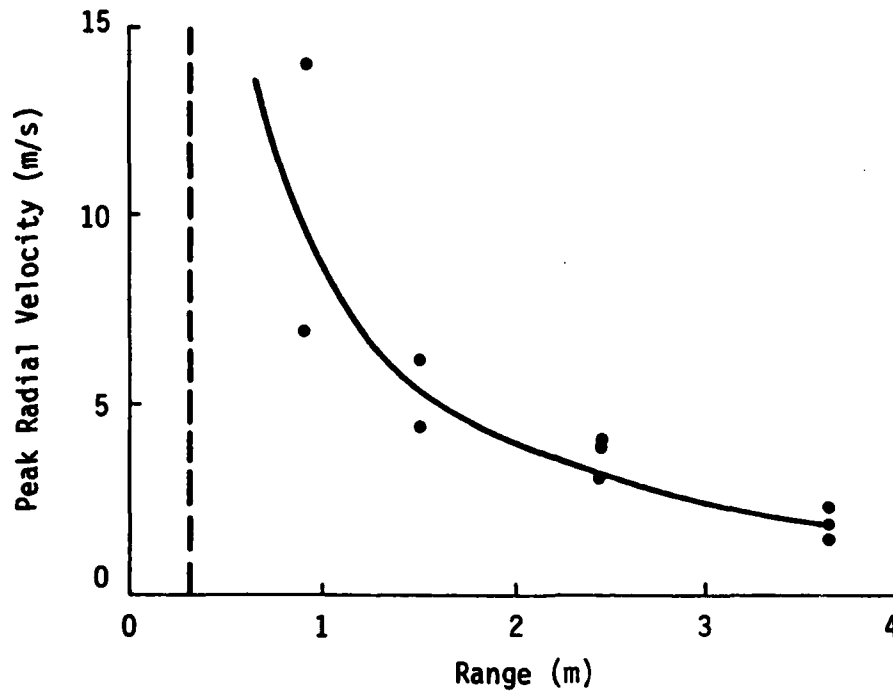
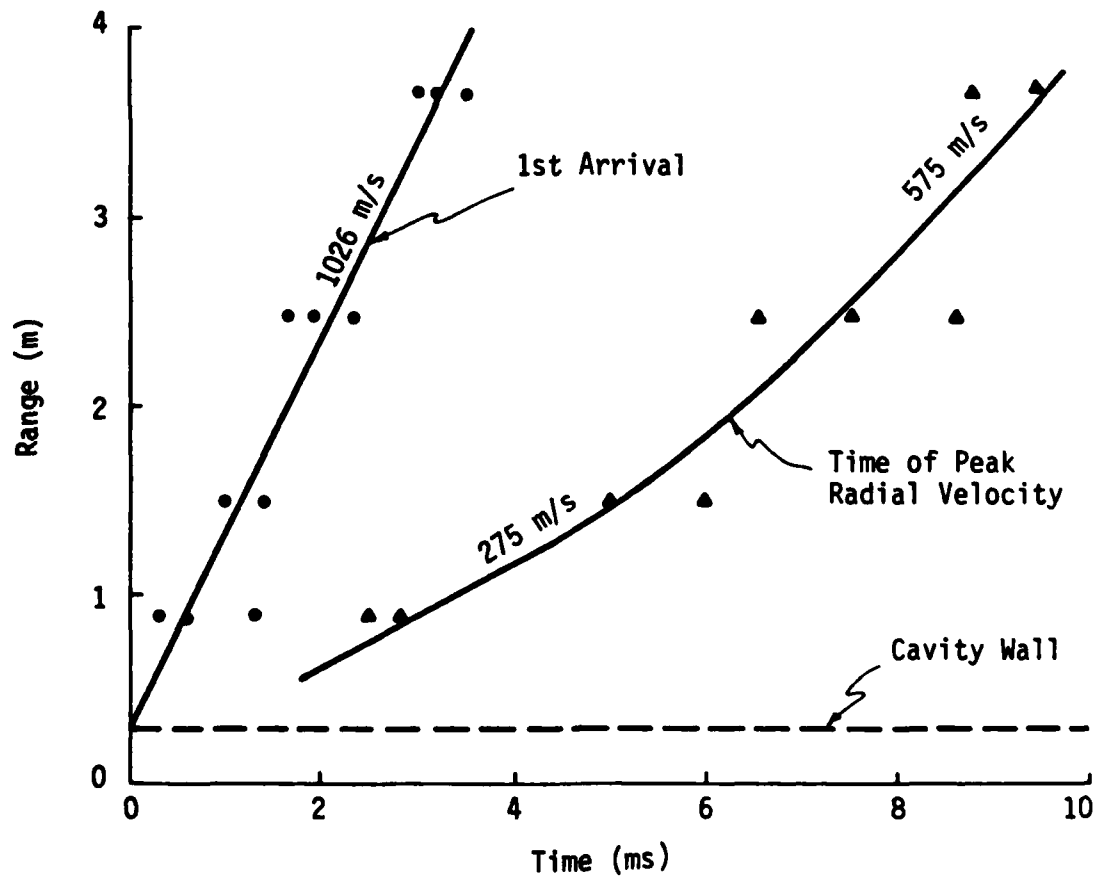


Figure 23. CIST 22 Composite Radial Velocity Data



A. Attenuation of Peak Radial Velocity



B. Arrival Times

Figure 24. CIST 22 Observed Attenuation and Arrival Times
47

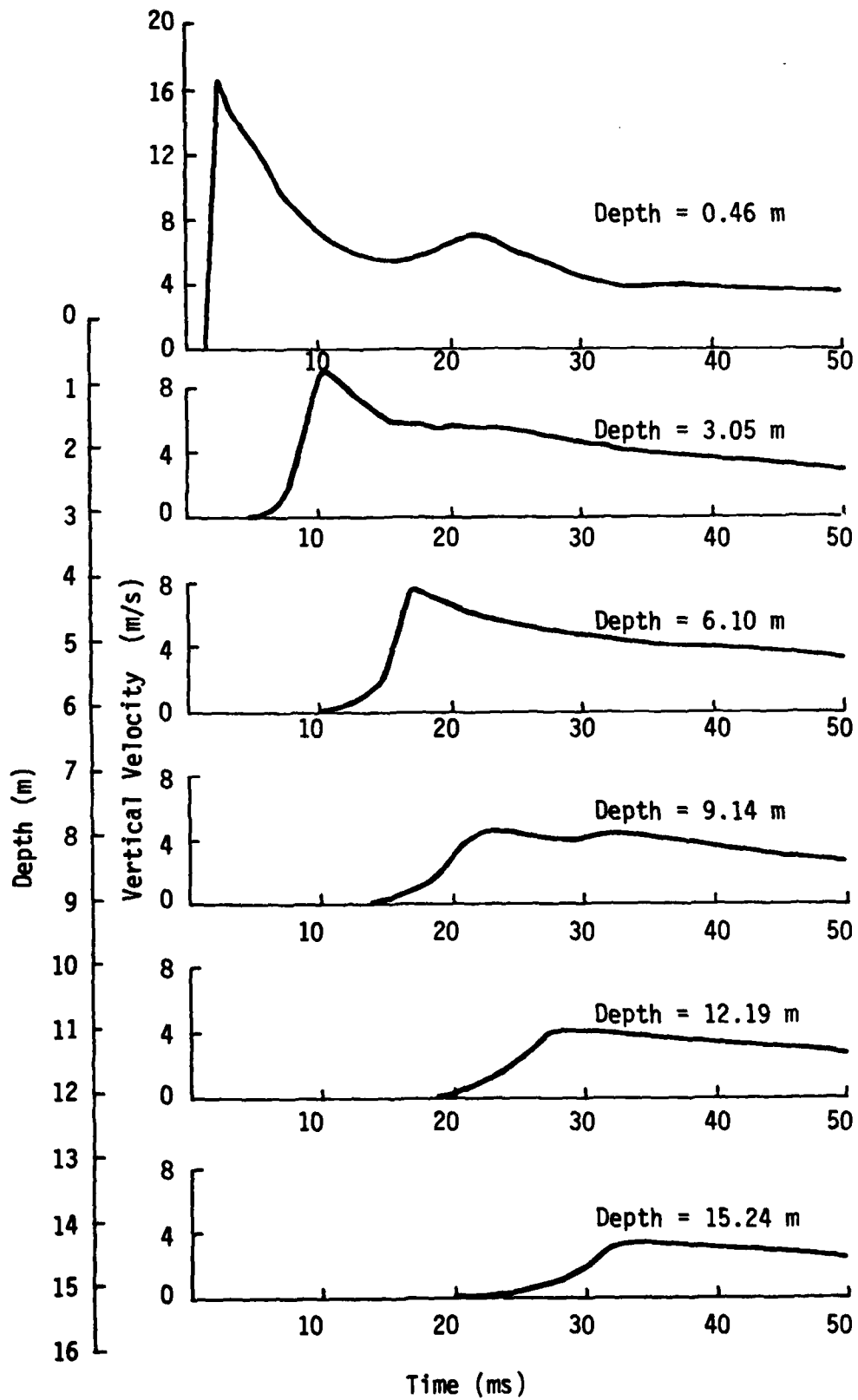
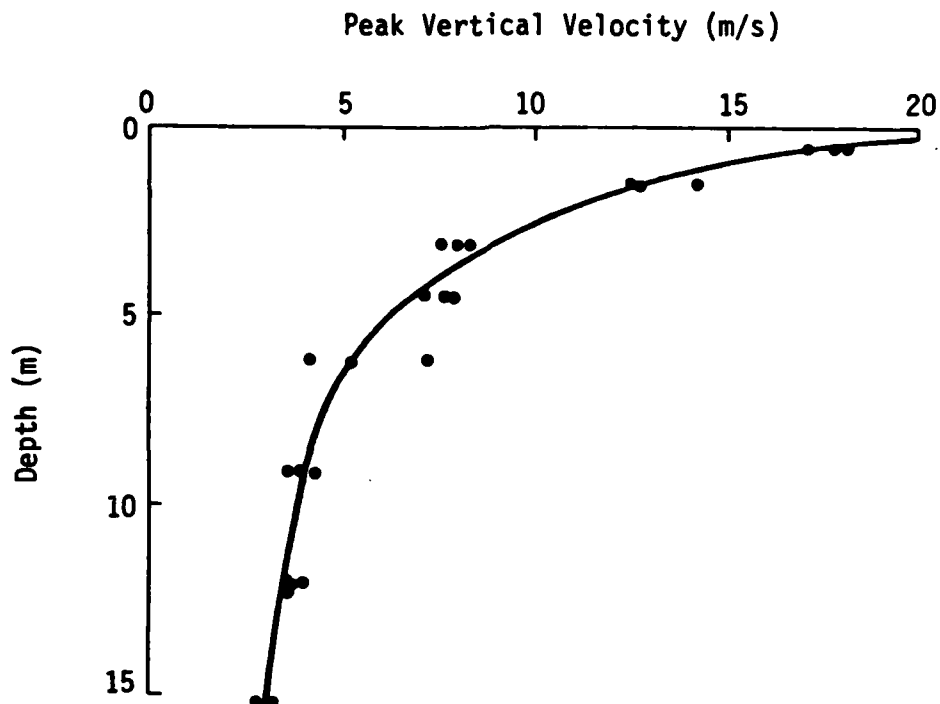
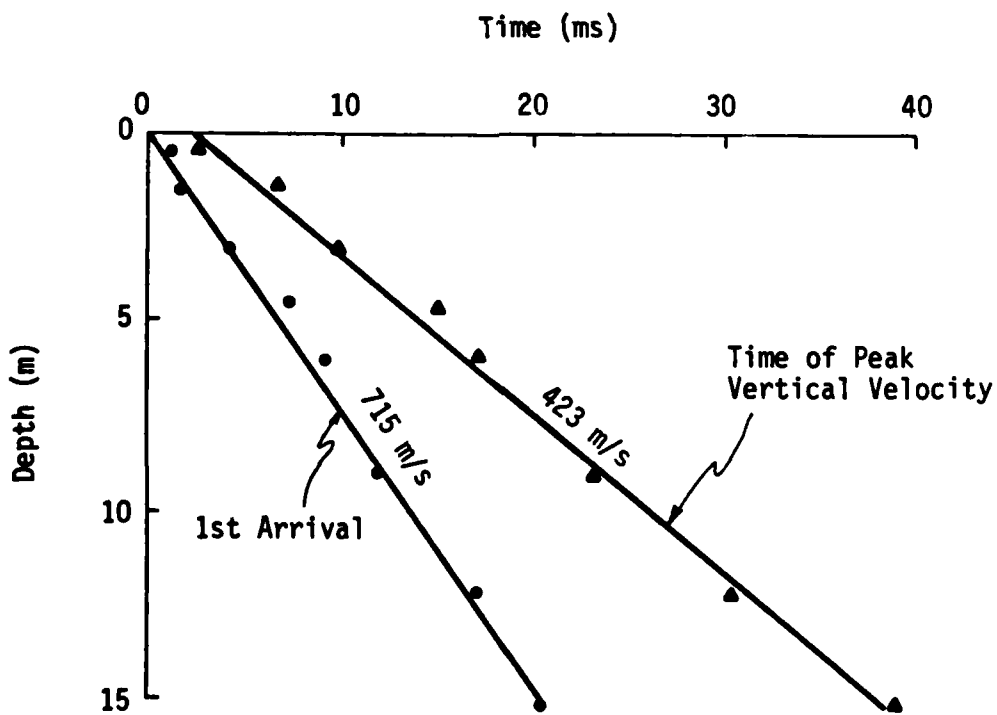


Figure 25. DISC Test II Composite Vertical Velocity Data



A. Attenuation of Peak Vertical Velocity



B. Arrival Times

Figure 26. DISC Test II Observed Attenuation and Arrival Times

6.0 MODELING THE INSITU BEHAVIOR OF SAND

6.1 Finite Difference Calculations

The CIST and DISC Test events in Ralston Valley alluvium were simulated with a series of finite difference calculations. The majority of calculations were either one-dimensional, axisymmetric or plane-strain. The one-dimensional code installed in the Soil Element Model (see Section 2.1) was used. In addition, a two-dimensional plane-strain calculation was done for DISC Test II using STEALTH-2D (Ref. 15). This illustrated the two-dimensional nature of motions generated in the DISC Test. The boundary conditions and grid definition for the one-dimensional calculations are shown in Figure 27. Edge and bottom boundary conditions were not important, because the grid was large enough to provide ample simulation time free of reflections.

Several constitutive relationships were used to calculate each event: a linear-elastic relationship, a simple elastic-plastic model, the AFWL Engineering model, and the cap model. The model parameters were those defined by laboratory test results (see values given in Appendix B). Additional calculations were done with revised model parameters to better match the measured waveforms. Table 3 provides a summary of the calculations performed.

6.2 Calculational Results

Results generated for each 1-D calculation consist of:

- a. Time-histories of stress, velocity, displacement, and any number of additional arbitrary quantities (e.g. cap position);
 - b. Snapshots of stresses and strains in the grid at various times;
- and

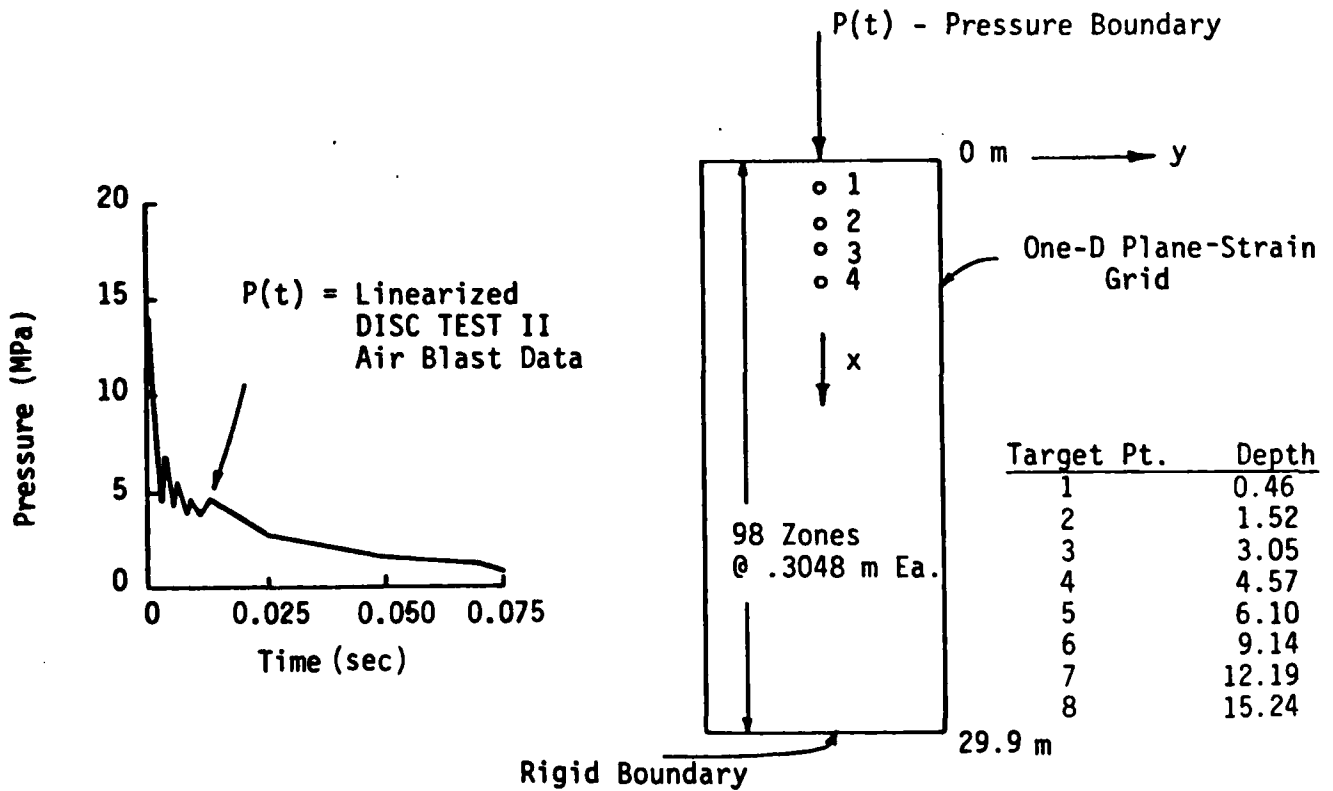
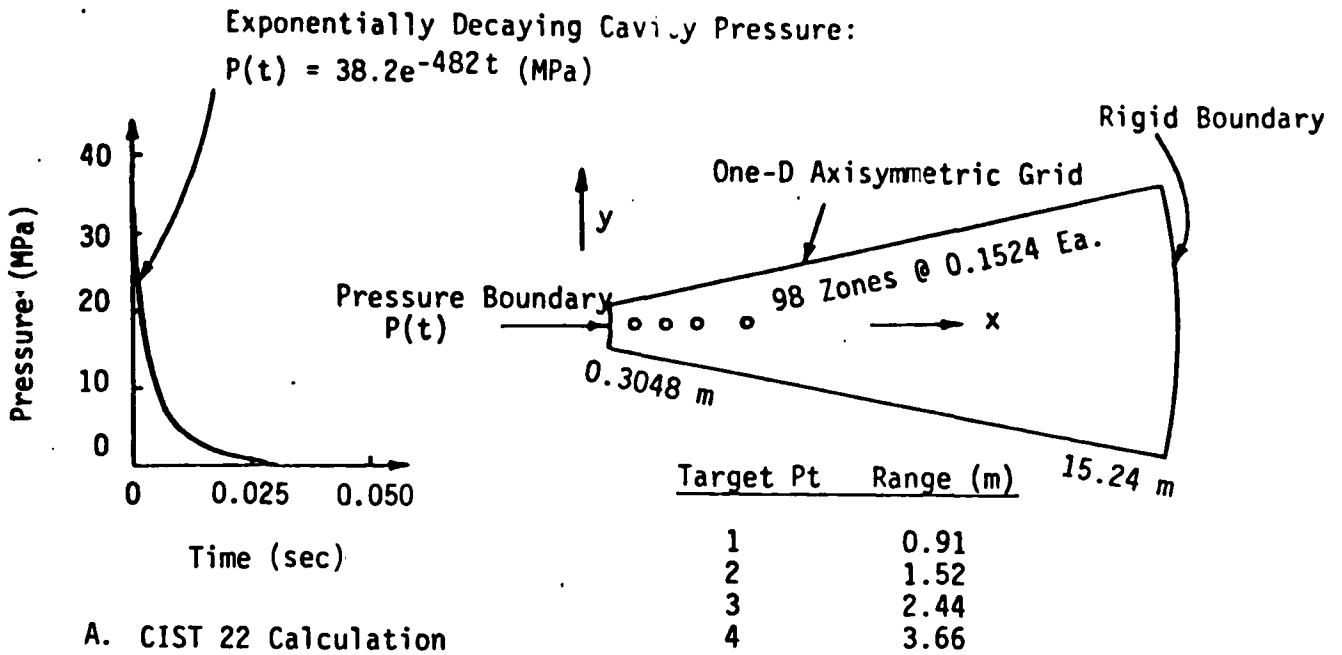


Figure 27. One-Dimensional Calculational Setups for CIST 22 and DISC Test II

Table 3. Finite-Difference Calculation Matrix

Event	Calc No.	Material Model	Notes
CIST 22	C22-1	Linear Elastic	No tensile failure
	C22-2	Elastic-Plastic	
	C22-3	AFWL	Laboratory based parameters
	C22-4	CAP	Laboratory based parameters
	C22-5	AFWL	Insitu based parameters
DISC Test II	DT-1	Linear Elastic	
	DT-2	Elastic-Plastic	
	DT-3	AFWL	Laboratory based parameters
	DT-4	CAP	High-pressure laboratory fit
	DT-5	CAP	Low-pressure laboratory fit
	DT-6	AFWL	2-D, laboratory parameters

c. SEM constitutive model plots at one target point.

Appendix C contains an example a set of complete results for a calculation. Three aspects of the calculations will be compared here: waveform shape, attenuation of peak values, and arrival times.

The elastic calculation of CIST 22 did not produce waveforms which resembled the observed motion, as shown in Figure 28. The remainder of the models, however, did match the general character of the data, as seen in Figure 29. Attenuation comparisons between the various models and the CIST data are shown in Figure 31A.

The character of motion produced in the DISC Test calculations was quite similar for all models. Figure 30 compares calculated waveforms with data near the center of the explosive bed. (The elastic model is not included, as it overlaid the elastic-plastic calculation.) Attenuation is shown in Figure 31B. Time of arrival of the first signal and velocity peaks are shown for CIST and DISC Test II in Figure 32.

Results from the two-dimensional DISC Test calculation are summarized in Figure 33. The figure shows how vertical and horizontal velocity waveforms vary throughout the test bed.

Some general conclusions can be drawn from the above calculations:

a) Necessary model complexity varies with calculational geometry. The elastic, elastic-plastic, AFWL, and cap models all produced similar results for the DISC Test. This is because motion is uniaxial, and the most important material response modeled is uniaxial compression, which all four models do fairly well within their bounds. Attenuation is a main difference between models. Note that an elastic model should theoretically not attenuate motion or stress at all. However, artificial

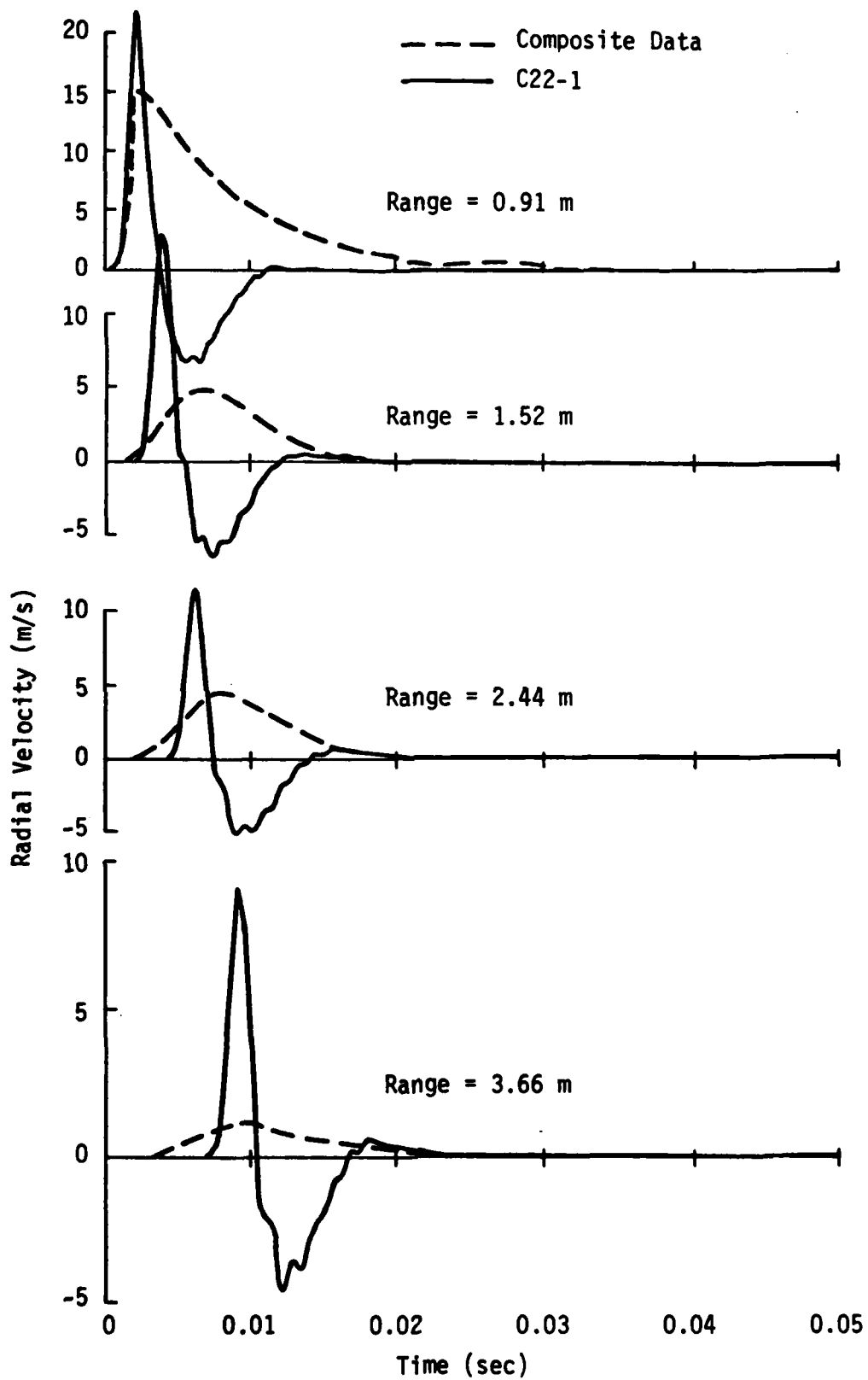
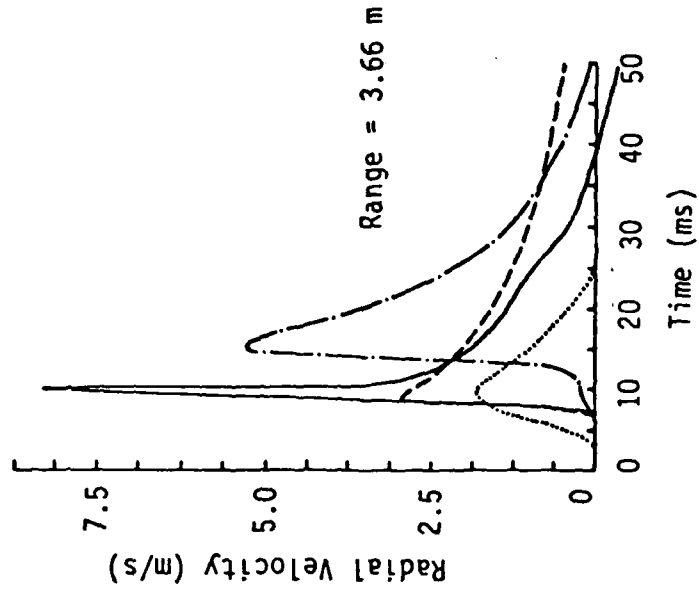
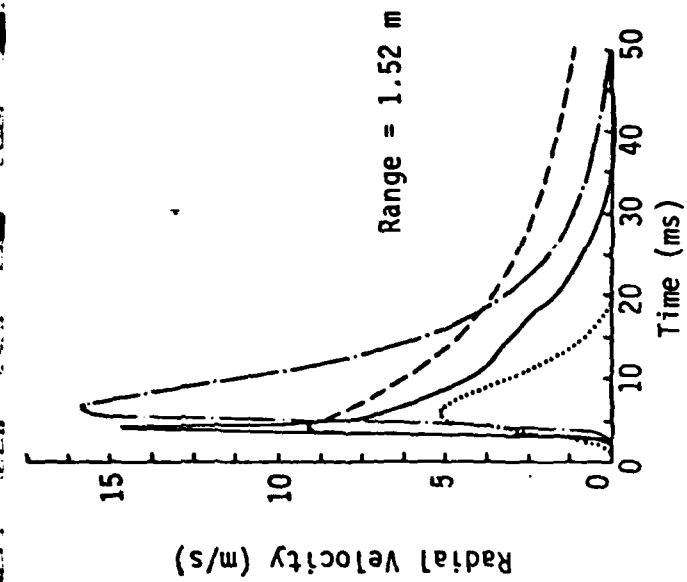


Figure 28. CIST 22 Elastic Calculation Compared with Data



..... Composite Data
 — ELPLA
 - - - AFWL
 - · - CAP

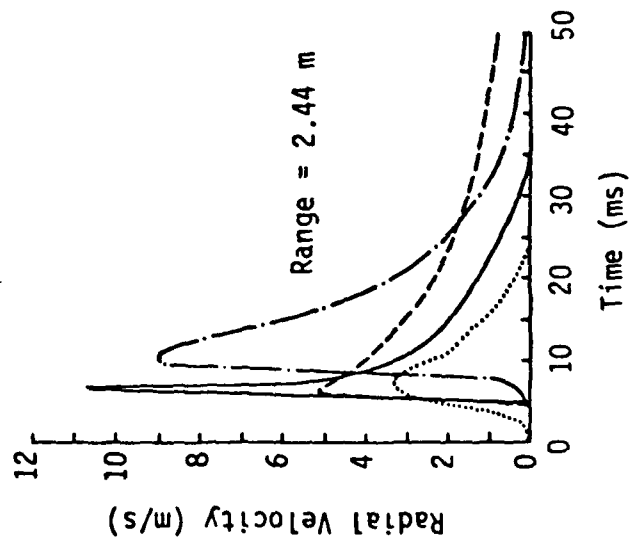
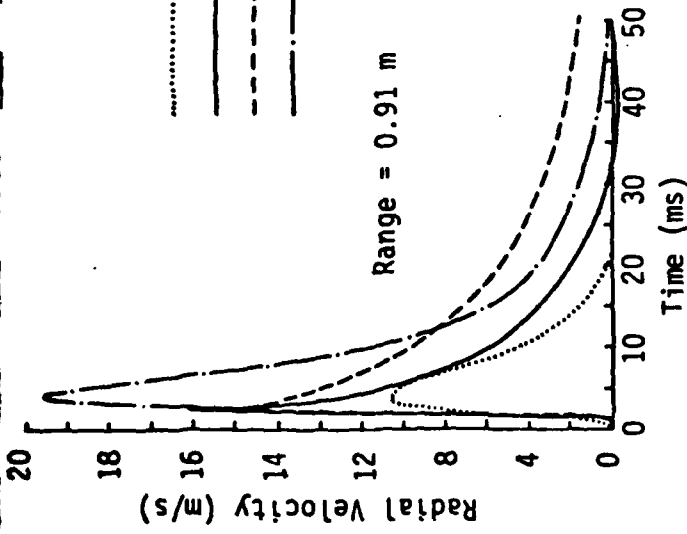


Figure 29. CIST 22 Calculated Radial Velocity Waveforms Compared with Data

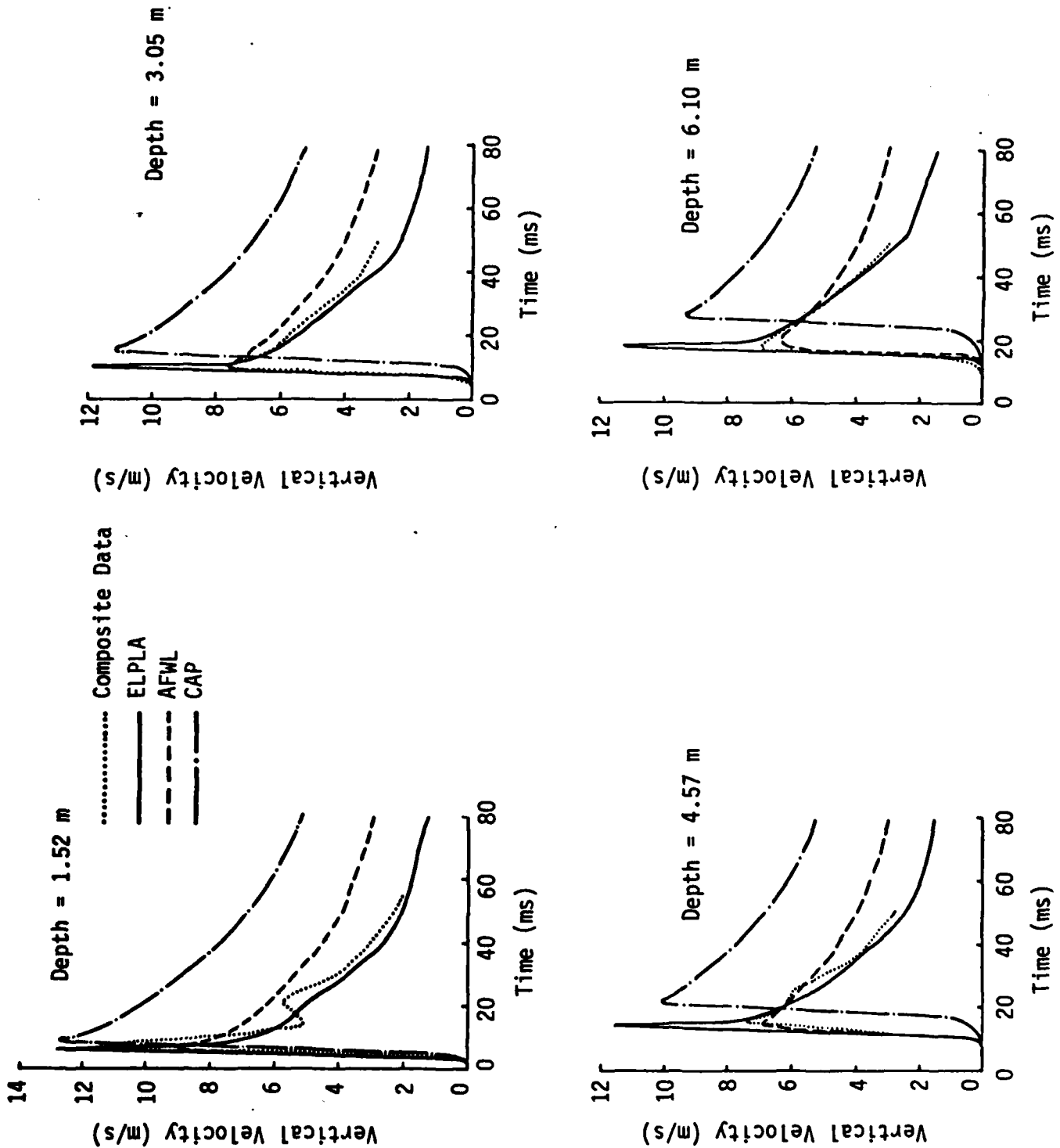
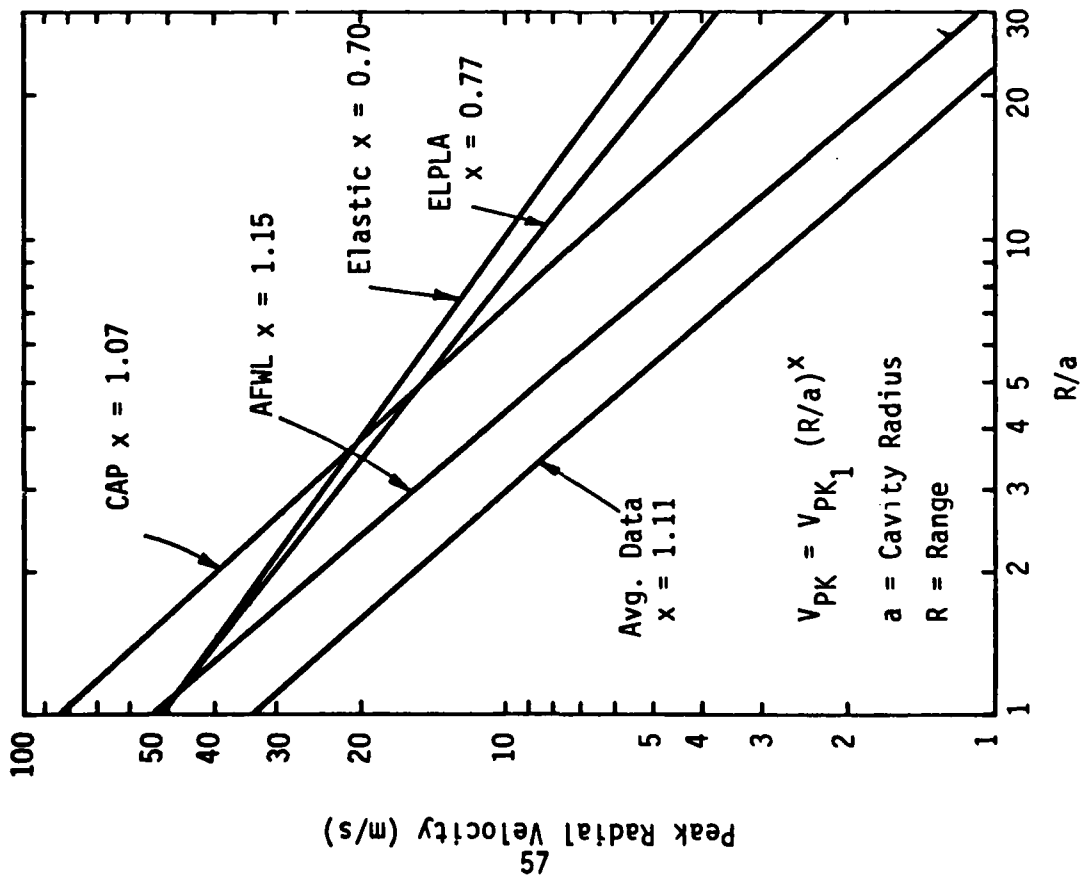
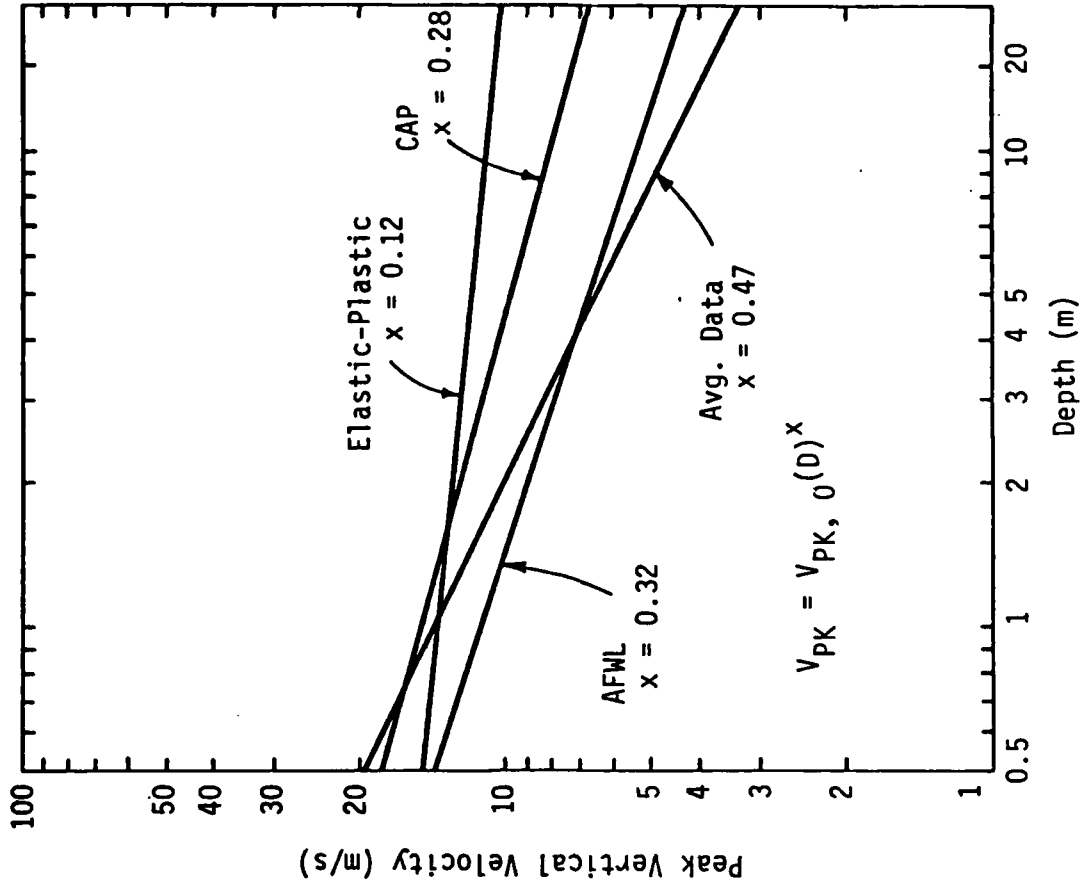


Figure 30. DISC Test II Calculated Vertical Velocity Waveforms Compared with Data



A. CIST 22



B. DISC Test II

Figure 31. Comparison of Calculated and Measured Attenuation Rates for CIST 22 and DISC Test II

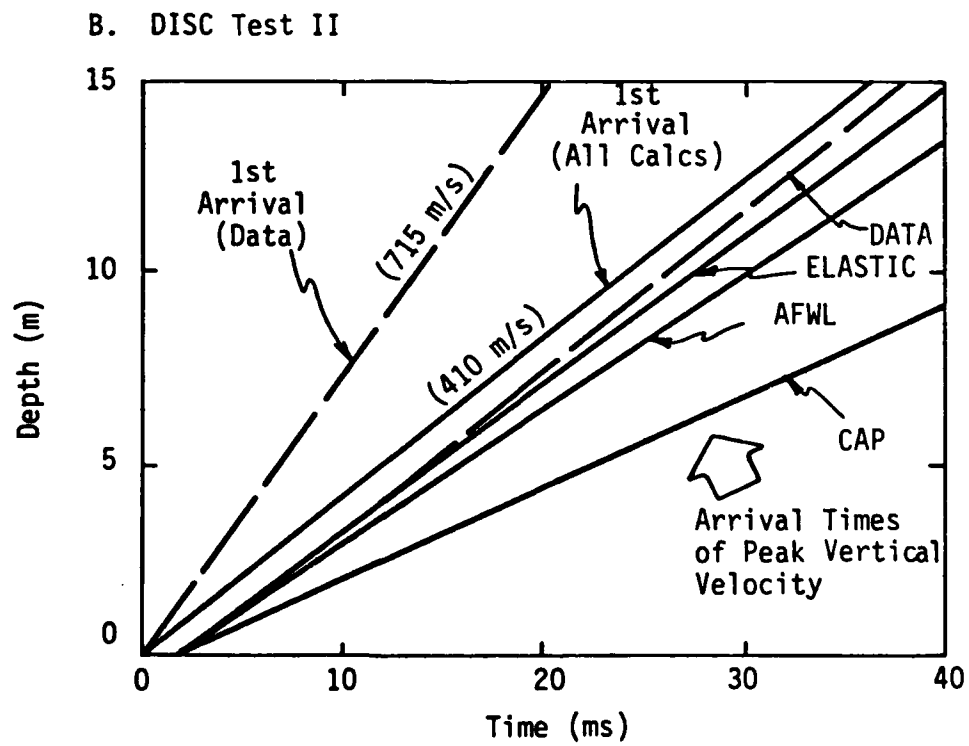
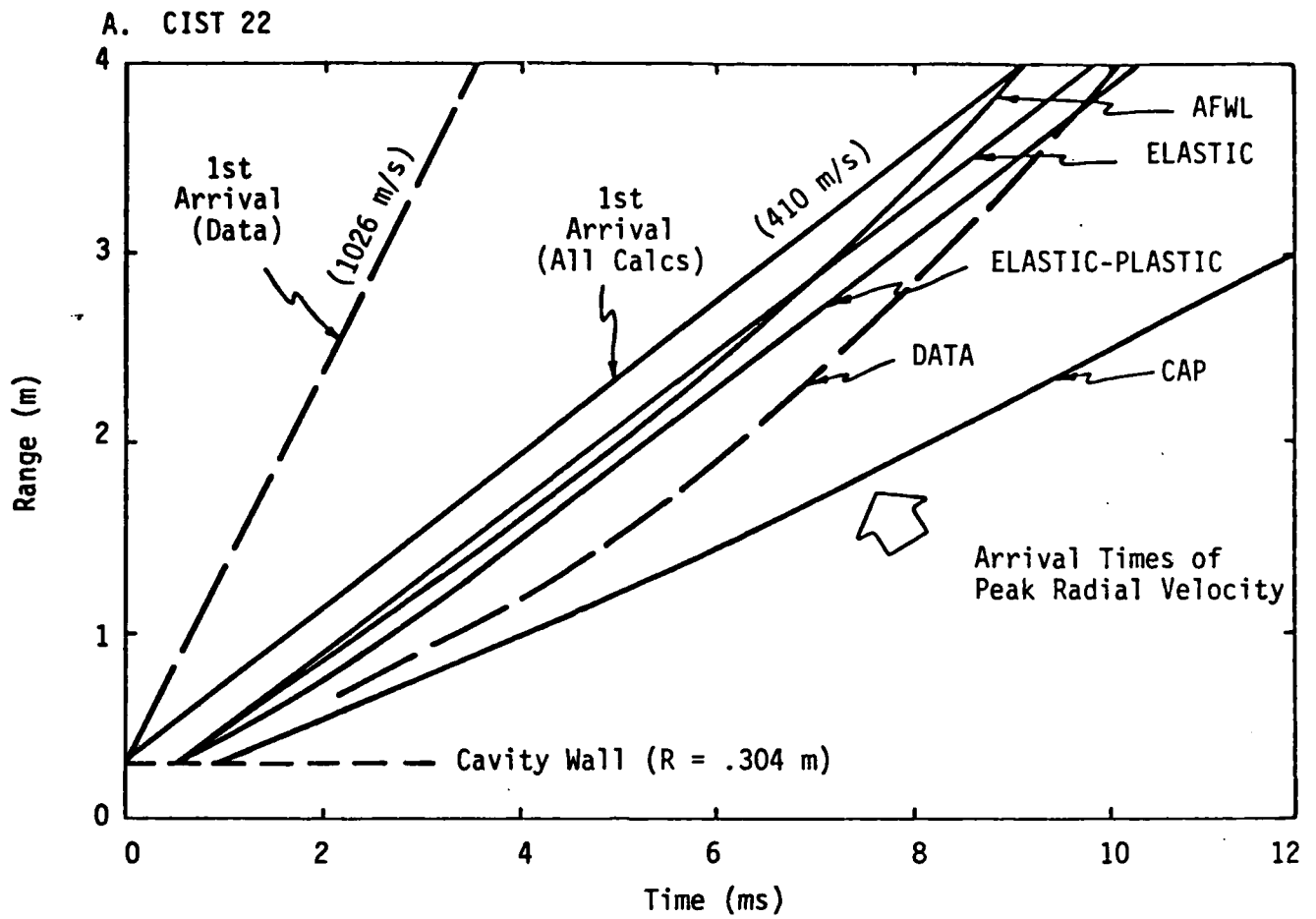


Figure 32. Comparison of Calculated and Measured Times of Arrival for CIST 22 and DISC Test II

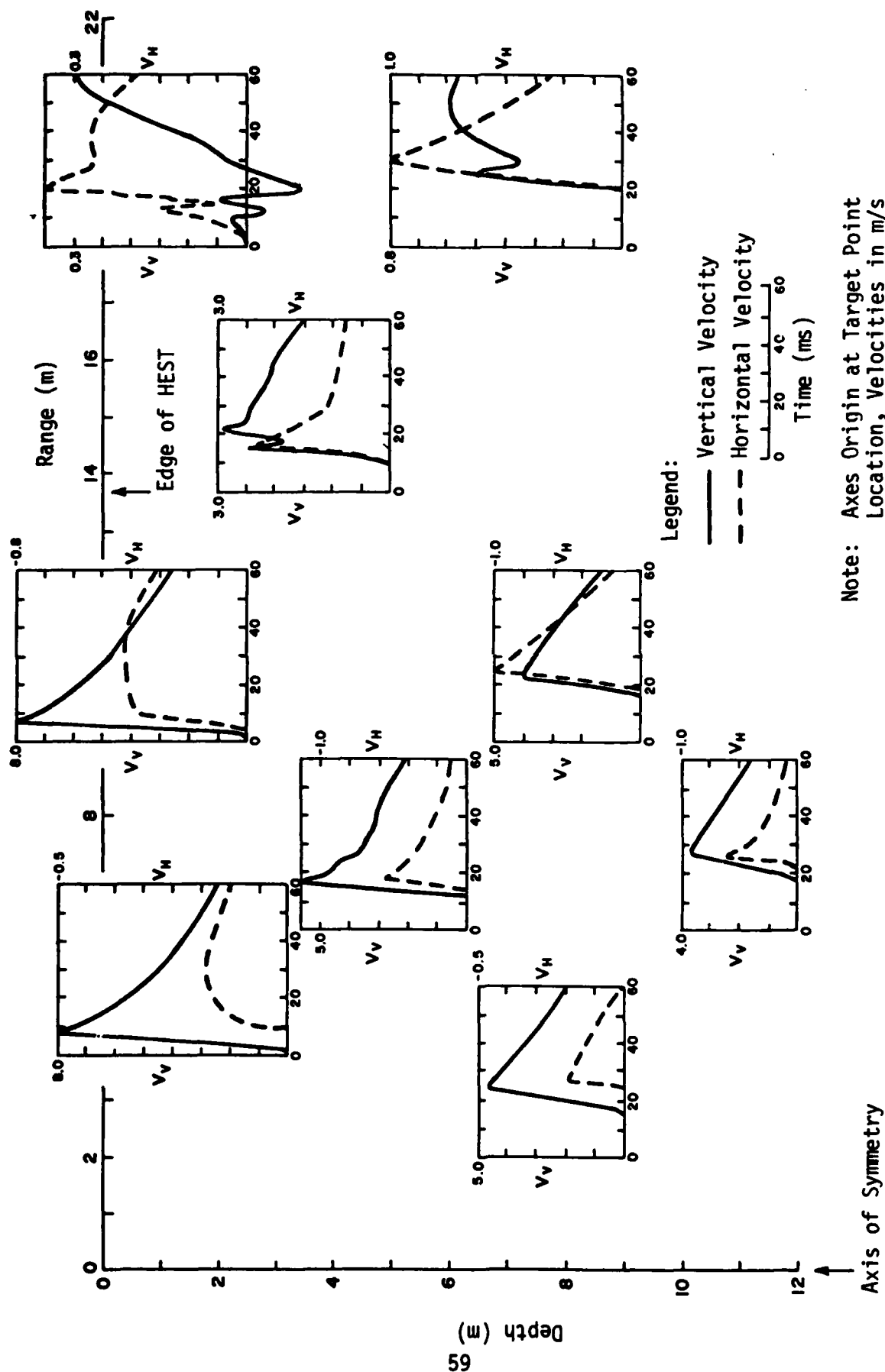


Figure 33. DISC Test II Calculated (2D STEALTH) Velocity Waveforms

viscosity reduces peaks, and this effect was seen in Figures 31B. In the CIST calculations the results change markedly in going from an elastic model to an elastic-plastic model with shear and tensile failure. This is due to the cylindrical symmetry of the problem. Stress relief in the hoop direction generates a more complex stress/strain field than in the uniaxial compression case, even in one dimensional (radial) wave propagation. In order of importance, the critical features of material response in the CIST calculations appear to be:

- i) Volumetric (compressional) behavior;
- ii) Shear failure and post failure behavior; and
- iii) Tensile behavior.

Cylindrical calculations therefore tend to reveal much more than planar calculations about the constitutive model employed.

b) Model parameters should be based on laboratory data at the same level of stress expected insitu. The cap model (which predicts insitu motions considerably larger than observed) was fit at the 70 MPa level in the uniaxial test, while actual stress levels were on the order of 5-10 MPa. At lower stresses the model is clearly too soft, but can easily be adjusted to better fit low stress level laboratory data. If a wide range of peak stress is expected in a particular problem, the model should match the data at all stress levels below the maximum. Although the models could be modified to facilitate curve fitting, detailed matching over a wide stress range was not possible with the implemented versions of the AFWL and cap models.

c) Two-dimensional effects can influence insitu model estimation. Based on waveform matching in one-dimensional calculations, an insitu-

based model can be selected. Inherent in the measured waveforms are relief and other two-dimensional effects, which must be recognized during modeling. Otherwise, the model may be biased by unloading effects, and may therefore significantly underpredict motion.

7.0 DISCUSSION OF SAND MODELING

7.1 Additional Laboratory Behavior of Sand

More is known about the laboratory behavior of cohesionless soil than is reflected in the data available for this study. The following is a summary of points which would be important in developing a complete constitutive relationship.

7.1.1 Multiphase Effects. Soil is a two-or three-phase medium, with a solid soil skeleton and water, air, or both filling the voids. The rate of pore fluid migration through the skeleton has a significant effect on effective stress, and therefore on behavior under both static and dynamic loads. The permeability of sand depends to a large degree on the amount of fines present, and is usually quite high compared with that for silts and clays. Depending on the type and rate of loading, pore fluid migration in sand may or may not occur. Lacking data, it is necessary to estimate the permeability of a sand based on void ratio and percent of fines.

When a soil is partially saturated, its behavior is considerably different from that in either the dry or the fully saturated condition. Pore pressure parameters may be defined to describe partially saturated behavior as done by Skempton in Reference 16. Under dynamic loads, pore air may enter into solution, and the soil may become fully saturated. The details of this phenomenon need to be quantified for modeling purposes.

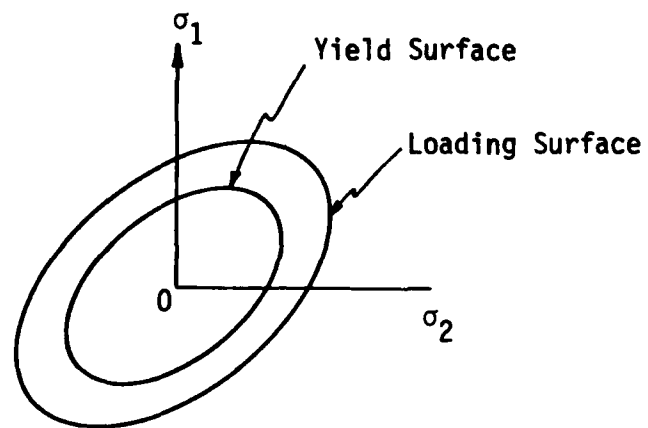
7.1.2 Anisotropy and Work Hardening. Soil in its natural state may be inherently anisotropic, or it may become anisotropic due to application of stress. A grain matrix with particles oriented in a preferred

direction will complicate definition of a constitutive relationship because complete symmetry can no longer be assumed.

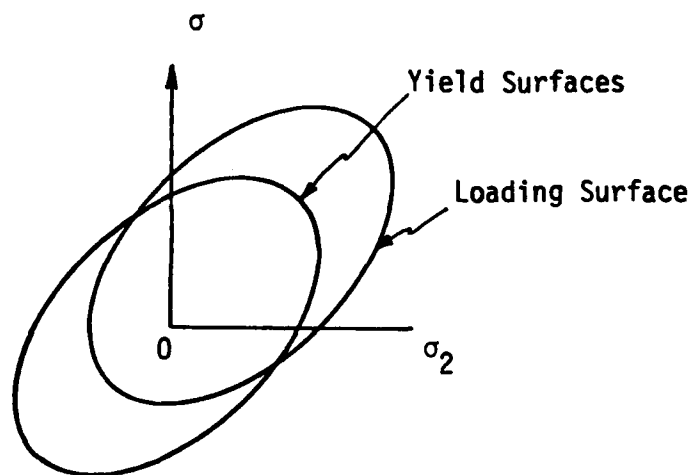
As a soil deforms, its strength characteristics often change. Two types of hardening/softening behavior have been postulated for soil: isotropic and kinematic. Figure 34 illustrates the basic concept behind each of these phenomena. For an isotropically hardening material, the loading surface expands uniformly about the origin in stress space and maintains the same shape, center, and orientation as the yield surface. In kinematic hardening, plastic deformation causes the loading surface to translate as a rigid body in stress space. Changes in properties as a result of loading are important for long duration and multi-directional loads, and for cases of multiple loading.

7.1.3 Strains. It has been well established that sands often change (or tend to change) volume as a result of shear deformation. This is known as shear-volume coupling, or dilatancy. This coupling is especially important in determining pore pressure response in saturated soils. Some evidence of this was noted in the triaxial behavior of MB and RB sand, but the exact relationship for coupled shear-volume behavior was not well defined.

Another aspect of strain behavior not explicitly covered thus far is the definition of plastic yield and potential functions. It has been postulated that soil deforms in the direction of the stress increment under small stress increments, and in the direction of total stress (and not stress increment) under large stress increments. It is therefore necessary to define a plastic potential, in addition to a failure or yield surface, which defines the plastic strain behavior of the material. The



A. Isotropic Hardening



B. Kinematic Hardening

Figure 34. Hardening Behavior

nature of the plastic potential with respect to the yield surface determines whether the flow rule is associative or nonassociative.

7.1.4 Loading Rate Effects. Test results on MB and RB sands indicate that properties were not dependent on loading rate, for the loading rates employed. It has been shown by Jackson, et al. (Ref. 17) that only submillisecond loading rates influence the compressibility of cohesionless sands. It is assumed that sandy soils with an increasingly higher percentage of fines are more sensitive to loading rate. This relationship needs to be quantified for poorly sorted alluvium, or silty soils such as playas.

7.1.5 Cyclic Loading Effects. The laboratory tests and calculations in this study dealt with explosive or impulsive loadings, which generate motions having only a few cycles at most. However, a substantial amount of research has been done to investigate cyclic loading effects on soils, because of their importance in other dynamic loading phenomena. Some of the more important aspects of cyclic behavior are:

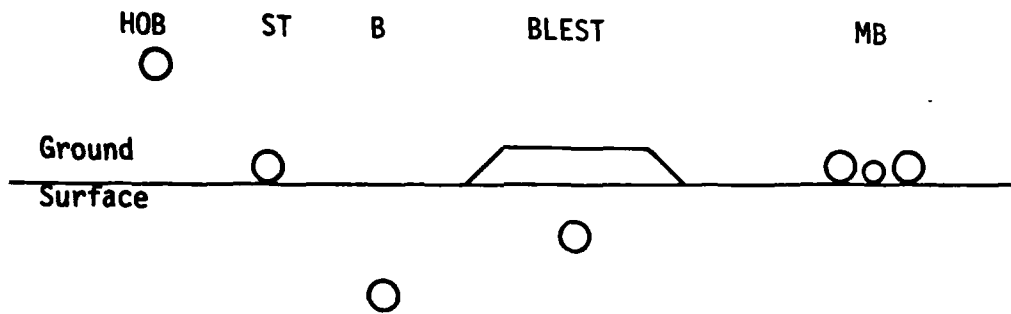
- a) Energy Dissipation. Each cycle of loading-unloading with hysteresis (even at low stress levels) represents a loss of energy through material damping. Damping characteristics are important for problems such as foundation vibration.
- b) Liquefaction. The tendency for changes in pore volume to occur during cyclic loading will cause excess pore water pressure buildup. This results in a drop in effective stress, which may cause shear failure.
- c) Modulus Degradation. As strains accumulate under many cycles of load, the shear modulus may decrease, resulting in an observed softening behavior.

7.1.6 High Pressure/Temperature Behavior. At very high pressures and temperatures the solid constituents of soil may undergo phase changes. These changes have important energy balance consequences for the soil system. The nature of these phenomena is typically explored through flyer plate and gas gun experiments.

7.2 Additional Aspects of the Insitu Behavior of Sand

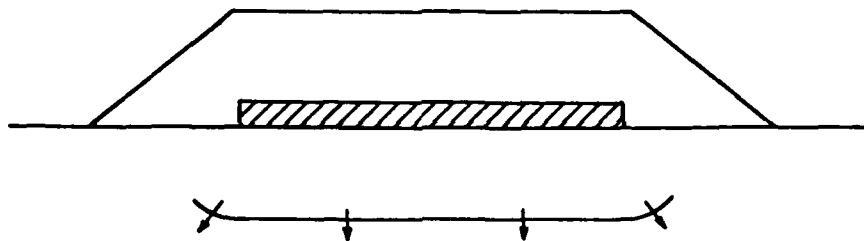
The calculations presented in this report address a specific aspect of dynamic soil behavior, insitu material property definition through high explosive tests. There are many other dynamic loading situations which involve additional responses fundamental to soils. They can be grouped into the following categories:

- a) Explosive Loading. These are high amplitude impulsive loads with relatively few cycles of motion. Several types of explosive load configurations are illustrated in Figure 35. Point sources may be either nuclear or high explosive, and vary in position with respect to the ground surface. HEST and DIHEST type loads are used to simulate nuclear environments, or to determine insitu material properties. There is a large amount of data on explosive effects in sandy soils, as shown in Table 4. The bulk of the data base comes from a few test sites, and is mostly for dry alluvium.
- b) Impact. Impact loads are similar to explosive loads, in that they are very impulsive and produce few cycles of motion.
- c) Earthquake. These loads usually have many cycles, and durations on the order of seconds. Transmission is typically in bedrock, and energy propagates to the surface through the soil. A common

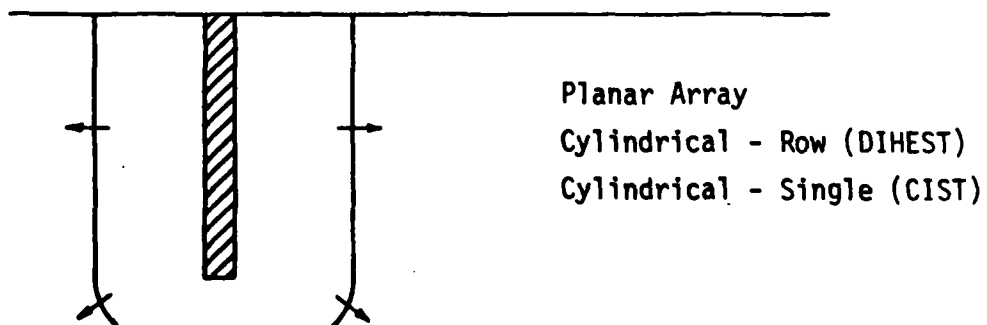


- HOB - Height of Burst
- ST - Surface Tangent
- B - Buried or Contained
- BLEST - Berm Loaded Simulation Technique
- MB - Multi-Burst

A. Point Sources



B. High Explosive Simulation Test (HEST)



C. Direct Induced

Figure 35. Types of Explosive Loading

Table 4. Summary of Major Explosive Events in Sandy Soils

Event	No. of Shots	Location	Date	Type of Explosive	Yield	Config.	HOB (ft)	Geology
Jungle 4	1	Area 10, NTS	Nov 51	NE	1.2 kt	SB	-17	Alluvium
Jungle 5	1	Area 10, NTS	Oct 51	NE	1.2 kt	SB	+3.5	Alluvium
Tumbler 1	1	FF, NTS	Apr 52	NE	1 kt	HOB	+800	Alluvium
Tumbler 2-4	3	FF, NTS	Apr 52	NE	1.2-30 kt	HOB	+1040-3450	Playa
W/K 1	1	FF, NTS	Mar 53	NE	16 kt	HOB	+300	Playa
W/K 9, 10	2	FF, NTS	May 53	NE	15, 26 kt	HOB	+500, 2400	Alluvium
Yacop ESS	1	Area 10, NTS	Mar 55	NE	1.2 kt	B	-67	Alluvium
Prifocilla	1	FF, NTS	Jun 57	NE	37 kt	HOB	+700	Alluvium
Johanna Bay	1	Area 10, NTS	Jul 62	NE	0.5 kt	SB	-2	Alluvium
Soda	1	Area 10, NTS	Jul 62	NE	100 kt	B	-635	Alluvium
Small Bay	1	FF, NTS	Jul 62	NE	-	SB	-10	Playa
Fisher	1	Area 3, NTS	Dec 61	NE	12.4 kt	B	-1190	Alluvium
Magnon	1	Area 3, NTS	Mar 62	NE	-	B	-784	Alluvium
Magnon	1	Area 3, NTS	Jun 62	NE	46 kt	B	-1340	Alluvium
Marlin	1	Area 3, NTS	Feb 65	NE	10 kt	B	-1972	Alluvium
Volcan	1	Area 2, NTS		NE	25 kt	B	-1067	Alluvium
Mugabelle	1	Area 2, NTS		NE	7.4 kt	B	-810	Alluvium
Peckard	1	Area 2, NTS		NE	10 kt	B	-810	Alluvium
Nite (200, 400)	26	Area 10, NTS	52-54	TNT	256 lb	SB-B	Var.	Alluvium
Sandia I, II	23	Area 10, NTS	Dec 58-Aug 59	TNT	256 lb	SB-B	-0-30	Alluvium
Toboggan	24	Area 6, NTS	Mar 59-Jun 60	TNT	8 lb	SB-B	-0-5	Playa
Stagcoach	3	Area 10, NTS	Mar 60	TNT	20 t	B	-17-80	Alluvium
Backboard	13	Area 10, NTS	Jun 60	TNT		B	-5-60	Alluvium
Scouter	1	Area 10, NTS	Oct 60	TNT	493 t	B	-125	Alluvium
Pre-Buggy	11	Area 5, NTS	62-63	TNT	1000 lb	B	-20	Alluvium
Air Vent I	1	Area 5, NTS	Dec 63	TNT	20 t	B	-18	Playa
Air Vent II	23	Area 5, NTS	Jan 64	TNT	256 lb	SB-B	-0-25	Playa
Flat Top II, III	2	Area 5, NTS	Feb-Mar 64	TNT	20 t	SB	+0	Playa
Nine Throw I	1	FF, NTS	Dec 71	ANFO	118 t	SH	+0	Alluvium
Pre-Nine Throw IV	9	FF, NTS	73-74	SH, TNT	0.128-100 t	SB	+0	Alluvium
CIST 5	1	Area 10, NTS	May 73	PETH	N/A	CIST	N/A	Dry Alluvium
CIST 6	1	Area 6, NTS	Jun 73	PETH	N/A	CIST	N/A	Playa
CIST 7	1	Area 5, NTS	Aug 73	PETH	N/A	CIST	N/A	Playa
BEK NEST 1	1	Mercury, NV	Sep 80	PETH	N/A	NEST	N/A	Dry Alluvium
CIST 22	1	Balston Val., NV	Mar 79	PETH	N/A	CIST	N/A	Dry Sand
BEK NEST	2	Balston Val., NV	Apr-Sep 81	PETH	N/A	NEST	N/A	Dry Sand
CIST 19	1	Pianet Ranch, AZ	May 77	PETH	N/A	CIST	N/A	Dry/Met Alluvium
Niners Bluff II	2	Pianet Ranch, AZ	Jun-Aug 78	ANFO	120 t	SB	+0	Dry/Met Sand
CIST 18	2	LAFBDR, AZ	Oct 76	PETH	N/A	CIST	N/A	Dry Alluvium/Granite
CAMEX-Dry	3+	LAFBDR, AZ	82-83	SH, PETH	N/A	B, SH	-68-0	Dry Alluvium
Pre-Bice Throw II	2	MSDR, NH	Aug-Sep 75	TNT, ANFO	100 t	SB	+0	Alluvium
CIST 15	1	MSDR, NH	Jul 75	PETH	N/A	CIST	N/A	Met Alluvium
CIST 16	1	MSDR, NH	Feb 76	PETH	N/A	CIST	N/A	Met Alluvium
Niners Bluff I	8	MSDR, NH	Aug-Dec 77	TNT	256 lb	SB, NB	+0	Alluvium
W11 Race	1	MSDR, NH	Sep 82	ANFO	500 t	SB	+0	Alluvium
Pre-Direct Course	1	MSDR, NH	Oct 82	ANFO	20 t	HOB	+57	Alluvium
Direct Course	1	MSDR, NH	Sep 83	ANFO	500 t	HOB	+166	Alluvium
Little Bitch	10	NCR, NH	Jun-Aug 60	TNT	256 lb	B	-3-13	Alluvium
Playa ANFO	1	NCR, NH		ANFO	1000 lb			Silty Playa
LD NEST II	1	NCR, NH	Dec 64	PETH	N/A	NEST	N/A	Dry Sand/Gravel
Pre-Cape	2	NCR, NH	Mar 65-Jun 68	TNT	256 lb			Alluvium
Cape	13	NCR, NH	Aug 66-Jul 68	TNT	977lb-15 t	B	-10-48	Alluvium
Bice Throw	1	NCR, NH	Oct 76	ANFO				Alluvium
Pre-Multiple Burst I	6	NCR, NH	Feb 77	C-4	10 lb	NB, NB	+0	Dry Alluvium
SIMPSON	4	NCR, NH	Mar 77-Oct 78	ANFO	N/A	DINEST	N/A	Dry Alluvium
Pre-Multiple Burst II	12	NCR, NH	Oct-Dec 78	TNT	256	B, SB, HOB	-18-+2	Dry Alluvium
Pre-Hybrid Burst	12	NCR, NH		C-4, TNT	30-256 lb	SB, NB	+0	Alluvium
Chert	1	NCR, NH	Aug 81	TNT	253 lb	B	-38	Dry Alluvium
3-1000 lb NB	1	NCR, NH	Aug 81	TNT	3 1000 lb	NB	+0	Dry/Met Alluvium
Jay Nite	1	Eniwetok, PPG	Oct 52	NE	10.4 Mt	SB	+10	Pacific Atoll
Castle Bravo	1	Bikini, PPG	Feb 54	NE	15 Mt	SB	+7	Pacific Atoll
Blackfoot	1			NE	-	HOB	+200	Pacific Atoll
Castle Koon	1	Bikini, PPG	Apr 54	NE	130 kt	SB	+14	Pacific Atoll
Eazy	1			NE	47 kt	HOB	+300	Pacific Atoll
George	1			NE	-	HOB	+300	Pacific Atoll
Lacross	1	Eniwetok, PPG	May 56	NE	39 kt	SB	+17	Pacific Atoll
Zuni	1	Bikini, PPG	May 56	NE	3.4 Mt	SB	+10	Pacific Atoll
Seminole	1	Eniwetok, PPG	Jun 56	NE	14 kt	SB	+7	Pacific Atoll
Tuna	1	Bikini, PPG	Jul 56	NE	4.6 Mt	SB	+12	Pacific Atoll
USA	1	Eniwetok, PPG	May 58	NE	1.4 Mt	SB	+3	Pacific Atoll
Cactus	1	Eniwetok, PPG	May 58	NE	18 kt	SB	+3	Pacific Atoll
Oak	1	Eniwetok, PPG	Jun 58	NE	9 Mt	SB	+7	Pacific Atoll
Peace	20	Eniwetok, PPG	Jun-Aug 72	TNT	1000 lb	SB	+0	Sat. Coral Sand
CIST 10	1	Eniwetok, PPG	Jul 74	PETH	N/A	CIST	N/A	Sat. Coral Sand
Wined Company	8	Grand Jct., CO	Jun-Nov 72	TNT	0.5-500 t	SB	+0	Sand/Sandstone
ESSE 2	1	McLaurin, MS	Aug-Nov 75	TNT	300 lb	B, SB, HOB	-3.3-+3.3	Met/Bry Clayey Silt
ESSE 1	9	Fort Polk, LA	74-75	TNT	8-12 t	B	0-35	Layered Sand, Silt, Clay
CIST 3	1	NH Site B1, ME	Nov 72	PETH	N/A	CIST	N/A	Dry Alluvium

Notes: NTS - Nevada Test Sites
 FF - Frenchman Flats
 YF - Yucca Flats
 LAFBDR - Luke Air Force Bombing and Gunnery Range
 MSDR - White Sands Missile Range
 NCR - McCormick Ranch Testing Range
 PPG - Pacific Proving Grounds
 NB - Nintaman
 SB - Surface Burst
 HOB - Height-of-Burst
 B - Buried
 NB - Half-Buried
 SH - Shaped
 NB - Multi-Burst
 Yield - TNT Equivalent
 N/A - Not applicable

assumption is that the waves in the soil are vertically propagating shear waves.

- d) **Wave-Induced.** Water waves produce oscillatory loads in underlying sediments.
- e) **Vehicular.** The wheels or tracks of a vehicle moving across the ground surface produce transient loads of a somewhat complicated nature.
- f) **Foundation Vibration.** These loads are transmitted from a moving foundation into the surrounding soil. Excitation may be due to machine vibrations, wind loads, impact, etc. Thus these loads can be either transient or steady state in nature, and can vary widely in magnitude and frequency.

Each type of dynamic loading may produce a different type of response. Several important types of dynamic soil behavior include:

- a) **Transient Waves.** Energy transmission through soil can be characterized by wave and phase velocity, peak stress, peak motion (acceleration, velocity, displacement), attenuation of peaks (energy dissipation), frequency content, rise time and duration.
- b) **Steady-State Waves.** A stationary wave pattern requires a steady-state source, due to the dissipative nature of soil.
- c) **Cratering.** The separation and ejection of material around a local source of energy.
- d) **Spall.** Soil may become distended (loss of particle-particle contact); also called lofting.
- e) **Creep.** Long term, time-dependent response.

f) Liquefaction. Loss of strength due to sudden drop in effective stress.

Table 5 shows the phenomena which are particularly important for each category of dynamic loading.

The dynamic phenomena mentioned above are manifestations of various aspects of soil behavior. Thus, on a fundamental level, soil behavior can be tied to specific observable phenomena, and this is done in Table 6. This table allows a material modeler to choose the behaviors which must be accounted for when a particular response is being calculated.

Table 5. Important Response Phenomena for Dynamic Loadings

Important Response Phenomena	Loading Case							
	Point Source Explosive	HEST	DIHEST	Impact	Earthquake	Wave Loads	Vehicle	Foundation Vibration
Transient Waves	X	X	X	X	X		X	X
Steady-State Waves						X		X
Cratering	X			X				
Spall	X		X	X			X	
Creep								X
Liquefaction	X	X	X	X	X	X	X	X

Table 6. Controlling Soil Behavior for Various Dynamic Response Phenomena in Sands

Controlling Soil Behavior	Dynamic Response Phenomena					
	Transient Waves	Steady State Waves	Cratering	Spall	Creep	Liquefaction
Non-Linear Volume and Shear	X	X	X	X	X	X
Permanent Deformation	X		X	X	X	
Elastic Unload	X			X		
Hysteresis		X				X
Shear-Volume Coupling	X	X	X	X		X
Pressure Dependent Shear Strength	X		X			
Strain Level Dependent Shear Strength	X	X				
Stress-History Dependency					X	X
Strain Rate Effects					X	
Anisotropy	X	X	X			
Effective Stress	X	X	X	X	X	X
Pore Fluid Movement				X		X
Minimal Tensile Strength			X	X		
Phase Changes	X		X			

8.0 TESTING CONSIDERATIONS

8.1 Ideal Testing Program

The purpose of a soil stress-strain test is to obtain data with which to predict the load-deformation response of a soil mass, for a particular field loading condition. In the context of the present research, the field loading of particular interest is an explosion, either nuclear or chemical, detonated above, at, or below the ground surface. The problem is how to make the prediction, i.e., what stress-strain data the soil test should yield, and how that stress-strain data should be used to calculate load-deformation response.

There are two principal philosophies or methods of soil stress-strain testing. The first is the Load Path philosophy. Under this philosophy the soil stress-strain test is designed to duplicate a representative field loading (stress or strain) path. The test data is then used directly in the field load-deformation prediction. An early example of this approach is use of confined compression (oedometer) data to predict foundation settlement. The two main problems with this method are: knowing what loading paths to use in the test; and for all but the simplest loading paths, constructing a test device capable of duplicating the desired loading paths.

The explosive loading problem involves a large variation in loading amplitudes, the interaction of propagating waves with materials of different properties and the free surface, the creation of new waves as a result of these interactions and the changes in the material states as these waves interact. Simplifying these complex conditions to a few

states of stress or strain has proven very difficult. Trullis (Ref. 9) has suggested that for a buried burst in a homogeneous media the strain paths are quite similar and independent of the properties of the media. Experiments to demonstrate the accuracy of this statement based on theoretical calculations have, to date, been unsuccessful. The strain paths calculated for surface burst are more complex and vary more, however, Trullis still maintains that they may be generalized. Experimental evaluation for this case is beyond the state-of-the-art in ground motion instrumentations. This analysis further requires that the soil sample be subjected to a tensile strain in a principal direction, which presents serious problems in developing a laboratory device to subject a sample to the required strain paths and allow measurement of the associated stresses.

The second philosophy is the Constitutive Model philosophy. Under this philosophy one assumes the existence of a mathematical constitutive model, sufficiently general and accurate to correctly predict soil stress-strain response for loading paths other than those used to formulate the model and evaluate its parameters. The constitutive model need not be the "one and only true model", but it must yield accurate predictions of load-deformation response for field loading cases of interest. The main elements in this method are: establishing what stress-strain mechanisms to model (and which ones to ignore), selecting a satisfactory model, deciding what tests are needed to evaluate the model parameters, constructing a test device capable of performing the required tests, and finally solving the field loading boundary value/propagation problem using the selected constitutive model.

The ideal soil stress-strain testing philosophy is a compromise between (or a combination of) the above two philosophies. It involves formulating a constitutive model based on test load paths as close as possible to the field loading paths. This approach combines the realism of the Load Path Method with the generality of the Constitutive Model Method.

The main decisions to be made in designing the above ideal laboratory soil stress-strain testing program for a given field (in this case explosive) loading situation involve:

- a) estimating the field loading path(s) and rates;
- b) selecting the constitutive model;
- c) defining the test loading path(s) and rates;
- d) stress versus strain control;
- e) effective versus total stress;
- f) sample shape;
- g) sample size;
- h) number of tests; and
- i) treatment of data scatter.

For a typical field explosive loading situation, the soil is initially in what approximates a K_0 condition, with an OCR ≥ 1 . The airslap-induced motion involves primarily vertical compression; and the upstream-induced motion involves primarily radial compression, outward radial displacement, and vertical compression. The outward radial displacement tends to produce circumferential tension; at least it relieves some of the Poisson compression caused by the radial and vertical compression. In addition, the combination of airslap and upstream-induced motion causes a rotation of principal planes about a circumferential axis.

One conceptually attractive soil stress-strain test device for the above situation is a strain-controlled hollow cylinder device, in which the inner and outer drums are capable of applying vertical shear stresses to the sample's inside and outside curved surfaces. A less ideal device, but one which already exists, is a stress-controlled hollow cylinder device, equipped to apply a torque along the cylinder axis. Both hollow cylinder devices have the advantage of being able to induce (circumferential) tension using (radial) compressive loading, but also have the disadvantage of creating a nonhomogeneous state of stress and strain in the sample. In addition, the axis of principal stress rotation in the stress-controlled hollow cylinder test is radial, rather than circumferential. Both devices will yield stress-strain and strength data for which the three principal stresses are distinct. A rapid method for plotting such data in the octahedral plane has been devised by Merkle (Ref. 18).

8.2 Modeling Requirements

The two principal requirements of a soil constitutive model for field explosive loading applications are that it include all important physical mechanisms, and be computationally efficient.

The principal requirements for the above model are:

- a) behavior is controlled by effective stress;
- b) considers pore fluid compressibility and flow characteristics;
- c) dynamic hydrostat may be concave to the strain axis at low stress, but is convex to the strain axis at high stress;
- d) shear (deviator) stress-strain curve concave to the strain axis up to the point of peak strength, but may exhibit strain softening beyond that point to approach a lower residual strength;

- e) peak and residual shear strengths increase with increasing confining pressure, with nonlinear effects often important at very high confining pressure;
- f) very low tensile strength, with post tensile failure stress redistribution;
- g) inelastic volumetric and deviatoric strains accumulate from the onset of loading;
- h) exhibits both volumetric and deviatoric hysteresis;
- i) exhibits shear strain/volume strain coupling (dilatancy), controlled by previous strain history;
- j) plastic flow rule may be nonassociative (i.e., plastic strain increments may not be normal to the yield surface);
- k) accomodates a geologically realistic initial (K_0 consolidation) condition, with an OCR > 1.

None of the soil constitutive models yet exercised by the SEM satisfied all the above requirements. However, the AFWL Engineering and cap models both have several desirable features, including familiarity within the groundshock community. They are therefore prime candidates for possible improvement in the next phase of this research, the objective of which is to develop a model satisfying as many of the above requirements as possible.

9.0 SUMMARY

The FY82 phase of the study Fundamental Properties of Soils for Complex Dynamic Loadings focused on dynamic constitutive modeling of sandy soils. Four constitutive models of explosively loaded sand were studied:

- a) elastic-plastic;
- b) AFWL Engineering;
- c) cap;
- d) hyperbolic.

A one-dimensional wave propagation feature was added to the Soil Element Model (SEM) to study the influence of a constitutive model on wave propagation effects. Insitu material property tests CIST 22 and DISC Test II were modeled in one and two dimensions, using the above four constitutive models, and the calculated and measured results were compared. The SEM was also used to assess the performance of the four constitutive models against the results of laboratory tests on three sands conducted by the U.S. Army Engineer Waterways Experiment Station.

A principal conclusion to be drawn from the above comparisons of calculated and measured results is that dilatancy, the coupling between shear and volumetric strain, needs additional attention in constitutive modeling of cohesionless soils.

The conceptually ideal laboratory soil testing device for explosive loading applications is a strain-controlled hollow cylinder device. Theoretically it has the capability to induce radial compression, hoop expansion due to outward radial displacement, vertical compression, and rotation of principal planes about the circumferential axis.

REFERENCES

1. Dass, W.C., Bratton, J.C., and Higgins, C.J., "Fundamental Properties of Soils for Complex Dynamic Loadings: Annual Technical Report," Report No. AFOSR-TR-82-0101, Applied Research Associates, Inc., Albuquerque, NM, January, 1982.
2. Duncan, J.M., and Chang, C.Y., "Nonlinear Analysis of Stress and Strain in Soils," Journal of the Soil Mechanics and Foundation Engineering Division, ASCE, Vol. 96, No. SM5, Proc. Paper 7513, September 1970, pp. 1629-1653.
3. Lade, P.V. and Nelson, R.B., "Incrementalization Procedure for Elasto-Plastic Constitutive Model with Multiple, Simultaneous Yield Surfaces," Implementation of Computer Procedures and Stress-Strain Laws in Geotechnical Engineering, Desai and Saxena, eds., Acorn Press, Durham, NC, August, 1981.
4. Hart, R.D., "A Fully Coupled Thermal-Mechanical-Fluid Flow Model for Nonlinear Geologic Systems," Thesis presented to the University of Minnesota, Minneapolis, MN, in partial fulfillment of the requirements for the degree of Doctor of Philosophy, March, 1981.
5. Phillips, B.R., "Mechanical Response of Dry Reid-Bedford Model Sand and Saturated Misers Bluff Sand," U.S. Army Engineer Waterways Experiment Station, January, 1982.
6. Phillips, B.R., "Mechanical Properties of Misers Bluff Sand," U.S. Army Engineer Waterways Experiment Station, Vicksburg, MS, May, 1982.
7. Phillips, B.R., "Mechanical Properties of Reid Bedford Model Sand," U.S. Army Engineer Waterways Experiment Station, Vicksburg, MS, September, 1982.
8. Workman, J.W., Trulio, J.G., and Stokes, E.S., "Modeling the Behavior of Geologic Materials in Explosive Field Events," Report No. AFWL-TR-80-66, Applied Theory, Inc., Los Angeles, CA, January, 1981.
9. Phillips, B.R., "MX Task V-1: Results of Laboratory Tests on the Subsurface Materials Obtained from the Ralston Valley and Dry Lake Valley Geotechnical Study Sites," U.S. Army Engineer Waterways Experiment Station, Vicksburg, MS, December, 1980.
10. Phillips, B.R., and Jackson, A.E., Jr., "Ralston Valley Soil Compressibility Study: Laboratory Test Results," U.S. Army Engineer Waterways Experiment Station, Vicksburg, MS, February, 1982.
11. "Baseline Material Properties of Dry Sand Alluvium for MX/DDB Ground Shock Calculations," letter from A.E. Jackson, U.S. Army Engineer Waterways Experiment Station, Vicksburg, MS, to Commander, Ballistic Missile Office, Norton AFB, CA, 16 June, 1982.

12. Lodde, P.F., and Thomas, J.N., "Ralston Valley, Nevada, Cylindrical In Situ Test (CIST 22): Data and Material Model Report," Report No. AFWL-TR-80-115, New Mexico Engineering Research Institute, University of New Mexico, Albuquerque, NM, May, 1981.
13. Jackson, A.E., Jr., Murrell, D.W., Zelasko, J.S., and Skinner, F.W., Jr., "Ralston Valley Soil Compressibility Study: Quick Look Report for DISC Test I," U.S. Army Engineer Waterways Experiment Station, Vicksburg, MS, May, 1981.
14. Jackson, A.F., Jr., and Zelasko, J.S., "Ralston Valley Soil Compressibility Study: Quick Look Report for DISC Test II," U.S. Army Engineer Waterways Experiment Station, Vicksburg, MS, January, 1982.
15. Hofmann, R., "STEALTH, A Lagrange Explicit Finite-Difference Code for Solids, Structural and Thermohydraulic Analysis," Report No. EPRI NP-176 (Summary), Electric Power Research Institute, Palo Alto, CA, June, 1976.
16. Skempton, A.W., "The Pore-Pressure Coefficients A and B," Geotechnique, Vol. 4, 1954, pp. 143-147.
17. Jackson, J.G., Jr., Ehrgott, J.Q., and Rohani, B., "Loading Rate Effects on Compressibility of Sand," Journal of the Geotechnical Engineering Division, ASCE, Vol. 106, No. GT8, Proc. Paper 15640, August, 1980, pp. 839-852.
18. Merkle, D.H., "The Effective Stress Mechanics of Undrained Shear Strength," Report No. AFWL-TR-71-85, Air Force Weapons Laboratory, Kirtland AFB, NM, July, 1971.

APPENDIX A

WES Laboratory Tests (Refs. 5 and 6)

The isotropic compression (IC) test subjects a cylindrically shaped specimen to an equal all-around confining pressure while measurements of the specimen's height and diameter changes are made. The data are normally plotted as pressure versus volumetric strain, the slope of which is the bulk modulus, K .

The triaxial compression (TXC) test is conducted after a desired confining pressure is applied during the IC test. While the confining pressure is held constant, axial load is increased and measurements of the specimen's height and diameter changes are made. The data can be plotted as principal stress difference versus axial strain, the slope of which is Young's modulus E , or as principal stress difference versus principal strain difference, the slope of which is twice the shear modulus G . The maximum principal stress difference the specimen can support or the principal stress difference at 15 percent axial strain during shear loading (whichever occurs first) is defined as failure and describes one point on a failure surface under positive principal stress difference states of stress. The failure surface is depicted as a plot of principal stress difference versus mean normal stress.

The triaxial extension (TXE) test is also conducted after a desired confining pressure is applied during the IC test. While lateral pressure is held constant, vertical pressure is decreased and measurements of the specimen's height and diameter changes are made. As with the TXC test, the data are plotted as principal stress difference versus axial strain or

as principal stress difference versus principal strain difference. The maximum negative principal stress difference or the point at which the material separates (whichever occurs first) is defined as failure and describes one point on a failure surface under a negative principal stress difference state of stress.

Three types of uniaxial strain (UX) tests were conducted:

- 1) The first (designated UX) is conducted by applying an axial (vertical) pressure to a wafer-shaped specimen that is physically constrained from deflecting radially. Measurements are made of the applied axial stress and the specimen's height change. The data are plotted as axial (vertical) stress versus axial (vertical) strain, the slope of which is the constrained modulus M .
- 2) The second type of UX test (designated UX/ K_0) is conducted by applying radial pressure to a cylindrically shaped specimen until a slight inward movement of the diameter is detected. Axial load is then applied until the specimen returns to its original radial position (zero radial strain). This process is repeated throughout the loading and unloading. As in the UX test, the data are plotted as axial stress versus axial strain, the slope of which is the constrained modulus M . When the data are plotted as principal stress difference versus mean normal stress, the slope is $2G/K$ or, in terms of Poisson's ratio ν , $3(1-2\nu)/(1+\nu)$.
- 3) The third type of UX test (designated UX/Null) is similar to the K_0 test in that both radial and vertical pressures are

controlled. A wafer-shaped specimen is remolded in a thin-walled steel cylinder which is strain gaged on the outside. As vertical pressure is applied, the circumferential strain (measured by the strain gages) on the steel cylinder is kept at zero by applying lateral pressure to the cylinder. This process is continued throughout the test. The data are plotted and properties deduced the same as those for the UX/K₀ test.

APPENDIX B

Material Model Descriptions

The following are brief descriptions of the models used to calculate the laboratory behavior of the sands discussed in this report.

B.1 Elastic-Plastic Model

This model uses a linear hydrostatic stress-strain relationship in both loading and unloading. The shear stress-strain response is also linear up to a failure state, after which the material behaves as an ideally plastic material. The failure condition is defined by a surface in stress space which is symmetric about the p-axis. Figure B-1 shows the model components and defines the model parameters as used in the SEM.

B.2 AFWL Engineering Model

This model is essentially a version of the elastic-plastic model, modified to allow piecewise elastic approximation of nonlinear behavior and volume compaction. The model is defined with a hydrostat (in pressure versus volume strain space), a constant Poisson's Ratio prior to failure, and a failure surface (in invariant stress space). Tensile stresses are limited by a minimum pressure cutoff. Plastic strains at failure are defined by a nonassociative flow rule, because stress excursions exceeding the failure surface are corrected vertically (i.e., at constant pressure) back to the failure state. Figure B-2 defines the SEM parameters for the AFWL model.

B.3 Cap Model

The behavior of the cap model in the elastic regime is governed by elastic bulk and shear moduli. The bulk modulus is a function of

pressure, and the shear modulus depends on the second invariant of the stress deviator tensor, J'_2 . The plastic behavior of the model is described in stress space by a modified Drucker-Prager failure surface and an elliptical strain-hardening cap. The failure surface is stationary (in this version), and the movement of the cap is controlled by the amount of plastic volumetric strain the material has experienced. The cap model is an effective stress model, in that it can represent both drained and undrained volumetric behavior simulating effective and total stress responses, respectively. Pore pressure response of the material is then readily calculated by subtracting effective from total stresses.

Figure B-3 illustrates the cap model and defines the SEM cap parameters.

B.4 Hyperbolic Model

This model combines a hyperbolic curve-fit to triaxial shear stress-strain response with a simple bilinear hydrostat for volumetric response. Figure B-4 shows the hydrostatic and shear response parameters, and how the shear parameters are calculated.

B.5 Model Parameters

Tables B-1 through B-4 list model parameters for MB and RB sands, and RV alluvium. These parameters were determined on the basis of laboratory results only.

HD-R131 284

FUNDAMENTAL PROPERTIES OF SOILS FOR COMPLEX DYNAMIC
LOADINGS: DYNAMIC CON. (U) APPLIED RESEARCH ASSOCIATES
INC ALBUQUERQUE NM W C DASS ET AL. APR 83
AFOSR-TR-83-0653 F49620-80-C-0088

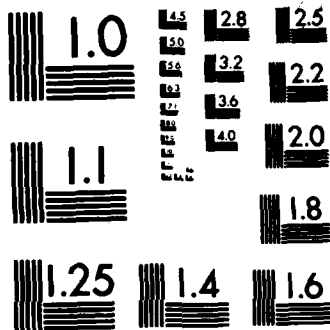
2/2

UNCLASSIFIED

F/G 8/13

NL

									END			
									FORMED			
									...			
									...			



MICROCOPY RESOLUTION TEST CHART
NATIONAL BUREAU OF STANDARDS-1963-A

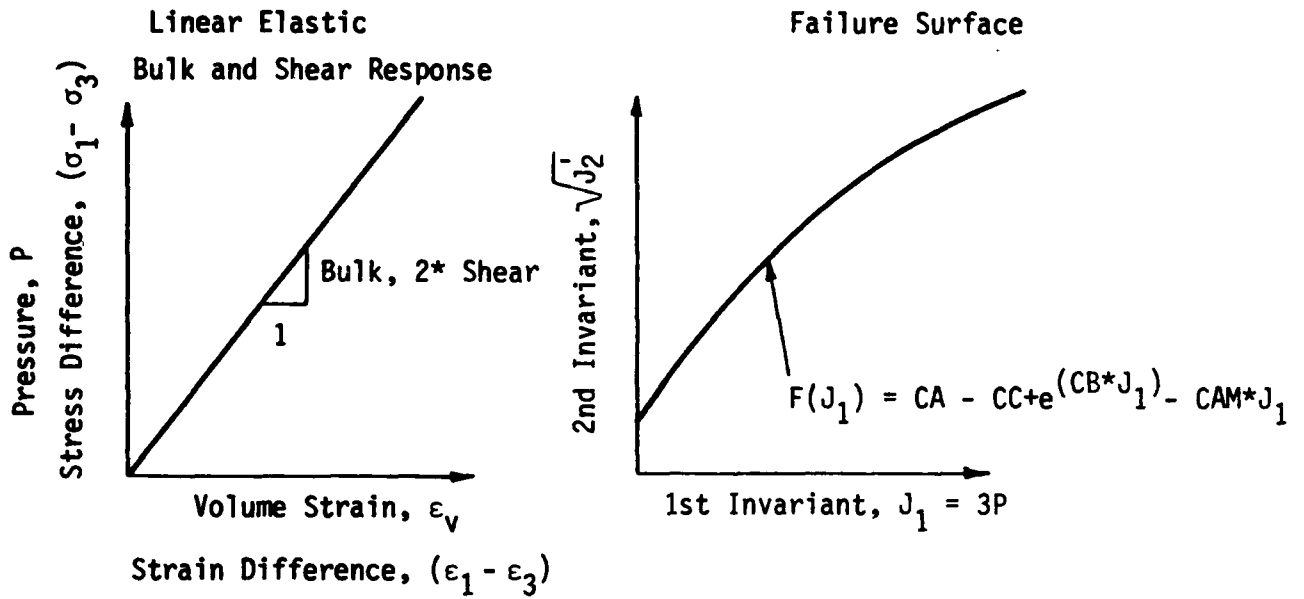


Figure B-1. Elastic-Plastic Model

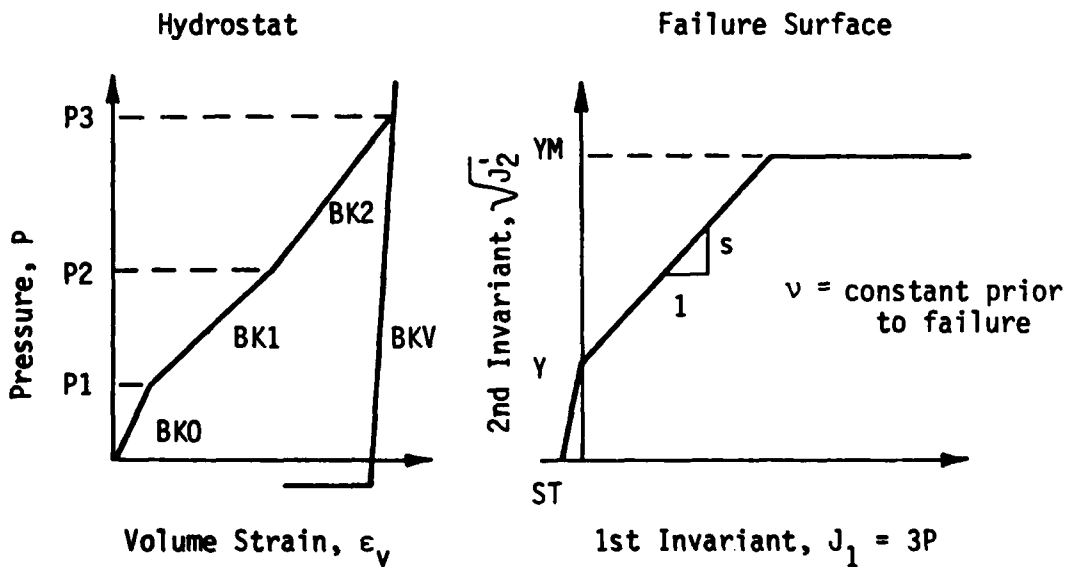


Figure B-2. AFWL Engineering Model

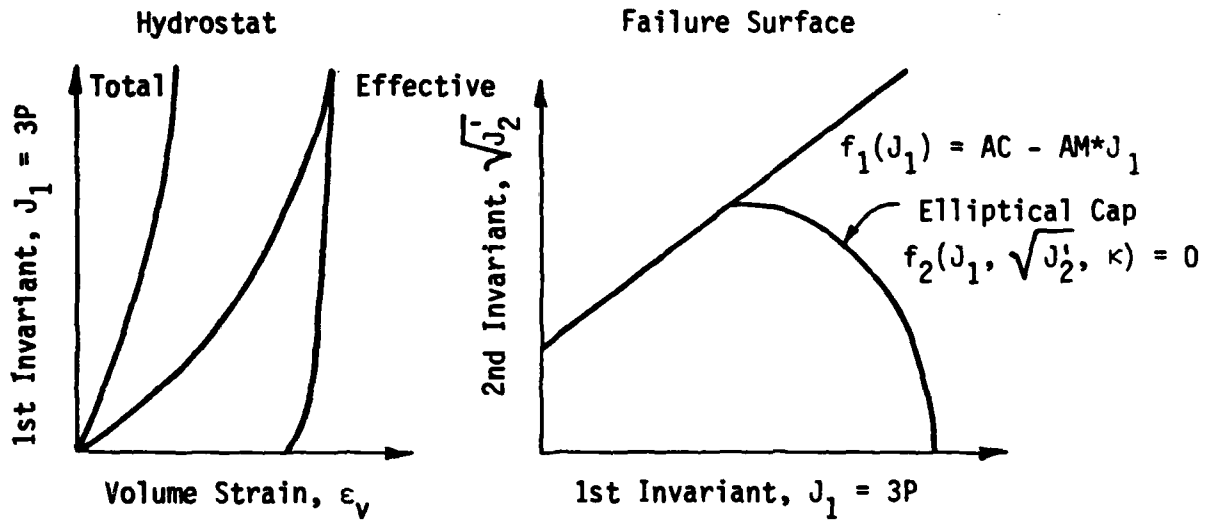
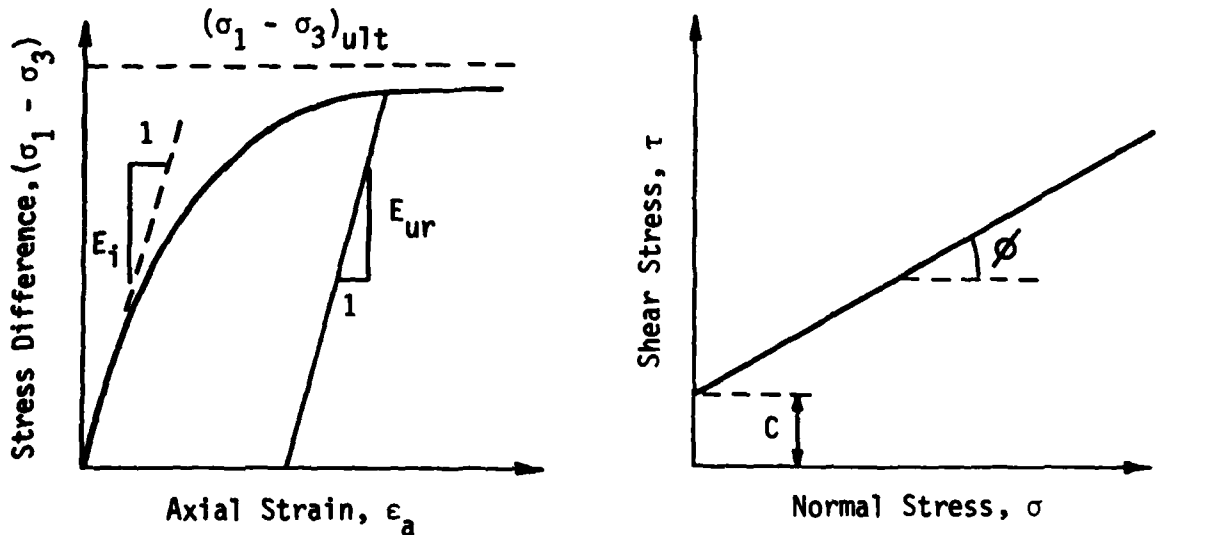


Figure B-3. Cap Model



$$(\sigma_1 - \sigma_3) = \frac{\epsilon}{\frac{1}{E_1} + \frac{\epsilon}{(\sigma_1 - \sigma_3)_{ult}}}$$

$$E_1 = K_{pa} \left(\frac{\sigma_3}{p_a}\right)^n$$

$$E_{ur} = K_{ur} p_a \left(\frac{\sigma_3}{p_a}\right)^n$$

$$(\sigma_1 - \sigma_3)f = \frac{2c \cos\phi + 2\sigma_3 \sin\phi}{1 - \sin\phi}$$

$$(\sigma_1 - \sigma_3)_{ult} = (\sigma_1 - \sigma_3)f/Rf$$

$$v = \frac{G - F \log(\sigma_3/p_a)}{(1 - d \epsilon_a)^2}$$

Figure B-4. Hyperbolic Curve-Fitting Model

Table B-1. Elastic-Plastic Model Parameters

Parameter	Name	Units	MB Sand (Dry)	MB Sand (Sat)	RB Sand (Sat)	RB Sand (Sat)	RV Alluvium (0-6 m)
Bulk Modulus	BULK	Pa	156E6	156E6	387E6	536E6	188E6
Shear Modulus	SHEAR	Pa	60E6	60E6	295E6	206E6	72E6
Failure Surface	CA	Pa	0.0	0.0	0.0	50E6	0.06E6
	CB	1/Pa	0.0	0.0	0.0	5.1E-9	0.0
	CC	Pa	0.0	0.0	0.0	50E6	0.0
	CAM	-	0.267	0.257	0.211	0.0	0.269
Tensile Strength	TCUT	Pa	0.0	0.0	0.6E6	0.0	0.0
Flow Rule	RULE	-	1.0	1.0	1.0	1.0	1.0
Density	RHOREF	kg/m ³	1710	2120	1650	2030	1930

Table B-2. Modified AFWL Engineering Model Parameters

Parameter	Name	Units	MB Sand (Dry)	MB Sand (Sat)	RB Sand (Dry)	RB Sand (Sat)	RV Alluvium (0-6 m)
Poisson's Ratio (load)	POISL	-	0.35	0.33	0.35	0.35	0.33
Poisson's Ratio (unload)	POISU	-	0.25	0.25	0.25	0.25	0.28
Loading Bulk Modulus	BKO	Pa	85E6	187E6	175E6	494E6	209E6
Unload Bulk Modulus	BKL1	Pa	191E6	114E6	518E6	597E6	153E6
	BKL2	Pa	346E6	274E6	439E6	543E6	330E6
Breakpoints	BKU	Pa	3600E6	5850E6	5622E6	4537E6	6667E6
	P1	Pa	2.2E6	2.8E6	1.7E6	4.3E6	2.3E6
	P2	Pa	14.8E6	10.1E6	11.6E6	15.7E6	20.0E6
Tensile Strength Intercept	P3	Pa	30.0E6	30.0E6	30.0E6	30.0E6	53.0E6
	ST	Pa	0.0	0.0	-0.6E6	0.0	-0.1E6
FS Slope	Y	Pa	0.0	0.0	0.12E6	0.0	0.058E6
Von Mises Limit	S	-	0.267	0.257	0.211	0.252	0.269
Density	VM	Pa	100E6	100E6	100E6	50E6	145E6
	RHOREF	kg/m ³	1710	2120	1650	2030	1930

Table B-3. Cap Model Parameters

Parameter	Name	Units	MB Sand (Dry)	MB Sand (Sat)	RB Sand (Dry)	RB Sand (Sat)	RV Alluvium (0-6 m)
Effective Stress	AKI	Pa	208E6	290E6	160E6	138E6	200E6
Hydrostat	AK1	-	0.978	0.984	0.969	0.977	0.983
Total Stress	AK2	1/Pa	4.12E-9	3.24E-9	1.41E-8	1.43E-8	5.89E-8
Hydrostat	AKIM	Pa	-	5840E6	-	8465E6	5840E6
Shear Response	AK1M	-	-	5.0E-4	-	5.0E-4	5.0E-4
	AK2M	1/Pa	-	1.19E-8	-	7.22E-8	1.20E-8
	AGI	Pa	110E6	170E6	96E6	65E6	90E6
	AG1	-	0.900	0.920	0.900	0.960	0.990
	AG2	1/Pa	4.7E-6	1.7E-7	3.3E-6	8.0E-6	5.0E-6
FS Cohesion	AC	Pa	0.05E6	0.0	0.12E6	0.1E6	0.06E6
FS Slope	AM	-	0.267	0.257	0.211	0.252	0.269
Cap Shape	ARI	-	2.5	3.0	3.5	3.5	2.3
Hardening	AW	-	0.36	0.36	0.30	0.30	0.50
Density	AD	1/Pa	1.2E-8	1.2E-8	4.4E-9	2.7E-9	7.5E-9
	RHOREF	kg/m ³	1710	2120	1650	2030	1930

Table B-4. Hyperbolic Model Parameters

Parameter	Name	Units	MB Sand (Dry)	RB Sand (Dry)
Modulus Number	K	-	990	21
Modulus Exponent	n	-	0.29	1.45
Failure Ratio	R _f	-	0.75	0.99
Cohesion	c	Pa	0.0	0.4E6
Friction Angle	ϕ	degrees	34	26
Unload/Reload Modulus No.	K _{ur}	-	24800	10946
Poisson's Ratio	G	-	0.44	0.44
	F	-	0.08	0.08
	d	-	8.2	8.2
Density	RHOREF	kg/m ³	1710	1650

APPENDIX C

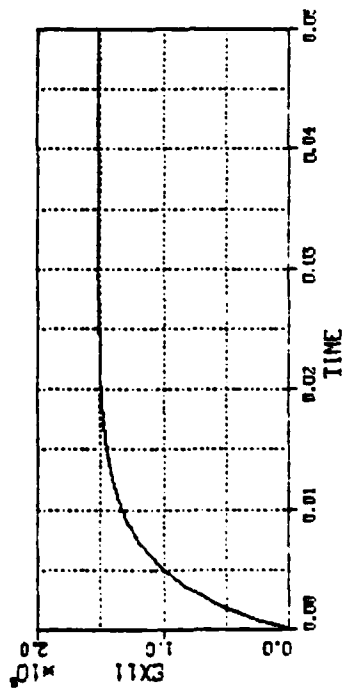
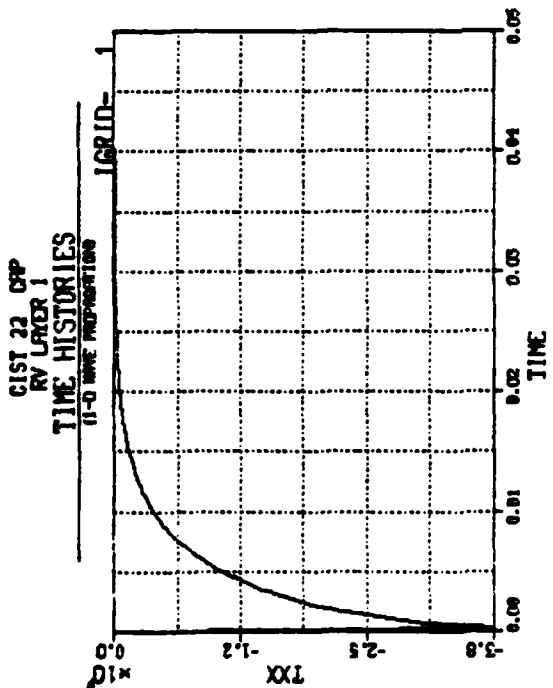
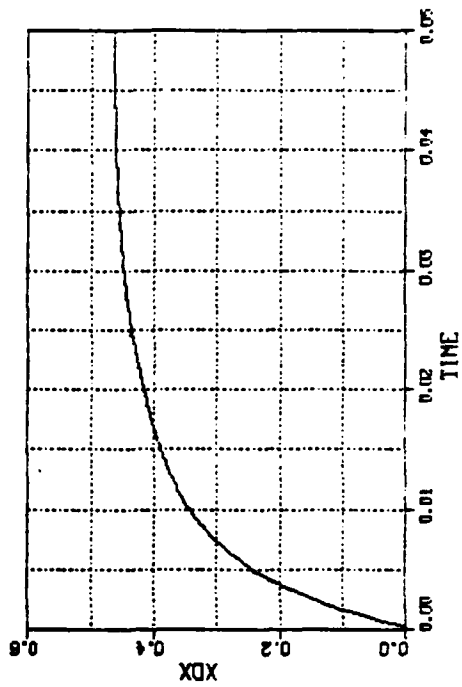
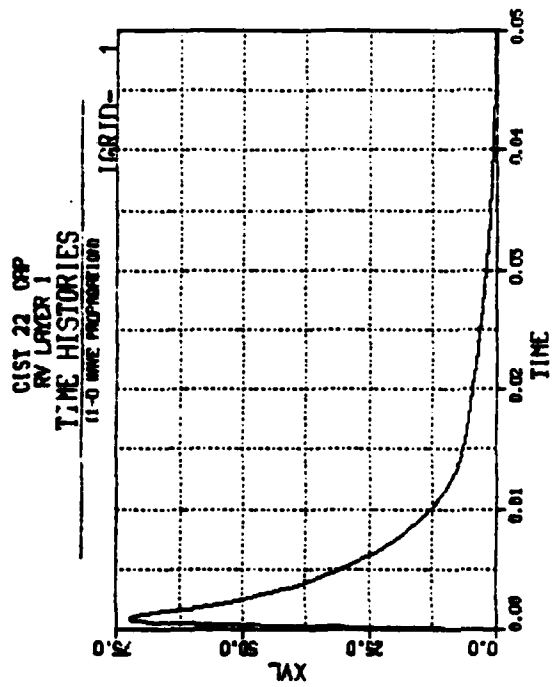
Sample Results from SEM Finite Difference Calculations

Notes

Problem No. - C22-4
Geometry - One-D Axisymmetric
Material - RV Alluvium
Model - Laboratory Based cap
Loading - CIST (Exponential)
Units - Meters, Pascals, Seconds
TXX - Normal Stress (Pa)
TYY - Hoop Stress (Pa)
EX11 - Impulse (Pa-s)
XVL - Velocity (m/s)
XDX - Displacement (m)
"Axial" - Radial Direction
"Radial" - Hoop Direction

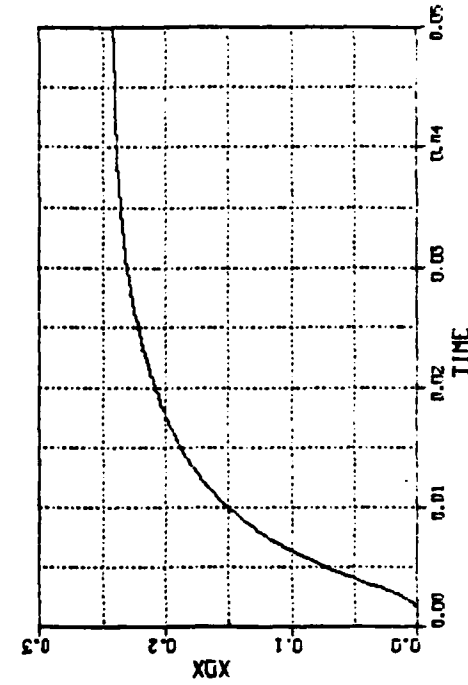
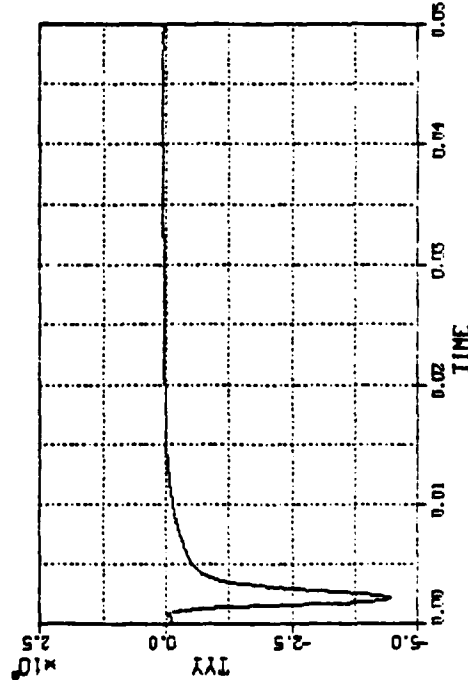
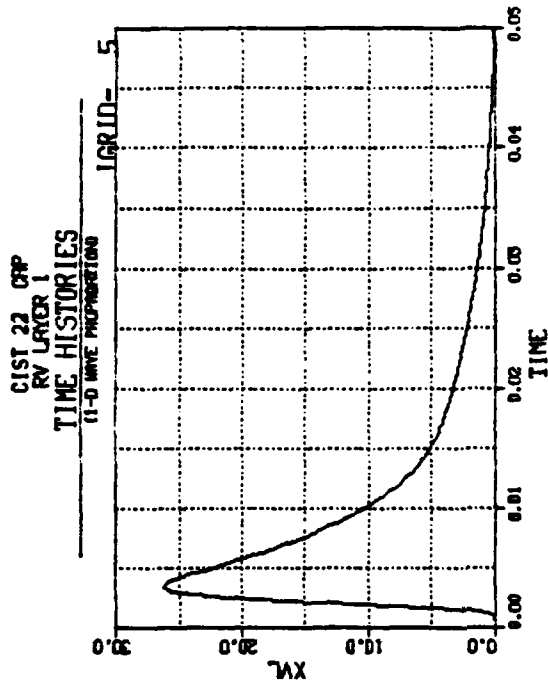
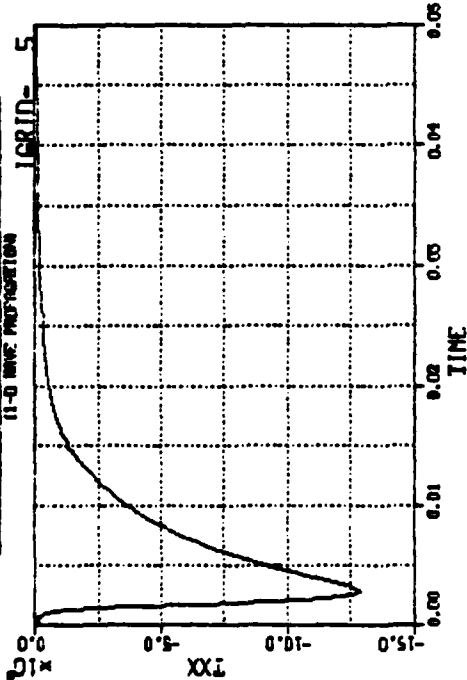
<u>Grid Point</u>	<u>Range (m)</u>
1	0.30
5	0.91
9	1.52
15	2.44
23	3.66

ARR SOIL ELEMENT MODEL VERSION 1 .JRN63



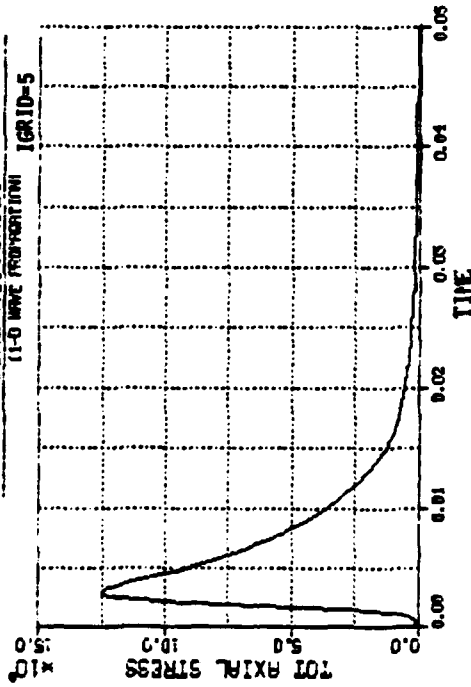
ARA SOIL ELEMENT MODEL VERSION 1 JUN83

CIST 22 OPP
RV LAYER 1
TIME HISTORIES
11-D WAVE PROPAGATION

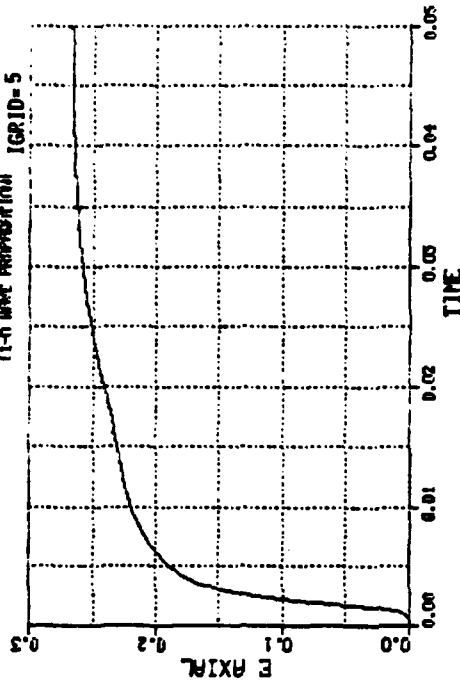


ARA SOIL ELEMENT MODEL, VERSION 1 JUN63

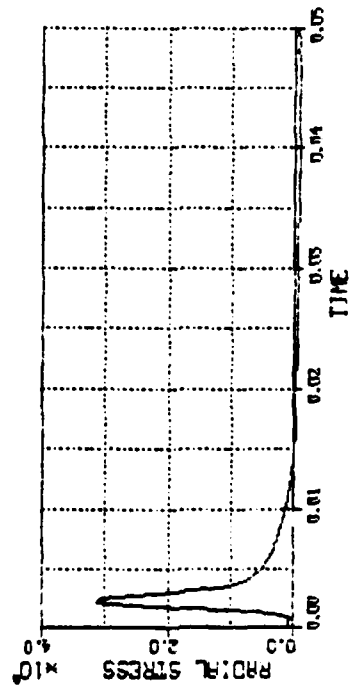
CIST 22 CAP
RV LAYER 1
TIME HISTORIES
(1-0 WAVE PROPAGATION) IGRID=5



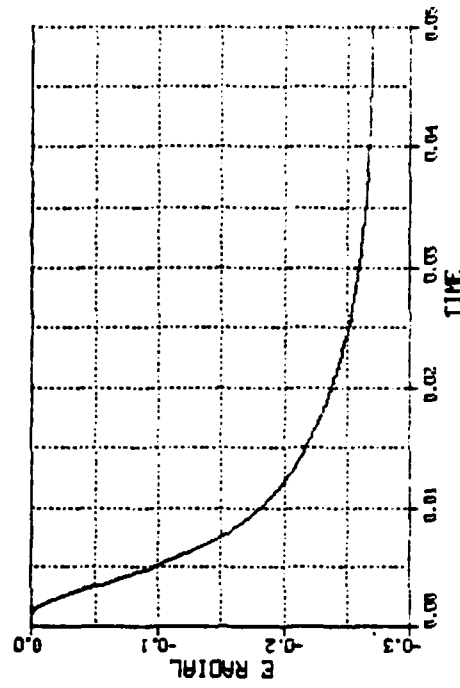
CIST 22 CAP
RV LAYER 1
TIME HISTORIES
(1-0 WAVE PROPAGATION) IGRID=5



CIST 22 CAP
RV LAYER 1
TIME HISTORIES
(1-0 WAVE PROPAGATION) IGRID=5

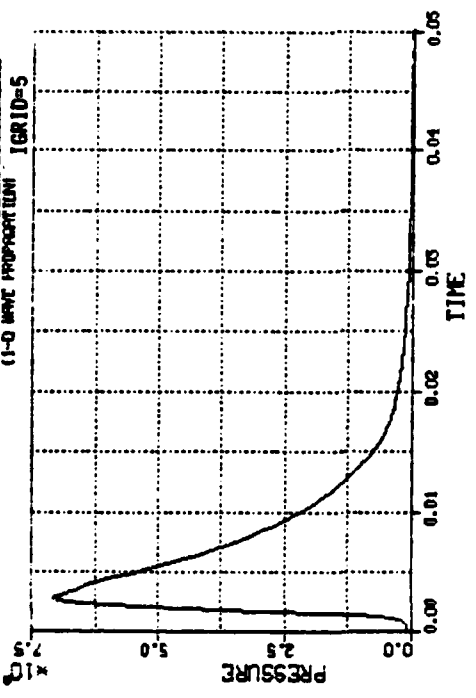


CIST 22 CAP
RV LAYER 1
TIME HISTORIES
(1-0 WAVE PROPAGATION) IGRID=5

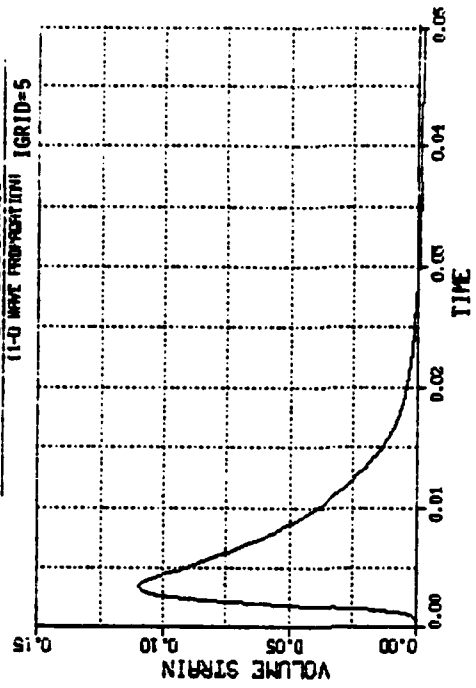


ARI1 SOIL ELEMENT MODEL VERSION 1 .FN83

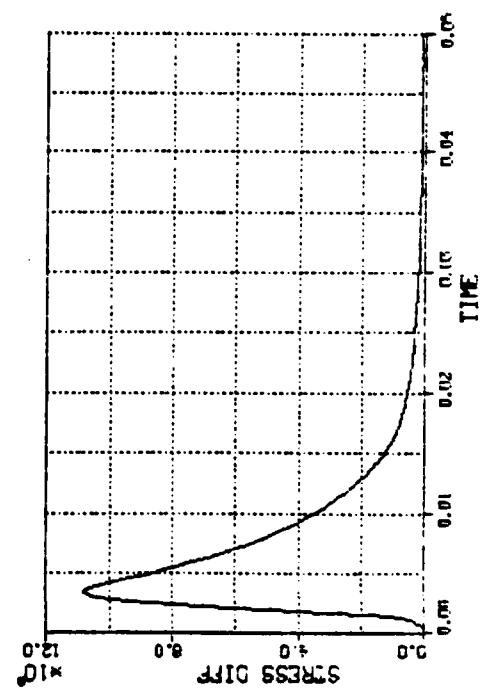
CIST 22 CPP
RV LAYER 1
TIME HISTORIES
(1-0 WAVE PROPORTION) IGRID=5



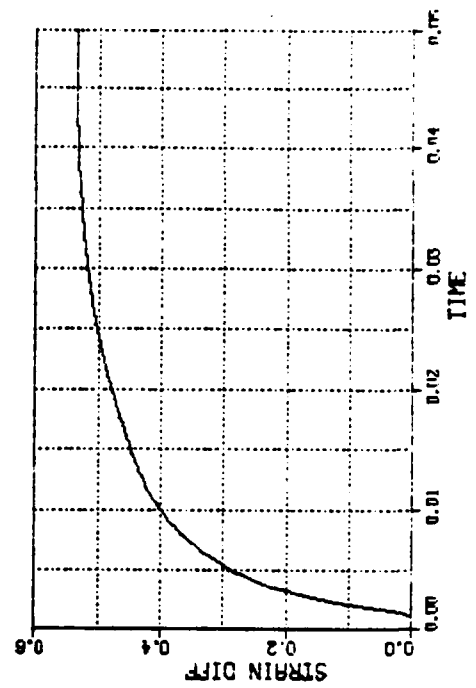
CIST 22 CPP
RV LAYER 1
TIME HISTORIES
(1-0 WAVE PROPORTION) IGRID=5



CIST 22 CPP
RV LAYER 1
TIME HISTORIES
(1-0 WAVE PROPORTION) IGRID=5



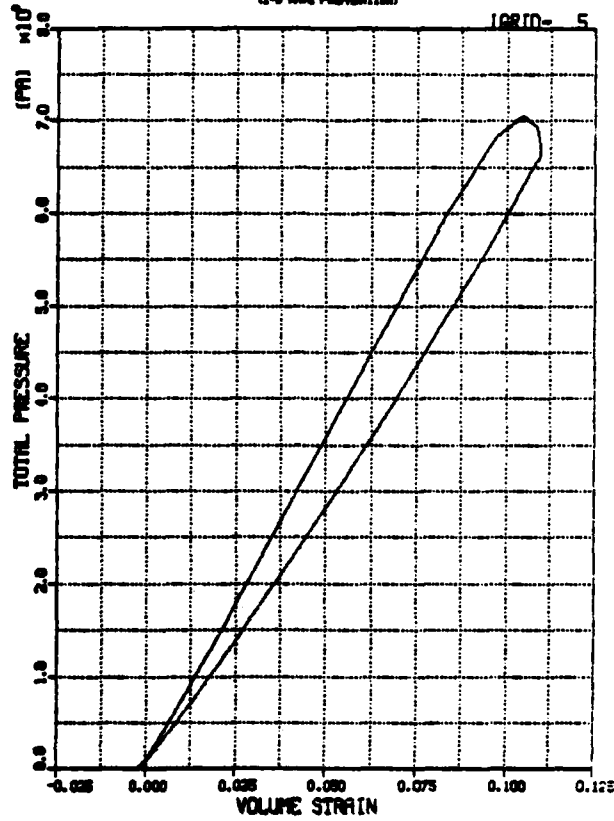
CIST 22 CPP
RV LAYER 1
TIME HISTORIES
(1-0 WAVE PROPORTION) IGRID=5



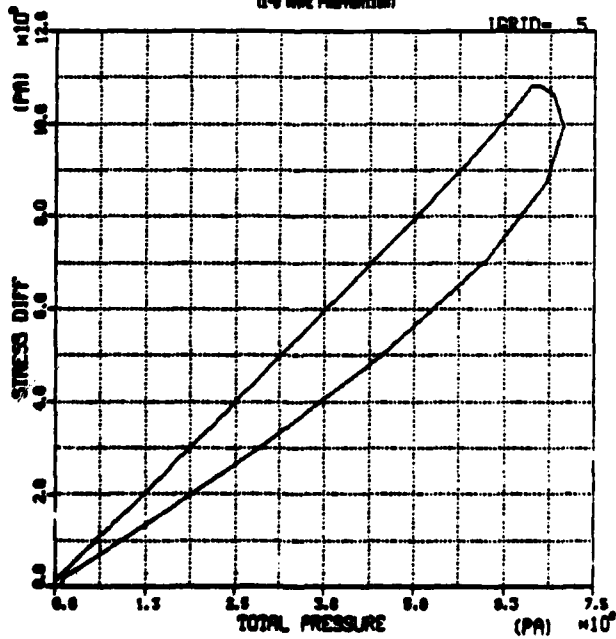
ABA SOIL ELEMENT MODEL VERSION 1 JAN83

CIST 22 OPP
RV LAYER 1

PRESSURE VS. VOLUMETRIC STRAIN
(1-0 HIVE PROPORTION)



CIST 22 OPP
RV LAYER 1
STRESS DIFFERENCE VS. PRESSURE
(1-0 HIVE PROPORTION)

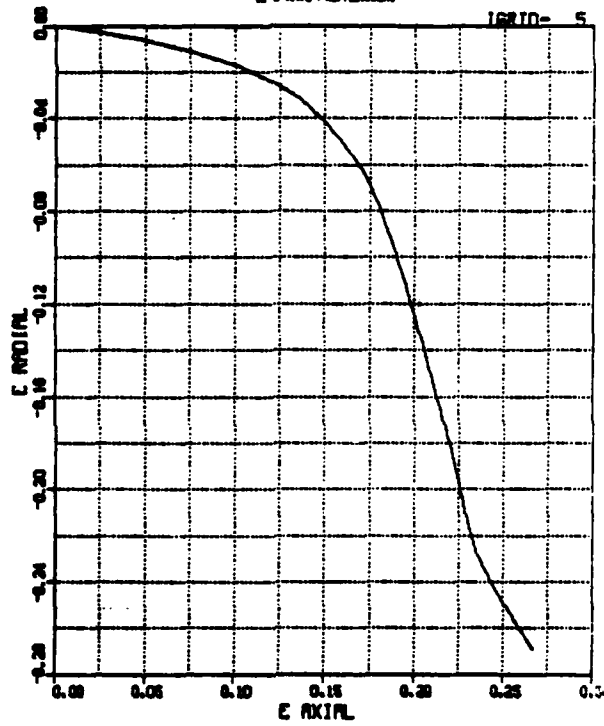


AAA SOIL ELEMENT MODEL VERSION 1 JAN83

CIST 22 OPP
RV LAYER 1

E RADIAL VS. E AXIAL

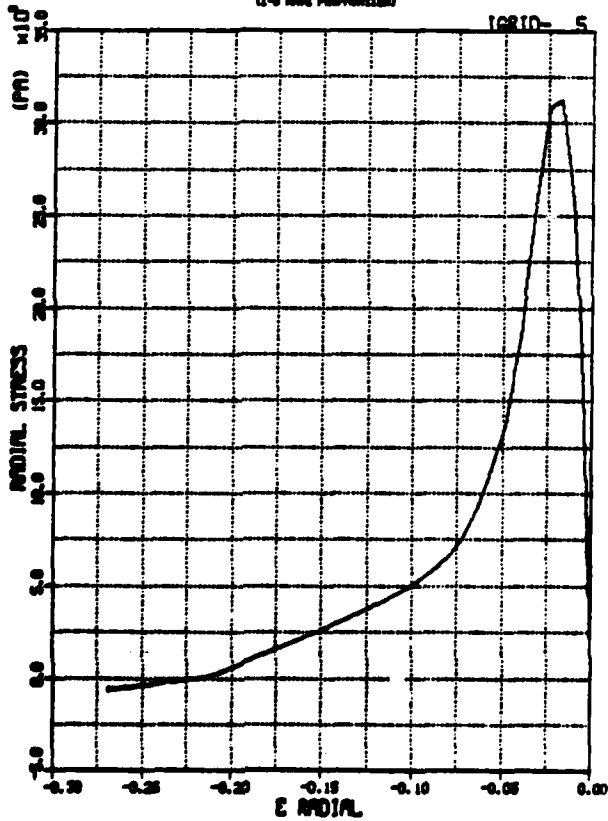
(1-8 MORE PREPARED)



CIST 22 OPP
RV LAYER 1

RADIAL STRESS VS RADIAL STRAIN

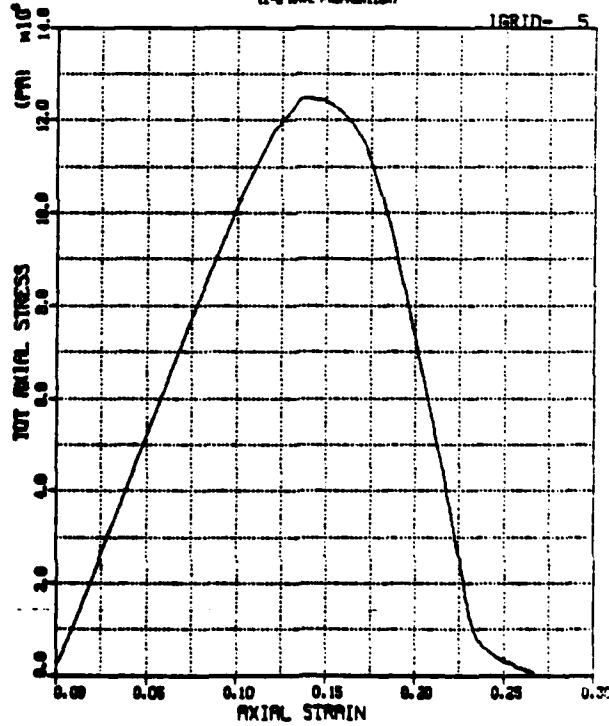
(1-8 MORE PREPARED)



CIST 22 OPP
RV LAYER 1

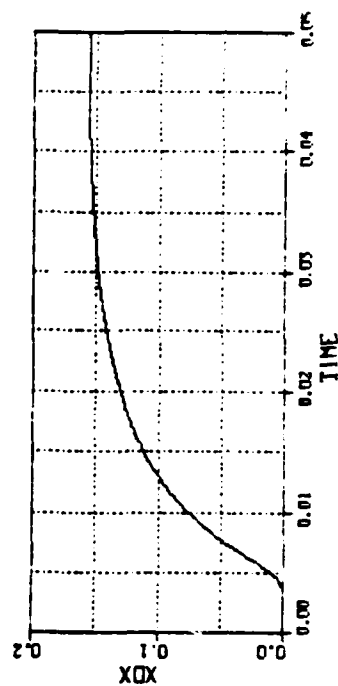
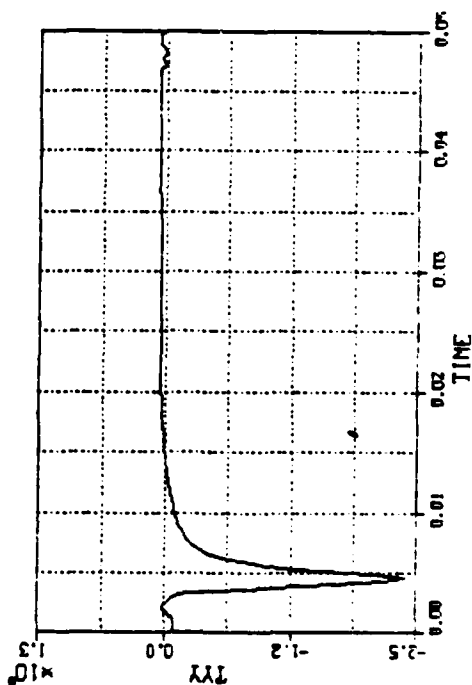
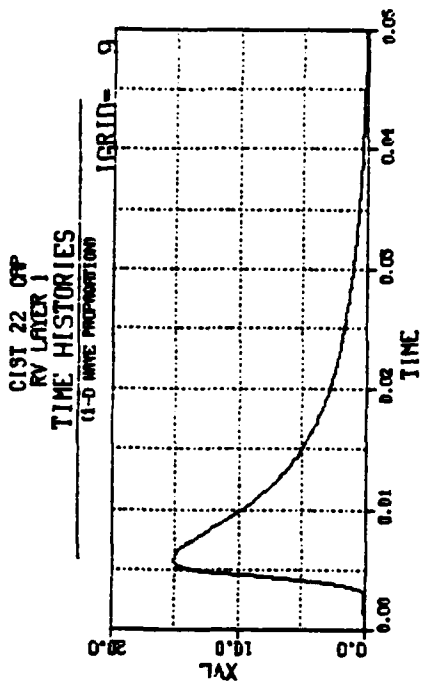
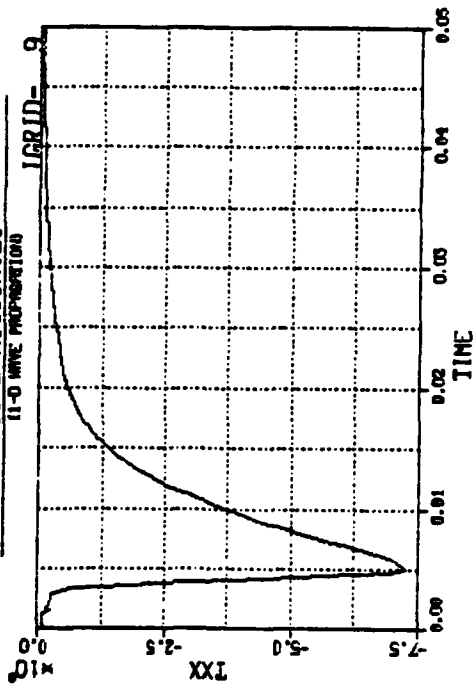
TOT AXL STRESS VS. AXIAL STRAIN

(1-8 MORE PREPARED)



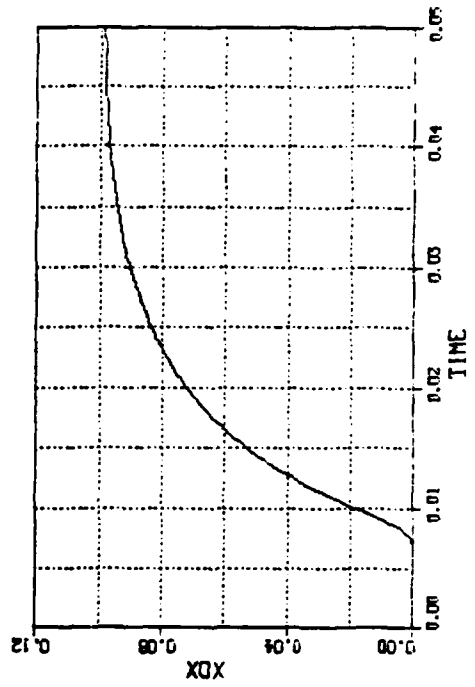
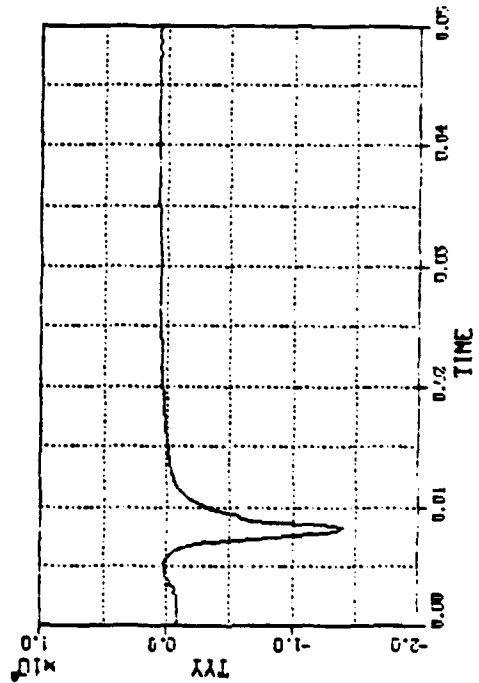
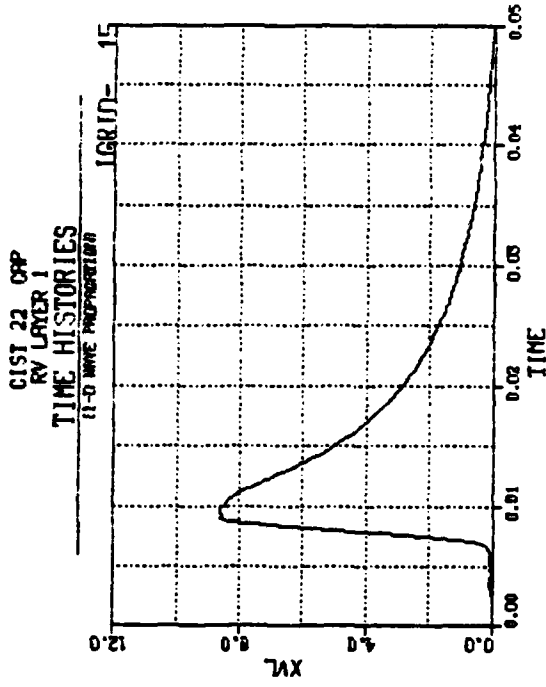
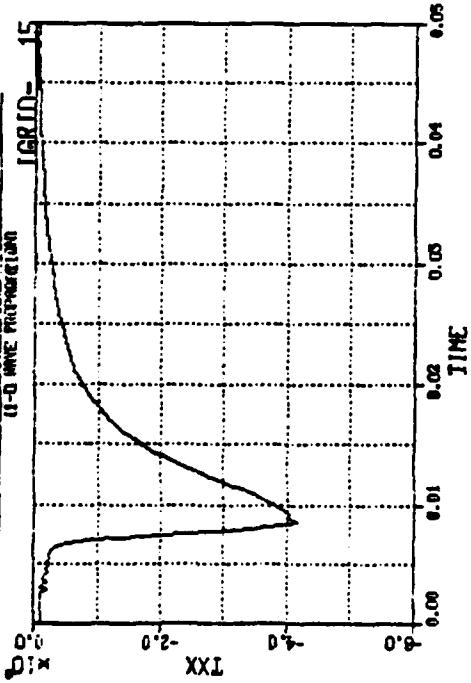
ARRA SOIL ELEMENT MODEL VERSION 1 JAN83

CIST 22 OFF
RV LAYER 1
TIME HISTORIES
11-0 WAVE PROPAGATION

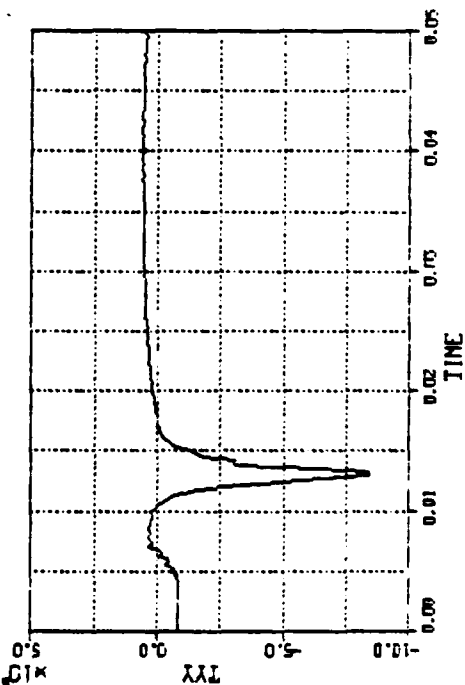
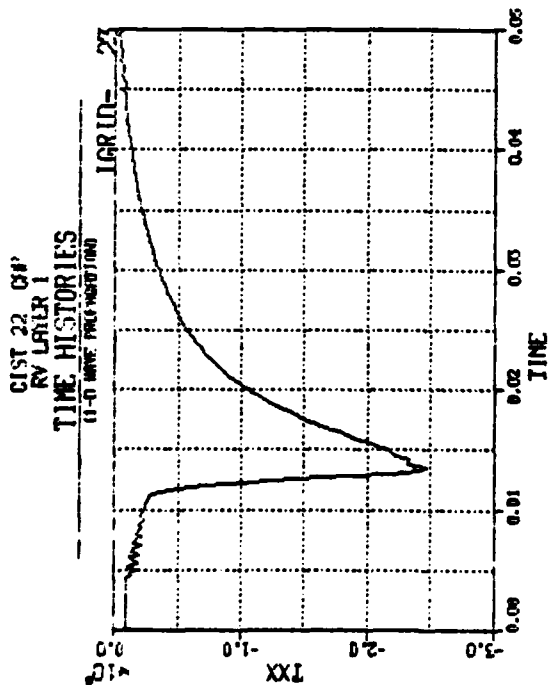
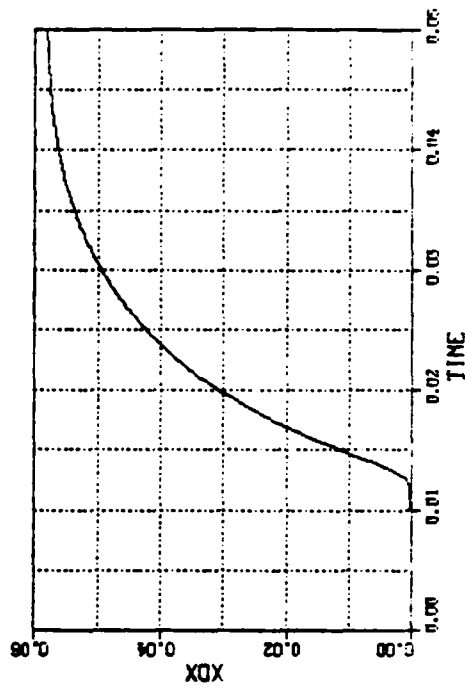
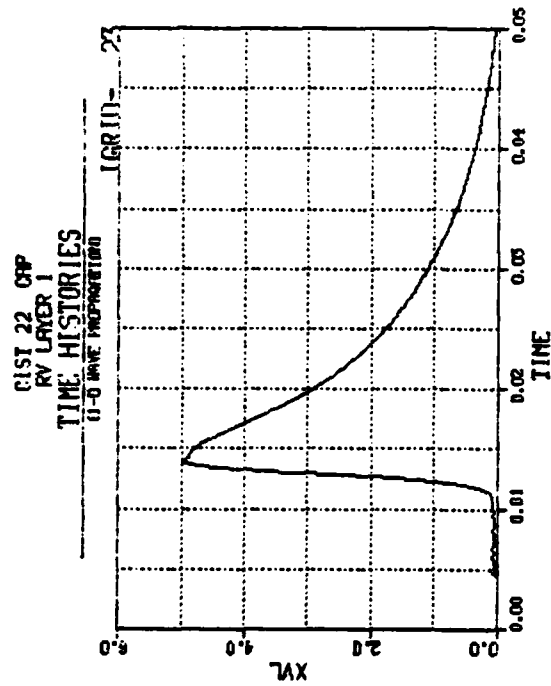


ARA SOIL ELEMENT MODEL VERSION 1 JUN83

GIST 22 OFF
RV LAYER 1
TIME HISTORIES
11-0 WAVE PROPAGATION



PRO SOIL ELEMENT MODEL, VERSION 1 JINBS



APPENDIX D

Publications

- D-1. Dass, W.C., "Comparison of Constitutive Models Subjected to Various Stress-Strain Paths," Proceedings, International Conference on Constitutive Laws for Engineering Materials, Desai, C.S., and Gallagher, R.H. (eds.), University of Arizona, Tucson, AZ, January 10-14, 1983.
- D-2. Dass, W.C., and Bratton, J.L., "Soil Model Evaluation Under Dynamic Loadings," Proceedings, Symposium on the Interaction of Non-Nuclear Munitions with Structures, USAF Academy, Colorado Springs, CO, May 9-13, 1983, (to be published).

COMPARISON OF CONSTITUTIVE MODELS SUBJECTED TO VARIOUS STRESS-STRAIN PATHS

William C. Dassl

¹Staff Engineer, Applied Research Associates, Inc., 2101 San Pedro NE,
Albuquerque, New Mexico 87110

SUMMARY. Many levels of constitutive models for geological materials are available today to the practitioner, from very complex to simple linear-elastic. As a result, there is often confusion when the time comes to choose a model which will give the appropriate combination of simplicity (and therefore cost-effectiveness) and accuracy. This paper describes a computer code which has been developed as a tool for studying material constitutive models. The code allows comparisons of model behavior and parametric studies to determine the influence of model components. It is intended that the "Soil Element Model", as it is called, be an aid in model development and also in choosing a model which best suits a particular boundary value problem. A study is presented which illustrates the use of this code to compare the ability of several material models to replicate laboratory test data. The test data (both static and dynamic) were taken in part from previous efforts, while some data were generated specifically for this purpose. The study concentrates on parametric effects and on isolating areas for model improvement and development. In addition, complex loading paths, typical of those which are induced by blast loadings, are imposed on the models and comparisons are made.

INTRODUCTION

There is a great amount of computer simulation currently being done to assess the response of soils to impulsive dynamic loadings. Finite difference and finite element calculations are heavily relied upon for prediction of ground motions and soil-structure interaction phenomena. Along with establishing suitable boundary conditions and the mathematical particulars of the finite difference (or element) code itself, choice of constitutive relationships and parameters seems to be most influential on calculated motions. It is often not known precisely what effect choosing one type of material model over another will have, so a particular type of model is usually chosen based on past experience of the calculator. Specific model parameters are determined by utilizing as much laboratory and/or in situ data as is necessary and available. The process of fitting parameters to data may range from quick and easy to tedious and time consuming, depending on the complexity of the model and the amount of experience the "user" has had with the model.

In an attempt to address some of the questions regarding dynamic soil modeling, a computer code called the Soil Element Model has been developed (1). The prime motivation behind the Soil Element Model is to allow comparison of different constitutive models when they are subjected to various kinds of static and dynamic stress and/or

strain paths. In addition, the code allows the user to become familiar with the response of each installed model through simple parameter variation studies. Finally, the Soil Element Model can be utilized as a model fitting tool. It facilitates the iterative fitting of parameters to data which is required by some models and can be used to determine the sensitivity of model response to small parameter variations.

SOIL ELEMENT MODEL

Description

The Soil Element Model (SEM) consists of a driver, a set of boundary condition algorithms, and a set of constitutive models. Fig. 1 illustrates the basic logic of the code.

The program is written in FORTRAN and is adaptable to most any computing system. The examples for this paper were done with a Cray 1-S computer at the Air Force Weapons Lab (AFWL), but the code is also functioning on an in-house Apple II microcomputer.

Capabilities

Three types of boundary conditions representing both laboratory tests and in situ conditions may be applied: stress controlled, strain controlled, and the equations of motion

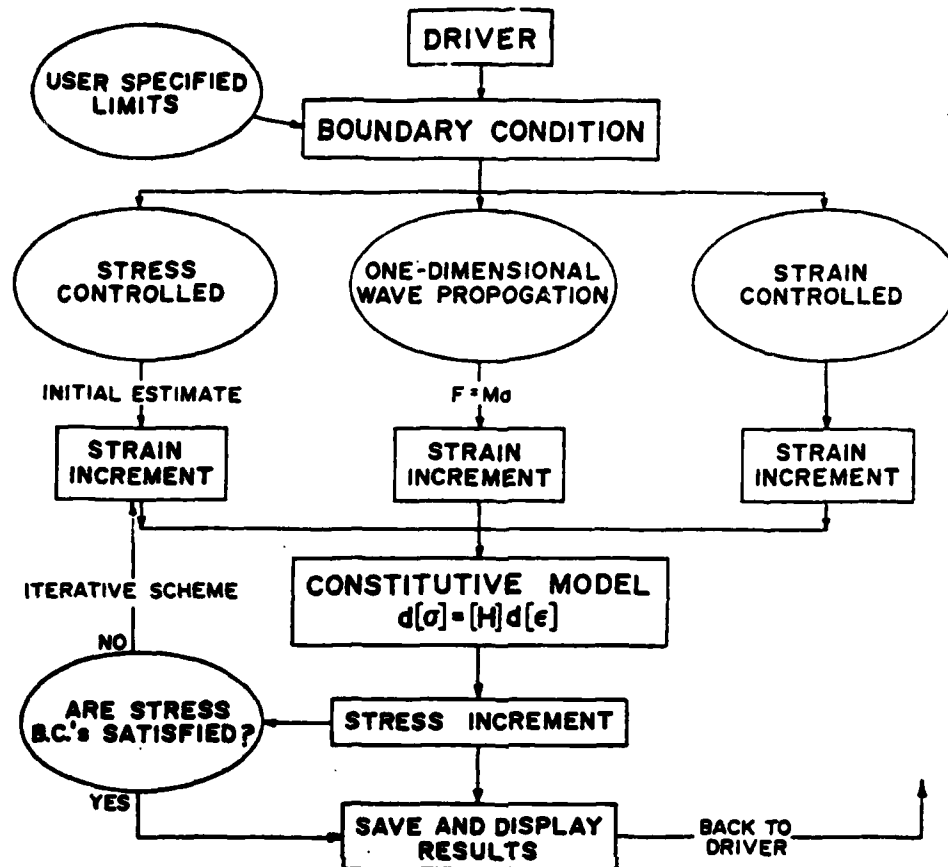


Fig. 1.--Basic Soil Element Model Logic

governing one-dimensional wave propagation. At present, the stress boundary options are hydrostatic compression, proportional loading, and standard triaxial shear. The strain boundary options are uniaxial strain, pure shear, true triaxial (rigid platens), and arbitrary strain paths.

Strain controlled boundary conditions are easily enforced because all of the models are formulated such that given a strain increment, they calculate a stress increment. Stress boundaries require an iterative scheme to establish a suitable strain increment which will produce the correct stress increment. When simultaneous iteration is necessary for more than one strain increment, the process becomes quite time consuming. (A true triaxial test with flexible platens, for example, may require determination of three independent strain increments.)

Exercising a material model over the above stress/strain paths provides insight into model response under many conditions. However, since the ultimate use of these models is in dynamic calculations, a relatively simple one-dimensional wave propagation code was incorporated into the SEM as a boundary condition option. This allows the user to establish, at least in one-dimension, whether differences observed in lab tests or hypothetical in situ model behavior produce

significant differences in an actual calculation. The explicit finite-difference scheme which was implemented is an adaptation of a more general code called SNEAKY written by Hart (2). Calculating wave propagation enforces conservation of mass and momentum between stacked elements (or zones). It requires maintaining a separate constitutive relation reflecting individual stress and strain histories (for each zone).

Constitutive Models

Although the SEM is used primarily to study soil modeling, the code is designed to accept arbitrary constitutive models which may be used for any material, not just soil. In fact, many of the models studied in conjunction with dynamic soil behavior have been either developed for or used to model other materials such as concrete and rock.

Models which are presently incorporated in the SEM include elastic, viscoelastic, elastic-perfectly plastic, one-dimensional curve-fits (3,4), AFWL Engineering (5), and the Cap model (6).

The elastic constitutive relationship is simply Hooke's Law for a linearly elastic, isotropic material. The model contains two constants, a bulk modulus (K) and a shear modulus (G), although any other two elastic constants may be substituted.

The three-element viscoelastic model consists of a spring (K_1) in parallel with a dashpot (n_1), both in series with a second spring (K_2). The governing equation for this model may be used to describe either volumetric or shearing behavior for soil. It may also be included in other models to account, when necessary, for rate dependent elastic behavior.

For the elastic-perfectly plastic model, a modified Drucker-Prager (pressure dependent) failure surface is defined which limits the deviatoric component of stress and allows plastic strain according to an associated flow rule. For stress states below the failure surface the material is linearly elastic. In all, six parameters are required, two for elastic behavior and four for the exponentially curved failure surface with tensile cutoff.

One-dimensional curve-fitting is a common empirical method for modeling soil behavior. Pyke's curve-fit (3) for shearing behavior fits a hyperbolic expression to the initial loading shear stress-shear strain curve, then uses extended Masing rules to model the hysteresis loops. At present, a simple linear elastic relation is used in the SEM to describe the volumetric response, but it is possible to combine Pyke's shear behavior with more complicated bulk responses for better overall behavior.

The hyperbolic curve-fitting method of Duncan and Chang (4) collapses triaxial shear stress-strain results quite well. In conjunction with a confining pressure-dependent bulk modulus, the hyperbolic relations can be used for strain predictions. Because the relations are direct representations of data, the lab response of many different types of soil may be adequately modeled. The models lack the capability to match more complex stress/strain paths, which may or may not be critical, depending on the particular application of the hyperbolic models.

The AFWL Engineering model may be classified as elastic-perfectly plastic with volume hysteresis. Behavior is defined by a piecewise-linear hydrostat and a Drucker-Prager failure surface with a von-Mises cutoff. The model is commonly used in ground shock calculations. The SEM version has twelve parameters which are relatively easy to determine from standard laboratory tests (uniaxial strain and triaxial shear), or they may be estimated from in situ test data.

The Cap model is also commonly used for calculating ground shock effects. It is available on several different levels of complexity which account specifically for various behaviors, such as rate dependence, anisotropy, kinematic hardening, etc. Anyone wishing to use the Cap model must first decide which behavioral phenomena are important to their particular problem and then be sure that the correct features are implemented. The version currently installed in the SEM is an effective stress model with linear-elastic behavior within the failure surface and cap, a curved or modified Drucker-Prager failure surface, and an elliptical cap. The failure surface is fixed and movement of the cap is controlled by plastic volumetric strain. To define both drained (total stress) and undrained (effective stress) behavior, 16 parameters must be

determined. A uniaxial strain or hydrostatic compression test and both drained and undrained triaxial shear tests (with pore pressure measurements) are necessary.

Additional models which can accommodate more complex soil behaviors are currently being installed in the SEM. Composite models, which combine various desirable features of different models, are also being studied.

SEM APPLICATION

The following section is an example of how the Soil Element Method is being applied to better understand and improve the modeling of dynamic soil behavior.

Material Description

The SEM exercises described here are aimed at evaluating the response of Misers Bluff (MB) sand, a medium to coarse grained silty sand (SW-SM) obtained at Planet Ranch, Arizona. Planet Ranch was the site for a cylindrical in situ test in 1977 (CIST 19; 8) and a series of high explosive events in 1978 (Misers Bluff II; 9). For these modeling studies, available lab data for the behavior of saturated MB sand was collected and additional tests were performed on air dry samples remolded to a density of 1.72 g/cc. The net result was a fairly complete set of data for the uniaxial strain and triaxial shear responses of wet and dry MB sand to stress levels as high as 60 MPa and confining pressures up to 6.9 MPa (see Phillips; 10).

Laboratory Behavior

Parameters for the elastic-plastic, AFWL Engineering, and Cap models were obtained by using the SEM to fit the model responses to the corresponding representative laboratory data. The elastic-plastic and AFWL models involve straight-forward linearization of data, while the Cap requires some iteration to find the right combination of parameters to match both the bulk and shear behaviors.

As shown in Fig. 2, the AFWL and Cap models can match the nonlinear uniaxial strain response fairly well, while the straight line approximation of the elastic-plastic is probably not acceptable for most purposes. At stress levels below failure, the elastic model is not able to produce irrecoverable deformations. The Cap model is the most capable of the three for matching the laboratory shear behavior, as seen in Fig. 3. Note that the Cap model's triaxial stress-strain response could be brought even closer to the data with more iteration.

All three models have a single pressure dependent failure surface with a circular intersection in the octahedral plane. This does not compare favorably with the data on MB sand, which indicates asymmetry of the failure surface about the P-axis. A Mohr-Coulomb shape would probably be more representative. An associative flow rule in the elastic-plastic and Cap models allows shear-dilatancy coupling to take place, while the AFWL model uses a nonassociative flow rule on the failure surface and has no coupling.

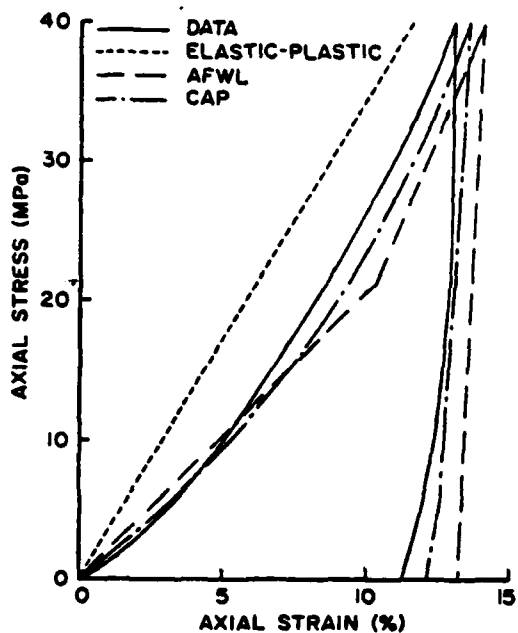


Fig. 2.--Misers Bluff Sand Uniaxial Strain Response

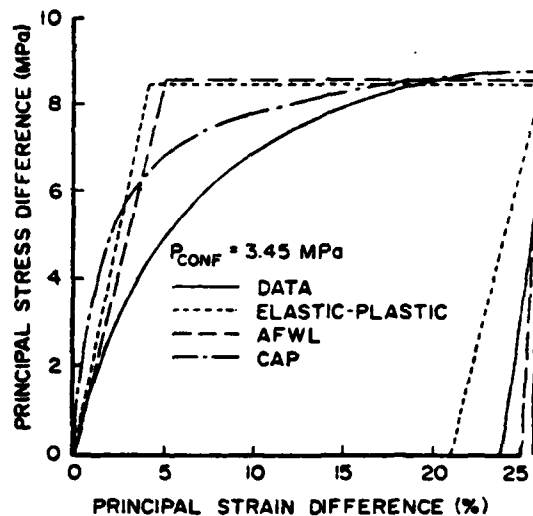


Fig. 3.--Misers Bluff Sand Triaxial Shear Response

In Situ Behavior

It is well known that soil behavior observed in the field cannot always be well predicted by constitutive models based on laboratory test results. The stress/strain paths encountered in situ are often much different and more complex than those in standard laboratory tests, especially in the case of impulsive loads. In addition, there are the problems involved with sampling soils which may create significant differences in lab versus in situ properties. There are various ways of coping with these problems. First, one could assume the lab model is adequate and proceed with calculating. Second, the laboratory-derived parameters could be adjusted to better reflect in situ response. Adjustments may be based on experience and/or intuition. Lab tests could be performed which try to simulate in situ stress paths more closely (e.g. true triaxial). Or finally, in situ data may be taken and improved models could be formulated based on these results. With each of these alternatives comes increased expense and, usually, more complex constitutive relationships.

A recent example of an attempt to simplify the in situ modeling process is the hypothesis of Workman, et al (11) that strain paths in explosively driven fields of motion are limited to a small region in strain space. These dominant strain paths are proposed to be insensitive to variations in geology and primarily dependent on shot geometry. If material behavior could be measured in the lab over these paths (indications are that this would require servo strain-controlled apparatus), modeling would be greatly simplified. In fact, the measured stress path would effectively become the constitutive model.

Fig. 4 is one hypothetical stress path for a spherically symmetric ground motion field. Note that the strain is nearly uniaxial until the point where radial relief occurs. This strain path was used in the SEM to drive the elastic-plastic, AFWL, and Cap models for MB sand. Three levels of initial K_0 consolidation were applied to study how predicted behavior might vary with depth. Results for the three models and three confining pressures are compared in Fig. 5. The differences in resultant stress paths reflect to some extent the same differences seen in lab shear behavior but also reflect basic model differences. Shear failure occurs upon unloading due to radial relief and the failure surface influences all cases. With depth, the K_0 condition diverges from the failure surface and the material undergoes increased stress relief. (Tensile relations are also quite important and effect the late time predicted response.)

The relative differences in predicted stress paths may indicate that strain paths seen in a calculation are in fact dependent on choice of constitutive relationships and may also vary with geology as determined by specific material parameters. Further SEM studies will be helpful in assessing the dominant strain path hypothesis.

In situ models are sometimes determined by iteratively performing finite difference calculations while varying model parameters until the data waveforms are matched. The inclusion of SNEAKY in the SEM facilitates the evaluation of various models in this context. Fig. 6 shows the setup for a one-dimensional, one layer simulation of a DISC TEST event (12). The MB sand models

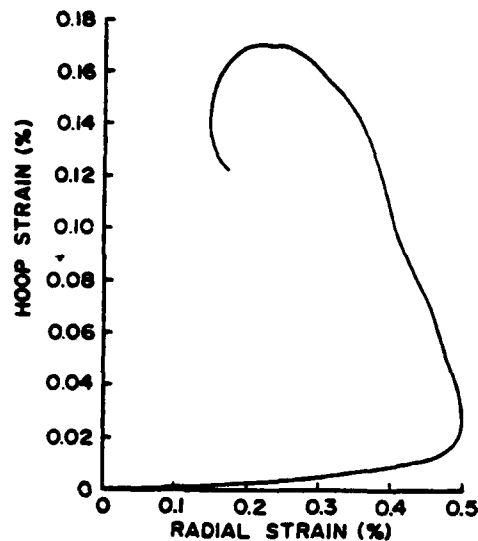


Fig. 4.--Characteristic Strain Path for Spherically Symmetric Ground Motion (Ref. 4, p. 70)

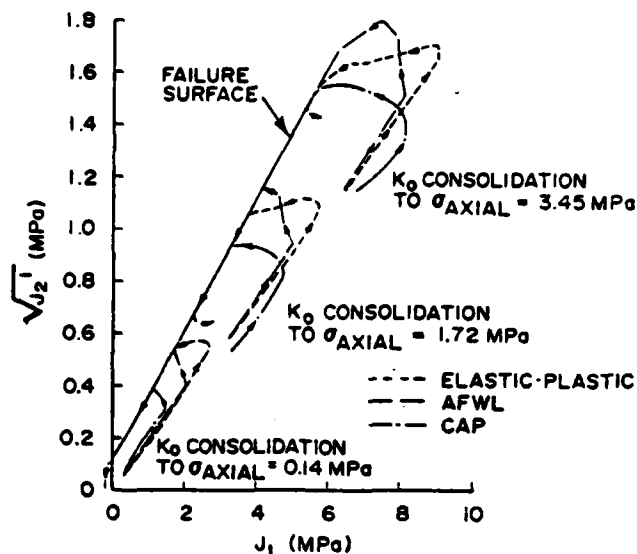


Fig. 5.--Resultant Stress Paths

used in the previous examples were again used. Simulation time is short (40 ms) and loading is typical of data from the DISC TEST I and II events.

Velocity waveform comparisons are shown in Fig. 7a. For the most part, differences in peak velocities and waveform shapes are due to differences in uniaxial strain behavior of the models below 10 MPa (Fig. 2). Note the similarity of the AFWL and Cap waveforms, the two models perform similarly in one-dimensional wave propagation. Attenuation of peak velocity with depth (Fig. 7b) is slightly faster for the AFWL model than for the Cap. Evidently the curved nature of the Cap model's unload volumetric relation has an appreciable effect on energy dissipation. As expected, the elastic-plastic model exhibits almost no attenuation with depth.

CONCLUSIONS

The complexity of each calculational problem dictates the nature of the constitutive relationship which must be used to accurately model material response. The available models are each adequate within the limits of the behaviors they were formulated to deal with. When these bounds are exceeded, the results from any model should be viewed with skepticism. An ideal model from the practitioner's viewpoint would be capable of reproducing all soil behaviors, but would be formulated such that unnecessary effects could be switched off. In this way, the modeler would be using the simplest model possible for each particular problem while maintaining consistency from one application to another.

The SEM is intended to be used as a tool for evaluating the bounds of a constitutive relationship, for both laboratory and more complicated in situ cases. This approach is necessary to make rational choices when considering the application of any particular constitutive model.

ACKNOWLEDGEMENTS

This research is sponsored by the Air Force Office of Scientific Research (AFOSR), United States Air Force, under Contract No. F49620-80-C-0088. The United States government is authorized to reproduce and distribute reprints for governmental purposes, notwithstanding any copyright notation hereon.

REFERENCES

- (1) Dass, W.C., Bratton, J.L. and Higgins, C.J., "Fundamental Properties of Soils for Complex Dynamic Loadings; Annual Technical Report", Report No. AFOSR-TR-82-0101, Applied Research Associates, Inc., Albuquerque, NM, September, 1981.
- (2) Hart, R.D., "A Fully Coupled Thermal-Mechanical-Fluid Flow Model for Nonlinear Geologic Systems", thesis presented to the University of Minnesota at Minneapolis, MN in partial fulfillment of the requirements for the degree of Doctor of Philosophy, March, 1981.

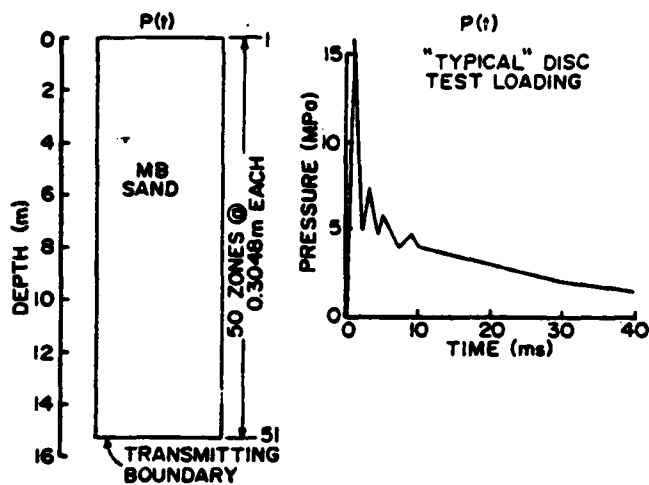


Fig. 6.--One-Dimensional (Uniaxial Strain) Wave Propagation--Example Problem

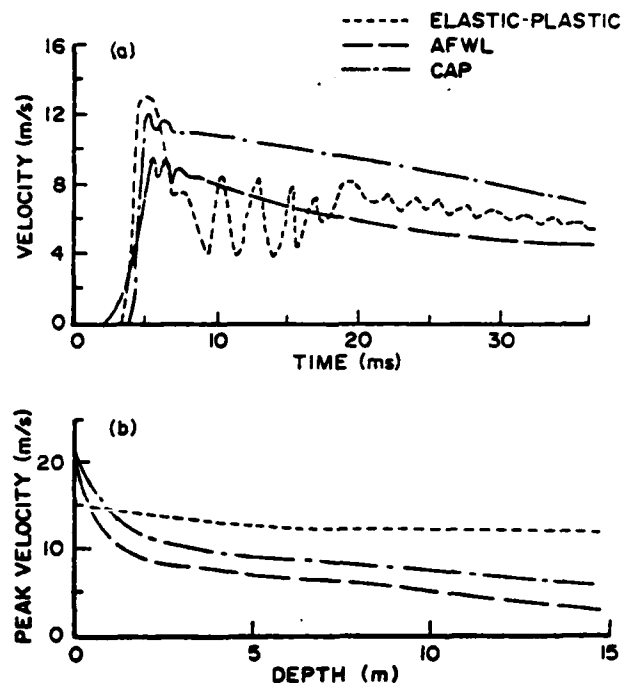


Fig. 7.--Comparison of Computed Motions:
(a) Velocity Waveforms; (b) Velocity Attenuation with Depth

- (3) Pyke, R., Nonlinear Soil Models for Irregular Cyclic Loadings, Journal of the Geotechnical Engineering Division, ASCE, Vol. 105, No. G16, Proc. Paper 14642, June, 1979, pp. 715-726.
- (4) Duncan, J.M. and Chang, C.Y., Nonlinear Analysis of Stress and Strain in Soils, Journal of the Soil Mechanics and Foundation Engineering Division, ASCE, Vol. 96, No. SM5, Proc. Paper 7513, September, 1970, pp. 1629-1653.
- (5) Fedock, J.L., Higgins, C.J., and Bratton, J.L., "Effects of Material Properties on Cylindrical Wave Propagation in Geologic Materials", Report No. AFWL-TR-77-184, Eric H. Wang Civil Engineering Research Facility, University of New Mexico, Albuquerque, NM, October, 1978.
- (6) Nelson, I., Baron, M.L., and Sandler, I., "Mathematical Models for Geologic Materials for Wave Propagation Studies", chapter 13 in Shock Waves and the Mechanical Properties of Solids, Syracuse University Press, Syracuse, NY, 1971.
- (7) Baladi, G.Y. and Akers, S.A., Constitutive Properties and Material Model Development for Marine Sediments in Support of the Subseabed Disposal Program, Subseabed Disposal Program Annual Report, Jan.-Dec., 1980, Vol. II, Part I, Report No. SAND81-1095/II, Albuquerque, NM, 1981, pp. 619-782.
- (8) Amend, J.H., and Brown, R.W., "Cylindrical In Situ Tests at Selected Test Sites", Air Force Weapons Laboratory, Kirtland Air Force Base, NM, August, 1980.
- (9) Strode, J.D. Jr., et al, "Proceedings of the Mises Bluff Phase II Results Symposium, Vols. I-III", Report No. PDR 7013-1, Field Command, Defense Nuclear Agency, Kirtland Air Force Base, NM, March 1979.
- (10) Phillips, B.R., "Mechanical Properties of Mises Bluff Sand", U.S. Army Engineer Waterways Experiment Station, Vicksburg, MS, May, 1982.
- (11) Workman, J.W., Trulio, J.G., and Stokes, E.S., "Modeling the Behavior of Geologic Materials in Explosive Field Events", Report No. AFWL-TR-80-66, Applied Theory, Inc., Los Angeles, CA, January, 1981.
- (12) Jackson, A.E. Jr., Murrell, D.W., Zelasko, J.S., and Skinner, F.W. Jr., "Ralston Valley Soil Compressibility Study: Quick-Look Report for DISC TEST I", U.S. Army Engineer Waterways Experiment Station, Vicksburg, MS, May, 1981.

SOIL MODEL EVALUATION UNDER DYNAMIC LOADINGS

by

William C. Dass¹
Jimmie L. Bratton²

Abstract

There are many different types of constitutive relationships available for calculating the response of geologic media to impulsive dynamic loading. Choosing a material model which is suitable for a particular situation can be difficult. Model selection is often based on personal experience of the calculator which may or may not result in optimum efficiency and best response. This paper describes a computer code which has been developed as an aid for studying material constitutive models. The Soil Element Model can calculate the response of a given material model to laboratory and in situ test conditions, arbitrary strain paths, or one-dimensional wave propagation. It is useful for developing models, performing parametric studies to determine model component influence, and comparing model behaviors. A study is presented which illustrates the use of this code to compare the ability of several material models to replicate laboratory and in situ data. The study focuses on a sand from the DRY CARES site near Yuma, Arizona, and examines the advantages and disadvantages of each model selected.

-
1. Staff Engineer, Applied Research Associates, Inc., 2101 San Pedro, NE, Albuquerque, New Mexico 87110
 2. Principal, Applied Research Associates, Inc., 2101 San Pedro, NE, Albuquerque, New Mexico 87110

94

1

END

FILMED

9-83

DTIC